A STUDY OF THE HEAVY RHENIUM ISOTOPES

A STUDY OF THE HEAVY RHENIUM ISOTOPES USING THE $(\vec{t},\alpha)$ REACTION

by

CHARLES ROSS HIRNING, B.Sc.

A Thesis

Submitted to the School of Graduate Studies

in Partial Fulfilment of the Requirements

for the Degree

Doctor of Philosophy

McMaster University

March, 1977

DOCTOR OF PHILOSOPHY (1977)
(Physics)

McMASTER UNIVERSITY
Hamilton, Ontario

TITLE: A Study of the Heavy Rhenium Isotopes Using the $(\vec{t},\alpha)$ Reaction

AUTHOR: Charles Ross Hirning, B.Sc. (University of Calgary)

SUPERVISOR: Professor D. C. Burke

NUMBER OF PAGES: x, 119

Abstract

The structures of the transitional nuclei ^{187}Re, ^{189}Re and ^{191}Re have been studied using the (t,α) proton pickup reaction. Beams of 15 MeV unpolarized tritons and 17 MeV polarized tritons were produced by the tandem Van de Graaff accelerator facility of the Los Alamos Scientific Laboratory. The reaction products were analyzed in a Q3D magnetic spectrometer and detected with a helical-cathode position-sensitive proportional counter. The unpolarized (t,α) reaction on thin targets of ^{188,190,192}Os produced spectra with energy resolutions of 8-12 keV (FWHM), from which level energies were accurately determined. Later, when the polarized-triton source became operational, the polarized (t,α) reaction on thicker osmium targets yielded angular distributions of analyzing powers and cross sections. Distorted-wave calculations were done to determine a set of optical model parameters which could reproduce the experimental results for known levels in ^{187}Re. The predictions of DWBA calculations were then used to assign spins and parities to other levels in ^{187}Re, and to levels in ^{189}Re and ^{191}Re. This is the first time the (t,α) reaction has been used to study deformed nuclei, and its usefulness for the purpose has been clearly demonstrated. The analyzing powers obtained were large, and their angular distributions were quite distinctive for different values of ℓ and j. This is also the first time level schemes have been assigned in the nuclei ^{189}Re and ^{191}Re. The results have been interpreted within the framework of the Nilsson model, with corrections for pairing and

Coriolis coupling included. The model has been found to provide a fairly good explanation for most of the experimental results. Some aspects of the data were better explained by including a hexadecapole component in the nuclear deformation. The hexadecapole deformation parameter which gave the best agreement with the experimental results was $\varepsilon_4 = 0.06 \pm 0.01$, which agrees well with theoretical predictions for nuclei in this mass region.

ACKNOWLEDGEMENTS

I would like to thank my supervisor, Dennis Burke, for his guidance, support and assistance, and for making possible the experiments at the Los Alamos laboratory.

The time spent on my behalf by the other members of my supervisory committee, Dr. J.A. Kuehner and Dr. H.G. Thode, is gratefully acknowledged.

Thanks to Oddmund Straume and Jim Waddington for many interesting and helpful discussions.

Thanks are also due to our collaborators at Los Alamos, Ed Flynn, Jules Sunier, Pierre-Antoine Schmelzbach and Richard Haglund, and to the technical and operations staff at LASL who provided excellent operating conditions for our experiments. In particular, Stu Orbesen was most helpful with setting up the spectrometer and detector, and Lou Morrison's assistance with the polarized-triton source was invaluable.

Finally, sincere thanks to all my friends and associates who have helped to make my stay in Hamilton a most enjoyable one. A very special thanks goes to Lily, for being herself.

Financial support was provided by the National Research Council of Canada in the form of a scholarship to the author and an operating grant to his supervisor, Dr. D.G. Burke.

TABLE OF CONTENTS

LIST OF TABLES

LIST OF FIGURES

LIST OF FIGURES (cont'd.)

CHAPTER I

INTRODUCTION

In general, there are two ways in which scientific progress is made (excluding fortuitous accidents). One is the origination of new theories which can account for existing data and predict new phenomena. The other is the development of new technologies which make possible the acquisition of previously inaccessible information. The theoretical background of the study reported in this thesis is not new; much of it was first introduced twenty years ago. Although many experiments of different types have since been done to test the predictions of the theory, a large amount of data has remained inaccessible. Very recently, technological innovation has provided a very powerful means of studying proton states below the Fermi surface in heavy deformed nuclei. The experiments reported here are the first to use this new technology in the rare-earth region.

In the past two or three decades, many improvements have been made to particle accelerators. Their energy capabilities have steadily increased and the stability of their beams has greatly improved. At the same time, magnetic spectrographs have been improving, giving better and better energy resolution. These evolutions have made the single-particle transfer reaction an increasingly useful method for studying the structure of nuclei. The (d,p) neutron stripping reaction was the first single particle transfer reaction used to populate neutron states, and it was followed by the (p,d), (d,t), (^{3}He,α) and (t,d) reactions.

Proton states have been populated by the (^{3}He,d) and (α,t) stripping reactions, and, more recently, by the (t,α) and (d,^{3}He) pickup reactions. For most of these reactions, different angular distribution shapes result from different values of the transferred orbital angular momentum, ℓ. It has been found that these shapes can usually be well reproduced by a distorted-wave Born approximation (DWBA) calculation. Thus, for reactions on even-even targets, it is possible to determine ℓ for the final state by comparing the angular distribution with either theoretical predictions or empirical distributions. In some cases, it is also possible to measure the ratio of the cross sections for two complementary reactions (e.g. (α,t) and (^{3}He,d)), and determine the ℓ transfer by comparing the experimental ratio to the theoretical value. For a given $\ell>0$, there are two possible values for the total transferred angular momentum, $j=\ell\pm1/2$. The choice between the two may often be made by combining the transfer reaction results with those from other types of experiments, or by appealing to model-dependent arguments.

Much interest has been shown in the structures of deformed nuclei in the rare-earth region. Neutron states in this region have been extensively studied, as have proton particle states. Proton hole states have been less well studied, and there are two main reasons for this. Although beams of tritons to initiate the (t,α) reaction have been available at a few laboratories for some time, this reaction is not as informative as most of the others. For triton energies presently available (up to $\sim$ 24 MeV), the (t,α) angular distributions are quite structureless, making the assignment of ℓ-values difficult or impossible. The (d,^{3}He) reaction has not been very useful in this mass region either,

because deuteron beams of $\gtrsim$ 30 MeV are required for the ^{3}He particles to have energies significantly above the Coulomb barrier. Accelerators capable of producing deuteron beams of sufficient energy and stability have not been available in conjunction with high-resolution particle spectrometers. Thus, neither $(d,^3He)$ angular distributions nor cross section ratios with the (t,α) reaction can be obtained. For these reasons, there is practically no particle transfer information available on proton hole states in deformed rare earth nuclei.

Single particle states in well-deformed odd-mass nuclei in the region $150<A<190$ have been found to be well described by the Nilsson model (Nilsson 1955) if pairing effects and Coriolis mixing are included (see, e.g., the review articles by Elbek and Tjøm 1969, and Bunker and Reich 1971). For the majority of these nuclei, most of the observed features at low excitations ($E\lesssim 2$ MeV) are reasonably well explained by assuming a simple quadrupole deformation. However, near the upper and lower limits of the region, the nuclear deformation changes quite rapidly with changing mass, and the Nilsson model is not as successful. The limit of its applicability is not yet well known, especially in the vicinity of $A\sim 190$. Several theoretical calculations (Lamm 1969; Nilsson et al. 1969; Götz et al. 1972; Nielsen and Bunker 1975) have indicated that a number of systematic energy trends throughout the deformed rare-earth region may best be explained by adding a hexadecapole component to the nuclear deformation. The magnitude of this component is largest near $A\sim 150$ and $A\sim 190$. Another study (Meyer-ter-Vehn 1975) has emphasized the importance of axial asymmetry in the $A\sim 135$ and $A\sim 190$ regions. The experimental evidence seems to support the hexadecapole deformation

hypothesis more strongly than triaxiality, although it is known that the quadrupole deformation is prolate in W and Os, but oblate in Pt (Baker et al 1976, and references therein).

Because of their position in a region of shape transition, the nuclear structure of the heavy odd-A rhenium isotopes is of considerable interest. A wide variety of experiments has been done to study the structure of the stable isotope ^{187}Re, including proton stripping reactions on ^{186}W, Coulomb excitation, inelastic scattering, resonance fluorescence, and γ-decay studies following the β-decay of ^{187}W (Ellis 1974, and references therein). These have resulted in a good understanding of many of the low-lying excitations in ^{187}Re. Very little is known about ^{189}Re, which is unstable with a half-life of 24 hours. An early γ-decay study using scintillation counters to examine the decay of ^{189}W has been reported (Kuaranen and Ihochi 1965). Some coincidence information was obtained, but no level scheme was proposed. A ground state spin and parity of $5/2^+$ is suggested by systematics, and is compatible with the measured log ft values for the decay to ^{189}Os (Lewis 1974). No information at all was available for ^{191}Re, which has a Half-life of about 10 minutes. The main reason for the scarcity of information on these nuclei is that stable targets do not exist for them to be populated in the most commonly used reaction and decay processes. In fact, the only stable neighbours of ^{189}Re and ^{191}Re are the osmium isotopes ^{190}Os and ^{192}Os. A proton pickup reaction is clearly necessary.

An historical review of the experiments which have contributed to the study reported here will help to clarify later discussion. Several odd-proton nuclei in the A~190 region have been found to have

low-lying $11/2^-$ states. Some authors interpret these as $h_{11/2}$ shell model states, while others believe them to be $11/2^-[505]$ Nilsson orbitals. Price et al. (1971) performed (^{3}He,d) and (α,t) reactions on targets of ^{190}Os and ^{192}Os, populating proton particle states in ^{191}Ir and ^{193}Ir. The observed proton stripping strengths for the $I^\pi = 11/2^-$ levels were consistent with either an $h_{11/2}$ shell model state below the Fermi surface or an $11/2^-[505]$ orbital above the Fermi surface. If the former description were correct, a proton pickup reaction would populate the $11/2^-$ states strongly, and therefore (t,α) studies on targets of Os and Pt were begun. The results obtained for the rhenium isotopes are reported here, while those for the odd iridium isotopes have been reported by Yamazaki et al. (1976).

The initial (t,α) experiments were performed on targets of ^{188}Os and ^{190}Os in 1971 (Burke et al. 1971) at the Los Alamos Scientific Laboratory (LASL). (Until very recently, this was the only Tandem laboratory in North America with the capability of producing a beam of tritons.) The reaction products were analyzed in an Elbek-type magnetic spectrograph, and were detected with nuclear emulsions. When the plates were scanned, it was found that the ^{187}Re spectra had very poor resolution; the peaks were wide and had very large low-energy tails. This was attributed to a non-uniform ^{188}Os target, but was discovered too late for the experiments to be repeated conveniently with a more uniform target. The ^{189}Re spectra were better, but without any (t,α) spectroscopic information for known levels in ^{187}Re, it was not possible to make any definite predictions regarding the nature of levels in ^{189}Re. The only useful result of these experiments was the determination of many

level energies in ^{189}Re.

The study was resumed in 1975. By this time, the accelerator laboratory at Los Alamos had put into operation a new, Q3D-type magnetic spectrometer with a helix detector system. (These will be described in detail in Chapter III). Thinner, more uniform targets of ^{188}Os and ^{190}Os were made, and a ^{192}Os target was also made so that the study could be extended to include ^{191}Re. Much better spectra were obtained this time. On the basis of relative (t,α) cross sections for known levels in ^{187}Re, and with the assistance of energy systematics in the lighter rhenium isotopes and the limited γ-decay study of Kauranen and Ihochi (1965), it was possible to suggest several Nilsson assignments in ^{189}Re. The situation in ^{191}Re was less clear, as the data served only to restrict the interpretation to three possible level schemes. However, the systematics of single proton states in the rhenium isotopes suggested some trends in nuclear structure which would be interesting to study further. One of these trends was a possible change of ground state configuration in going from ^{189}Re to ^{191}Re.

Shortly after the (t,α) experiments were completed, the world's first polarized-triton ion source went into operation at LASL. It was soon found (Flynn et al.1976; Flynn et al.1976a) that the $(\vec{t},\alpha)$ reaction is a very useful spectroscopic tool for spherical nuclei. Not only is it possible to discriminate between spin-orbit partners, it is also often possible to determine the ℓ-value of the transferred proton from the shape of the angular distribution of analyzing powers. Earlier studies (e.g. Casten et al.1973a) had demonstrated that the vector analyzing powers of (d,p) reactions could be used to determine the

transferred ℓ and j for spherical nuclei, but it was also found (Casten et al.1973b) that the technique did not work nearly as well for deformed nuclei.. The vector analyzing powers for the $W(\vec{d},p)$ reaction were found to be smaller than predicted by DWBA calculations and not very useful. It was not clear whether the reduction in analyzing powers from the DWBA predictions was a general property of deformed nuclei, or something peculiar to the particular $(\vec{d},p)$ study. No other analyzing power measurements of single particle transfer reactions in heavy deformed nuclei have been found in the literature. In view of these results, it was not at all certain that the $(\vec{t},\alpha)$ reaction could be successfully used with deformed nuclei. It was decided that a useful test case might be the $^{188}Os(\vec{t},\alpha)^{187}Re$ reaction, since many spins and parities of levels in ^{187}Re were known. If the analyzing powers were found to depend strongly on j and ℓ in this reaction, the technique could be used to make spectroscopic assignments in ^{189}Re and ^{191}Re, resolving the ambiguities that remained after the (t,α) study. The $(\vec{t},\alpha)$ experiments were done in May, 1976, and the successful results are the main subject of this thesis.

CHAPTER II

THEORY

The results of the experiments presented here have been interpreted within a theoretical framework which is well known. The unified model (including the deformed shell model), pairing theory, Coriolis mixing and the distorted-wave Born approximation (DWBA) have all been described in detail in a variety of published works. In this chapter, the basic assumptions and fundamental equations of these theories will be presented. Emphasis will be placed on those aspects which directly concern the present study. Further details and more rigorous treatments may be found in the references cited.

2.1 The unified model for rotations.*

The quantum mechanical description of a rotating body was first applied to the field of molecular spectroscopy, where it was found that the theory reproduced observed energy level spacings very well. Later, when a similar I(I+1) spacing pattern was observed in the spectra of certain nuclei, which were also observed to have large permanent quadrupole moments, a similar model was adopted. The nucleus is considered to have a permanently deformed shape which is rotating in space. The rate of rotation is assumed to be much slower than the intrinsic motion of

*This model is discussed in more detail by Rowe (1970) and Preston and Bhaduri (1975).

the nucleons, so that their motion is not greatly affected by the rotation. This model is of course phenomenological, but its success has been so great that for many purposes it has not yet been replaced by one more fundamental.

In the adiabatic approximation, the Hamiltonian for a deformed nucleus can be separated into an intrinsic part and a rotational part:

$$H = H_{int} + H_{rot} \qquad (1)$$

Defining $\vec{R}$ as the rotational angular momentum, $\vec{J}$ as the intrinsic angular momentum and $\vec{I} = \vec{R} + \vec{J}$ as the total angular momentum of the nucleus, the rotational Hamiltonian may be expanded as:

$$H_{rot} = \sum_{i=1}^{3} \frac{\hbar^2}{2\mathcal{I}_i} R_i^2$$

$$= \sum_{i=1}^{3} \frac{\hbar^2}{2\mathcal{I}_i} (I_i - J_i)^2 \qquad (2)$$

where $\mathcal{I}_i$ is the mean value of the i^{th} component of the moment of inertia tensor. If it is further assumed that the nucleus is axially symmetric, so that $\mathcal{I}_1 = \mathcal{I}_2 = \mathcal{I}$, and $R_3 = 0$, then eq. (2) simplifies to:

$$H_{rot} = \frac{\hbar^2}{2\mathcal{I}} \sum_{i=1}^{2} (I_i - J_i)^2 \qquad (3)$$

Defining the raising and lowering operators $I_\pm = I_1 \pm iI_2$ and $J_\pm = J_1 \pm iJ_2$, and expanding eq. (3) gives:

$$H_{rot} = \frac{\hbar^2}{2\mathcal{J}} (\vec{I}^2 - I_3^2 - J_3^2) - \frac{\hbar^2}{2\mathcal{J}} (I_+ J_- + I_- J_+) + \frac{\hbar^2}{2\mathcal{J}} \vec{J}^2 \qquad (4)$$

The second term on the right couples the rotational and intrinsic motions; in analogy to classical mechanics it is often called the Coriolis term, and is represented by H_{rpc}. The last term in eq. (4) operates only on intrinsic coordinates, so it is usually absorbed into the intrinsic part of the Hamiltonian:

$$H_0 = H_{int} + \frac{\hbar^2}{2\mathcal{J}} \vec{J}^2 \qquad (5)$$

For axial symmetry, $I_3 = K$ and $J_3 = \Omega$ are constants of motion, and since $R_3 = 0$, $K = \Omega$. The rotational Hamiltonian may then be written

$$H_{rot} = \frac{\hbar^2}{2\mathcal{J}} \left[I(I+1) - 2K^2 \right] - \frac{\hbar^2}{2\mathcal{J}} (I_+ J_- + I_- J_+) \qquad (6)$$

Next the eigenfunctions of H_0 are defined by

$$H_0 \chi_K^\alpha = \epsilon_K^\alpha \chi_K^\alpha \qquad (7)$$

where α represents the quantum numbers needed in addition to K to completely specify the state. If the nucleus is odd-A, the wavefunction χ_K^α may be further specialized to refer to the odd nucleon moving in the field of an even-even core. In this way the single particle model is introduced, and with its introduction the unified model is realized.

The properly normalized and symmetrized eigenfunction of the total Hamiltonian may now be written

$$|\alpha IMK\rangle = \left(\frac{2I+1}{16\pi^2}\right)^{1/2} \left[D^I_{MK} \chi^\alpha_K + (-1)^{I-1/2} \pi_\chi D^I_{M-K} \chi^\alpha_{-K} \right] , \quad (8)$$

where D^I_{MK} is the rotation matrix, and π_χ is the parity of the wavefunction χ^α_K. It may be readily seen that for K=1/2, the Coriolis term in Eq. (6) contributes directly to the energy of the state:

$$\langle \alpha IMK | H_{rpc} | \alpha IMK \rangle = \frac{\hbar^2}{2\mathcal{J}} a(-1)^{I+1/2}(I+1/2) , \quad (9)$$

where the decoupling parameter, a, is given by

$$a = -\langle \chi^\alpha_K | J_+ | \chi^\alpha_{-K} \rangle . \quad (10)$$

The total energy of an odd nucleus is given by:

$$E^\alpha_{I,K} = \epsilon^\alpha_K + \frac{\hbar^2}{2\mathcal{J}} [I(I+1) - 2K^2 + \delta_{K,1/2} a(-1)^{I+1/2}(I+1/2)] . \quad (11)$$

This equation indicates that there is a rotational band built on each intrinsic excitation. The energy relative to the bandhead energy is

$$E_{I,K} - E_{K,K} = \frac{\hbar^2}{2I}\left\{I(I+1) - K(K+1) + \delta_{K,1/2}\left[(-1)^{I+1/2}(I+1/2)-1\right]\right\}$$

(11a)

The energy spacing is predicted to follow the I(I+1) rule, except for K=1/2 bands, in which the spacing may be strongly perturbed. No mention has been made of vibrational states so far. Because they are difficult to treat properly, these states are commonly neglected in theoretical structures of the sort described here. Many fewer vibrational excitations are generally found than intrinsic or rotational excitations, but their omission does represent a significant shortcoming of the model. In what follows, the nucleus is assumed to be always in its vibrational ground state.

2.2 The deformed shell model.

The problem of calculating the wavefunction and energy of a particle bound to an even-even deformed core was first considered by S.G. Nilsson (1955). He assumed a Hamiltonian of the form

$$H = \frac{p^2}{2m} + \frac{m}{2}\left[\omega_1^2 x_1^2 + \omega_2^2 x_2^2 + \omega_3^2 x_3^2\right]$$

$$+ C\,\vec{\ell}\cdot\vec{s} + D\,\vec{\ell}^2 \quad , \qquad (12)$$

where the subscripts refer to a body-fixed coordinate system, and the ω_i are harmonic oscillator frequencies. If the nucleus is further assumed to be cylindrically symmetric, one may define a deformation

parameter δ such that:

$$\omega_1^2 = \omega_2^2 = \omega_0^2(\delta)(1 + 2/3\delta)$$
$$\omega_3^2 = \omega_0^2(\delta)(1-4/3\delta) \quad . \tag{13}$$

Prolate spheroidal shapes are given by $\delta>0$, oblate shapes by $\delta<0$. The function $\omega_0(\delta)$ is determined by requiring the volume enclosed by an equipotential surface to be the same at all deformations. The third term in Eq. (12) splits the degeneracy of the shell model levels, and the last term reproduces the observed lowering of high ℓ states relative to the other states in a major oscillator shell. New parameters, κ and μ, are introduced by defining

$$C = -2\hbar\omega_0\kappa$$
$$\text{and} \quad D = -\hbar\omega_0\mu\kappa \quad . \tag{14}$$

The values of κ and μ are chosen so that the shell model level ordering is reproduced in the spherical limit, $\delta=0$. Making a transformation to spherical coordinates, which are easier to work with, the oscillator potential becomes:

$$V(\vec{r}) = 1/3\, m\omega_0^2 r^2 [1-2\beta Y_{20}(\theta,\phi)] \quad . \tag{15}$$

The new deformation parameter, β, is related to δ by

$$\beta = \frac{4}{3}\sqrt{\frac{\pi}{5}}\,\delta = 1.06\delta \quad . \tag{16}$$

The complete Hamiltonian is then

$$H = -\frac{\hbar^2}{2m}\nabla^2 + \frac{1}{3}m\omega_0^2 r^2[1-2\beta Y_{20}(\theta,\phi)]$$

$$-\hbar\omega_0(2\kappa\vec{\ell}\cdot\vec{s}+\mu\kappa\vec{\ell}^2) \qquad (17)$$

Single particle wavefunctions and energies may conveniently be found by diagonalizing the Hamiltonian (17) in a basis $|N\ell jK\rangle$ defined by (c.f. Chi 1966):

$$1/2(-\nabla^2+p^2)|N\ell jK\rangle = (N+3/2)\hbar\omega|N\ell jK\rangle,\ N=0,1,2,\ldots$$

$$\vec{\ell}^2\ |N\ell jK\rangle = \ell(\ell+1)\hbar^2|N\ell jK\rangle$$

$$\vec{j}^2\ |N\ell jK\rangle = j(j+1)\hbar^2|N\ell jK\rangle \qquad (18)$$

$$j_3\ |N\ell jK\rangle = K\hbar|N\ell jK\rangle$$

In the present development, the resulting wavefunctions are identified with the intrinsic wavefunctions of Eq. (8), which may then be written:

$$\chi_K^\alpha(N) = \sum_j C_{j\ell}^K(\alpha)\,|N\ell jK\rangle \qquad (19)$$

Note that the sum need only be over j, since ℓ is determined by j ($j=\ell\pm1/2$) and N ($(-1)^N = (-1)^\ell$). The phase convention relating the expansion coefficients in (19) and those of the time reversed state, $\chi_{-K}^\alpha(N)$, is

$$c^{K}_{j\ell} = (-1)^{j-1/2}\,\pi_{\chi}\, c^{-K}_{j\ell} \qquad (20)$$

In the limit of very large deformations, the number of oscillator quanta along the symmetry axis, n_3, and the projection of $\vec{\ell}$ on the symmetry axis, Λ, become good quantum numbers. The Nilsson states $\chi^{\alpha}_{K}(N)$ are therefore labelled by $K^{\pi}[Nn_3\Lambda]$. These orbitals are doubly degenerate, each being able to accommodate two particles in time-reversed orbits. Thus, each (2j+1) - degenerate shell model state is split into (j+1/2) Nilsson orbitals, as shown in Fig. 1. For prolate deformations, low-Ω orbitals are depressed in energy relative to the shell model state, while the energy of high-Ω orbitals is raised.

The model outlined above has been found to predict energies, spins, parities and particle transfer strengths very well for single particle states in most well-deformed nuclei. It does have several shortcomings, however. One is that the Hamiltonian, Eq. (17), has non-zero matrix elements between states differing in N by 2, so that N is not strictly a good quantum number. In most calculations, this coupling is ignored, and the diagonalization is restricted to a single major oscillator shell. This results in a significant error only when two Nilsson orbitals having $\Delta N=2$ are predicted to come close together in energy. Another problem is that the $\vec{\ell}^2$ term reduces the average energy spacing between the major oscillator shells with increasing N. And finally, experimental evidence indicates that a simple quadrupole deformation does not always provide an adequate description of the nucleus; it is sometimes necessary to consider higher-order deformations.

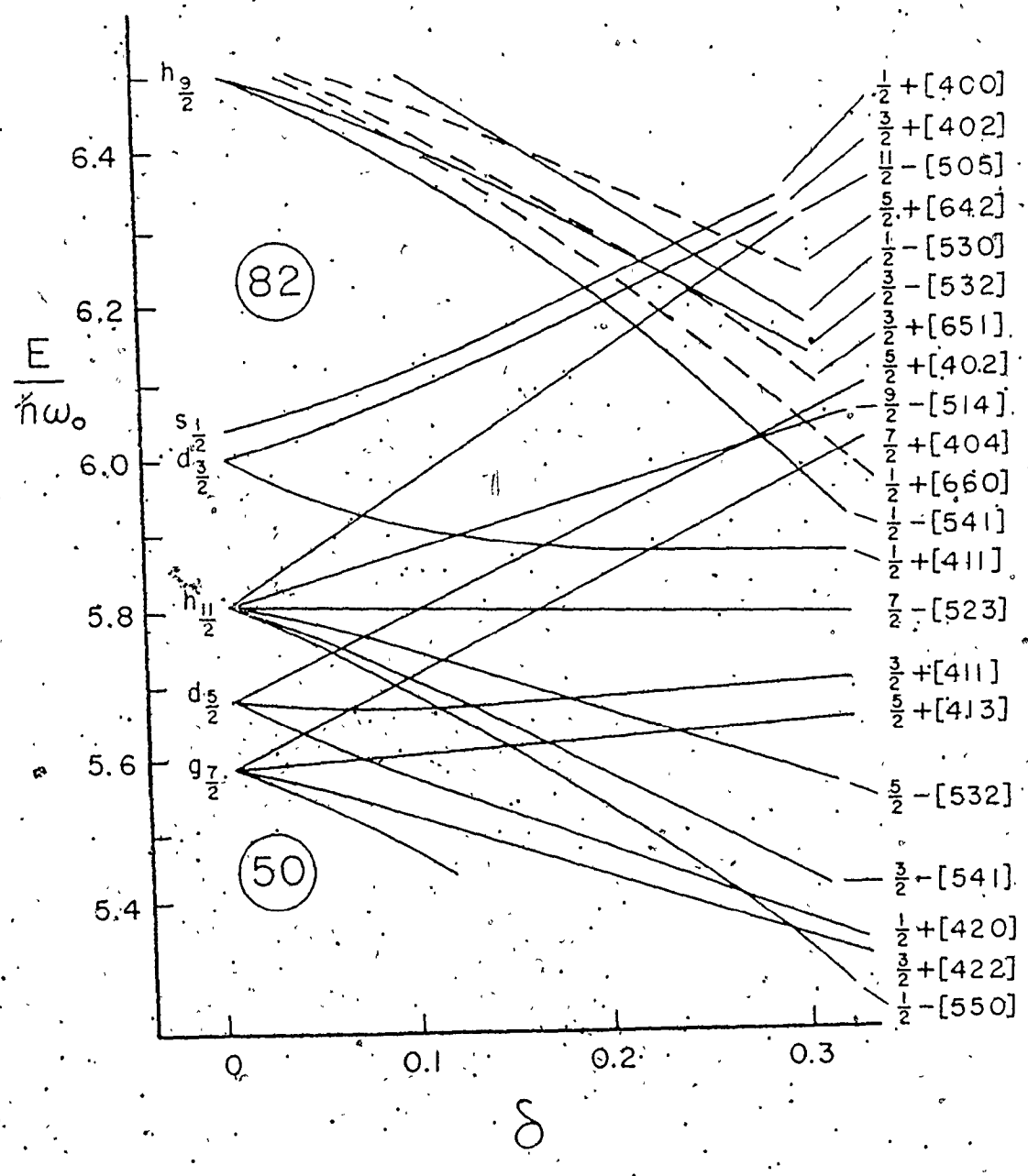

Figure 1. Single-particle energies predicted by the Nilsson model for proton states; $50 \leq Z \leq 82$, and prolate quadrupole deformations.

It was in an attempt to overcome these difficulties that B. Nilsson (1969) proposed a modified Hamiltonian. He began with a variation on the model described above which was also proposed by S.G. Nilsson (1955, Appendix A). A new deformation parameter, ε, is introduced such that

$$\omega_1 = \omega_2 = \omega_0(\varepsilon)(1+1/3\varepsilon) \quad ,$$
$$\omega_3 = \omega_0(\varepsilon)(1-2/3\varepsilon) \quad , \tag{21}$$

It is related to the previous deformation parameter, δ, by the expression

$$\varepsilon = \delta + 1/6\,\delta^2 + \mathcal{O}(\delta^3) \quad , \tag{22}$$

so that, for example, $\delta = 0.30$ corresponds to $\varepsilon \approx 0.32$. The coordinates are transformed according to the relation

$$\xi_i = \left(\frac{m\omega_i}{\hbar}\right) x_i \quad , \tag{23}$$

which has the effect of defining a different scale along each axis. This transformation eliminates the $\Delta N = 2$ coupling for a quadrupole deformation. Defining a radial paremeter ρ:

$$\rho^2 = \sum_{i=1}^{3} \xi_i^2 \quad ,$$

and a differential operator ∇_ξ^2 :

$$\nabla_\xi^2 = \sum_{i=1}^{3} \frac{\partial^2}{\partial \xi^2} \quad ,$$

the Hamiltonian becomes

$$H = 1/2\,\hbar\omega_0(\varepsilon)\left[-\nabla_\xi^2 + \rho^2 + \frac{2}{3}\,\varepsilon P_2\left(\frac{\partial}{\partial\xi_1},\frac{\partial}{\partial\xi_2},\frac{\partial}{\partial\xi_3}\right)\right.$$

$$\left. - \frac{2}{3}\,\varepsilon\rho^2 P_2(\hat{\xi}_1,\hat{\xi}_2,\hat{\xi}_3)\right]$$

$$- \kappa\hbar\omega_0(0)\,(2\vec{\lambda}.\vec{s} + \mu\vec{\lambda}^2) + V_{corr.} \qquad (24)$$

The term $V_{corr.}$ which arises from the coordinate transformation, may be neglected (see S. G. Nilsson 1955, for discussion). The contribution of B. Nilsson was to add two terms to the potential. One term is $-D\langle\vec{\lambda}^2\rangle_{shell} = -DN(N+3)/2$, which maintains the correct spacing of the oscillator shells. The other term adds a hexadecapole component to the deformation. The new Hamiltonian is then

$$H = \frac{1}{2}\hbar\omega_0(\varepsilon_2,\varepsilon_4)\left[-\nabla_\xi^2 + \rho^2 + 2/3\;\varepsilon_2 P_2\left(\frac{\partial}{\partial\xi_1},\frac{\partial}{\partial\xi_2},\frac{\partial}{\partial\xi_3}\right)\right.$$

$$-2/3\;\varepsilon_2\rho^2 P_2(\hat{\xi}_1,\hat{\xi}_2,\hat{\xi}_3) + 2\varepsilon_4\rho^2 P_4(\hat{\xi}_1,\hat{\xi}_2,\hat{\xi}_3)$$

$$\left. -\kappa\hbar\omega_0(0)\,[2\vec{\lambda}.\vec{s} + \mu(\vec{\lambda}^2 - \langle\vec{\lambda}\rangle^2_{shell})]\right] \qquad (25)$$

where ε_2 is the old ε. The shapes of the nuclear potential corresponding to various values of ε_2 and ε_4 are shown in Fig. 2 (from S.G. Nilsson et al. 1969). With the introduction of the hexadecapole deformation, states from different major shells of the same parity are again mixed. The effect tends usually to be small, however, and matrix elements

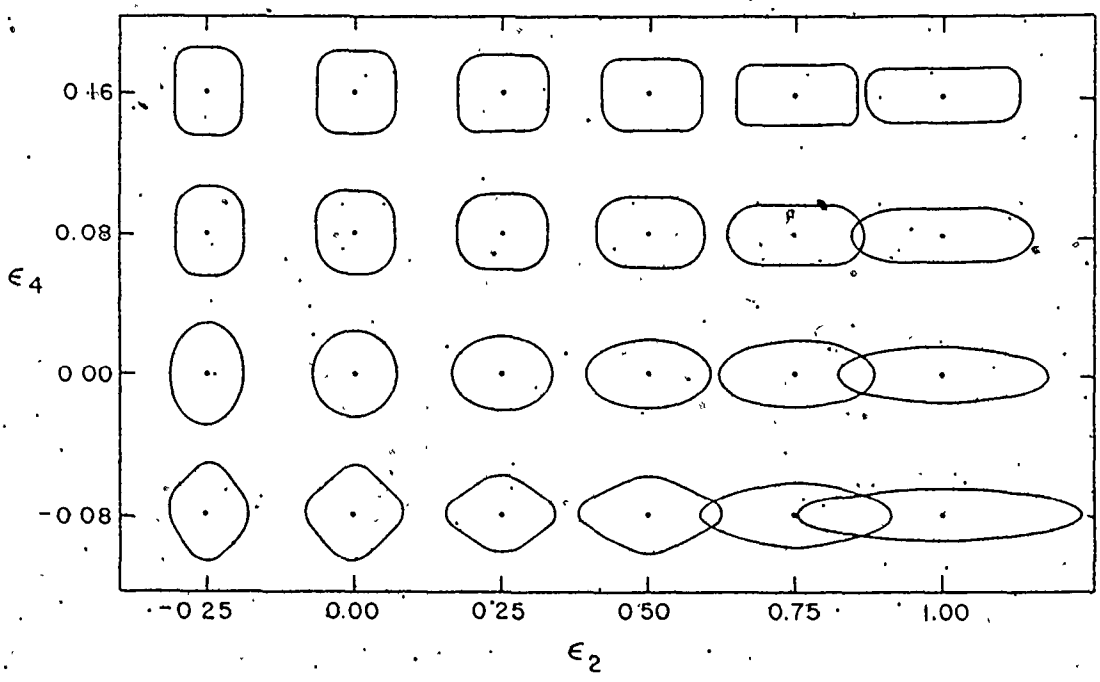

Figure 2. Nuclear potential shapes for various values of the deformation parameters ε_2 and ε_4 (from Nilsson et al. 1969).

between shells differing in N by more than 2 are neglected.

B. Nilsson (1969) went on to calculate the total nuclear energy, including Coulomb and pairing energies, for even-even nuclei in the actinide region. Equilibrium distortions $(\varepsilon_2,\varepsilon_4)$ are defined as those for which the total potential energy is a minimum. A similar calculation was done by Lamm (1969) for odd-A nuclei in both the actinide and rare-earth regions. More extensive calculations were done by S.G. Nilsson et al. (1969) for even-even nuclei in both high mass deformed regions. They used essentially the same Hamiltonian as B. Nilsson and Lamm, but they also employed a generalized Strutinsky (1967) prescription to normalize the average behavior of the potential energy surface to that of a liquid drop. Ground state deformations of even-even rare-earth nuclei were also calculated by Götz et al. (1972), using a slightly different procedure. They assumed a Saxon-Woods potential rather than a harmonic oscillator potential, and considered the possibility of axially asymmetric shapes, as well as quadrupole and hexadecapole deformations. They calculated deformation parameters β_2 and β_4, which are defined by an equation representing the radius of an equipotential surface (Bohr 1952):

$$R(\theta,\phi) = R_0(\beta,\gamma,\beta_4,\ldots)\,[1+\beta_2 Y_{20}(\theta) + \beta_{22}\{Y_{22}(\theta,\phi)+ Y_{2,-2}(\theta,\phi)\}+ \beta_4 Y_{40}(\theta)\} \qquad (26)$$

The relation between β_2 and β_{22} and the more common shape parameters β and γ is given by the equations

$$\beta_2 = \beta \cos\gamma \quad , \qquad (27)$$

$$\beta_{22} = \frac{1}{\sqrt{2}} \beta \sin\gamma \quad .$$

Hence, for $\gamma=0$, $\beta_2=\beta$ and $\beta_{22}=0$. The parameters (β_2,β_4) are related to the other parameters $(\varepsilon_2,\varepsilon_4)$ in a nontrivial way; the connection is shown graphically* in Fig. 9 of S.G. Nilsson et al. (1969). Götz et al. found that triaxial shapes were not predicted for most nuclei. Their values for the quadrupole and hexadecapole deformation parameters were similar to those found in the earlier studies, and agreed quite well with the experimental data available. Finally, in a recent study by Nielsen and Bunker (1975) the equilibrium deformations and energies of proton states in odd-A rare-earth nuclei were calculated. The procedure was very similar to that used by S.G. Nilsson et al. (1969) for even-even nuclear ground states. It was found that observed energy trends are fairly well reproduced by the calculation, and that some trends may be attributed to the hexadecapole deformation. The results of all of the above calculations which are relevant to the present study will be presented in Chapter VI.

2.3 Pairing effects**

In addition to the long range nuclear forces which tend to produce

---

*There is an error in this figure. The signs of the ε_4 values should be reversed.

**Pairing is discussed by Nathan and Nilsson (1965), and is treated more rigorously by Rowe (1970).

deformed nuclei away from closed shells, there are short range forces which tend to keep the nucleus nearly spherical. These latter forces result in nucleons filling available energy levels in time reversed pairs with angular momenta coupled to J=0. One consequence of this is that the ground state spins of all even-even nuclei are I=0. To treat the pairing force correctly, an appropriate term should be included in the nuclear Hamiltonian. This procedure results in extremely long and difficult calculations, so the effects are usually approximated using a formalism due to Bardeen, Cooper and Schrieffer (1957), and first applied to the nucleus by Bohr, Mottelson and Pines (1958). In this formalism (called BCS), the Fermi surface of an even-even nucleus is diffuse, so that, for deformed nuclei, an orbital near the Fermi surface is occupied by a pair with some probability V^2, and is empty with a probability U^2 ; $V^2+U^2=1$. If a single nucleon is now put into the orbital ν, the resulting configuration is a particle state to the extent U_ν that ν was empty , and it is a hole state to the extent V_ν that ν was full. The dual character is indicated by using the term "quasi-particle" for states of this type. The energy of a quasi-particle state is given by

$$E_\nu = \sqrt{(\varepsilon_\nu-\lambda)^2+\Delta^2} \quad , \tag{28}$$

where λ is the Fermi energy (for which $U^2=V^2=1/2$), Δ is a measure of the diffuseness of the Fermi surface, and ε_ν is the single particle (e.g., Nilsson) energy of the state ν. The occupation probability is

given by

$$v_\nu^2 = \frac{1}{2}\left[1 - \frac{\varepsilon_\nu - \lambda}{E_\nu}\right] \qquad (29)$$

If the single particle energy of the ground state of an odd-A nucleus is ε_0, the excitation energy of a quasi-particle state is

$$E = \sqrt{(\varepsilon_\nu-\lambda)^2+\Delta^2} - \sqrt{(\varepsilon_0-\lambda)^2+\Delta^2} \qquad (30)$$

$$\approx \sqrt{(\varepsilon_\nu-\lambda)^2+\Delta^2} - \Delta \qquad (31)$$

Eq. (31) follows from the fact that, usually, $\varepsilon_0 \approx \lambda$. The parameter Δ for a given nucleus may be calculated from the nucleon separation energies in adjacent nuclei, and this has been done for even rare-earth nuclei by Neergård and Vogel (1970).

The BCS formalism also predicts attenuation factors for matrix elements between quasi-particle states, and it gives an additional factor in the expression for the single particle transfer cross section. These will be discussed further in the appropriate sections below.

2.4 Mixing effects.

Mixing between states of different N was discussed briefly in section 2.2. Since it becomes a significant factor in this mass region only for deformations larger than those considered in the present work, it will not be pursued further here. Also neglected is mixing between quasiparticle states and vibrational states. A more detailed theory is

required to account for this phenomenon; Bunker and Reich (1971) give a survey of studies that have been done.

An effect which is important in this study and which can be treated with the theory as outlined is Coriolis mixing. The Coriolis term appears in the expansion of the rotational Hamiltonian, Eq. (4), and is made up of cross products of the intrinsic and total angular momenta. As stated in Section 2.1, it contributes directly to the energy of a state only for K=1/2. In addition, it couples wavefunctions of the form (8) which differ in K by one, and which have the same N. The coupling is particularly strong between Nilsson orbitals originating from the same high-j shell model state, such as $h_{11/2}$. The effect of the mixing is calculated by diagonalizing the Hamiltonian (1) in the basis defined by (8). Diagonal matrix elements are given by Eq. (11), and off-diagonal matrix elements are given by:

$$\langle \alpha IMK | H_{rpc} | \alpha' IMK+1 \rangle$$

$$= -\frac{\hbar^2}{2\mathcal{I}} \sqrt{(I-K)(j+K+1)}\, \langle \chi^{\alpha}_{K} | J_- | \chi^{\alpha'}_{K+1} \rangle P_{K,K+1}(\alpha,\alpha') \qquad (32)$$

The intrinsic matrix element is easily calculated if the expansion (19) is used for the wavefunctions χ^{α}_{K}:

$$\langle \chi^{\alpha}_{K} | J_- | \chi^{\alpha'}_{K+1} \rangle = \sum_{jj'} c^{K}_{j\ell}(\alpha) c^{K}_{j'\ell'}(\alpha') \langle N\ell_j K | J_- | N\ell'_{j'} K+1 \rangle$$

$$= \sum_{j} c^{K}_{j\ell}(\alpha) c^{K+1}_{j\ell}(\alpha') \sqrt{(j-K)(j+K+1)} \qquad (33)$$

Pairing effects tend to attenuate the matrix elements; the correction factor $P_{K,K+1}(\alpha,\alpha')$ is given by (Rowe 1970; Chap. 11):

$$P_{K,K+1}(\alpha,\alpha') = (U_K U_{K+1} + V_K V_{K+1}) \quad (34)$$

The mixed nuclear wavefunctions resulting from diagonalizing the Hamiltonian matrix may be expressed by

$$\psi_I = \sum_i a_i |\alpha_i IMK_i\rangle \quad , \quad (35)$$

where the sum is over all states included in the diagonalization. Note that K is no longer a good quantum number. Usually, however, one state $|\alpha_j IMK_j\rangle$ has a dominant amplitude a_j ($a_j > a_i, i \neq j$), so that the Nilsson quantum numbers for this state are often, for convenience, used as a label for the mixed wavefunction. In the simplest case, when only two states are involved, the effect of the mixing is to lower the energy of the state which had initially the lower energy, and to raise the energy of the other state. To first order, the effect of Coriolis mixing on the energy spacing of a rotational band may be reproduced by renormalizing the rotational parameter $\hbar^2/2\mathcal{I}$, since the strength of the mixing increases with increasing I. Another result of the mixing is the shift of single particle transfer strength (as expressed by the nuclear structure factor; see section 2.5) from the upper state to the lower state, for levels from the same shell.

2.5 Calculation of cross sections.

The general expression for the cross section for a single particle transfer reaction is (Satchler 1958):

$$\frac{d\sigma}{d\Omega}(\theta) = \frac{2I_f+1}{2I_i+1} \sum_{j\ell} S_{j\ell}\, \phi_{j\ell}(\theta) \qquad (36)$$

Here, I_i and I_f are initial and final nuclear spins, $S_{j\ell}$ is the nuclear spectroscopic factor and $\phi_{j\ell}(\theta)$ is the intrinsic single particle cross section. This last factor is independent of nuclear structure, and is usually calculated using the DWBA theory as outlined in the next section. The spectroscopic factor may be expressed in terms of a reduced width, $B_{j\ell}$:

$$S_{j\ell} = |B_{j\ell}|^2 \qquad (37)$$

An expression for $B_{j\ell}$ for rotational nuclei was originally proposed by Bromley et al. (1957), and subsequently further developed by Satchler (1958). Later, pairing corrections were incorporated by Yoshida (1961). Here a recent and rather elegant derivation due to Ikeda (1974) will be given. Using the second quantization formalism, the reduced width for a pickup reaction may be written

$$B_{j\ell} = \sum_{m,M_i} (-1)^{j-m} \langle j-m I_i M_i | I_f M_f \rangle \times \langle \Psi_{I_f,M_f} | a_{j\ell m} | \Psi_{I_i,M_i} \rangle \qquad (38)$$

where $a_{j\ell m}$ is the single particle annihilation operator for a nucleon in the state $|j\ell m\rangle$. The Nilsson model is incorporated by making the expansion

$$a_{j\ell m} = \sum_{\nu} C^{\Omega}_{j\ell}(\nu) a_{\nu\Omega} \quad , \quad m=\Omega \quad , \tag{39}$$

with the same phase convention for the expansion coefficients as that given in Eq. (20). Since the wavefunctions ψ_{IM} are described in a body-fixed coordinate system, the annihilation operator must be transformed to this system (indicated by primes):

$$a_{j\ell m} = \sum_{m'} D^{j}_{mm'}(\theta_i) a'_{j\ell m'} \tag{40}$$

where θ_i, $i=1,2,3$, are the Euler angles. Pairing effects are taken into account by making the Bogolyubov-Valatin transformation (see Rowe 1970, Chapter 11):

$$\begin{aligned} a_{\nu\Omega} &= U_\nu \alpha_{\nu\Omega} + V_\nu \alpha^{\dagger}_{\nu\tilde{\Omega}} \\ &= U_\nu \alpha_{\nu\Omega} + (-1)^{\Omega-1/2} V_\nu \alpha^{\dagger}_{\nu-\Omega} \end{aligned} \tag{41}$$

where $\tilde{\Omega}$ is the time reversal of Ω, and

$$\alpha^{\dagger}_{\nu\tilde{\Omega}} = (-1)^{\Omega-1/2} \alpha^{\dagger}_{\nu-\Omega}$$

The operators α and $\alpha^{\dagger}$ are quasiparticle annihilation and creation

operators. The ground state of an even-even nucleus is a quasi-particle vacuum state $|0\rangle$. For a reaction on an even-even target the initial state wavefunction is

$$|I_i M_i K=0\rangle = \left(\frac{2I_i+1}{8\pi^2}\right)^{1/2} D^{I_i}_{M_i 0}|0\rangle \qquad (42)$$

and the final state wavefunction is

$$\begin{aligned}|I_f M_f\rangle_0 &= \sum_\xi a_\xi \left(\frac{2I_f+1}{16\pi^2}\right)^{1/2} \left[D^{I_f}_{M_f K_\xi} \chi_{K_\xi} \right. \\ &\quad \left. + (-1)^{I_f-1/2} \pi_\chi D^{I_f}_{M_f -K_\xi} \chi_{-K_\xi} \right] \\ &= \sum_\xi a_\xi \left(\frac{2I_f+1}{16\pi^2}\right)^{1/2} \left[D^{I_f}_{M_f K_\xi} \alpha'^{\dagger}_{\nu_\xi K_\xi} \right. \\ &\quad \left. + (-1)^{I_f-1/2} \pi_\chi D^{I_f}_{M_f -K_\xi} \alpha'^{\dagger}_{\nu_\xi -K_\xi} \right] |0\rangle \end{aligned} \qquad (43)$$

The a_ξ are mixing amplitudes as defined in Eq. (35). Substituting (39), (40), (41), (42) and (43) into (38), using (20) and some angular momentum algebra, ultimately gives the surprisingly simple result

$$B_{j\ell} = \left(2\,\frac{2I_i+1}{2I_f+1}\right)^{1/2} \sum_\xi a_\xi C^{K_\xi}_{j\ell}(\nu_\xi) V_\xi \langle j K_\xi I_i 0 | I_f K_\xi\rangle \qquad (44)$$

Since the target nucleus is generally assumed to be in its rotational and vibrational ground state, $I_i=0$ and $I_f=j$. Hence Eq. (44) becomes

$$B_{j\ell} = \left(\frac{2}{2j+1}\right)^{1/2} \sum_\xi a_\xi C^{K_\xi}_{j\ell}(\nu_\xi) V_\xi \qquad (45)$$

and the differential cross section from Eq. (35) is

$$\frac{d\sigma}{d\Omega}(\theta) = 2\left[\sum_{\xi} a_{\xi} C^{K_\xi}_{j\ell}(\nu_\xi) V_\xi\right]^2 \phi_{j\ell}(\theta) \qquad (46)$$

The sum over j and ℓ has been dropped because only a single combination of these quantities can yield a particular final I^π. All the nuclear structure information is contained within the square brackets; this quantity is called the nuclear structure factor. For simplicity, consider the case of an unmixed final state:

$$\frac{d\sigma}{d\Omega}(\theta) = 2C^K_{j\ell} V^2 \phi_{j\ell}(\theta) \qquad (47)$$

In any rotational band, V^2 is the same for all members. The nuclear structure factors, $(d\sigma/d\Omega)/2\phi_{j\ell}$, of the members of a band based on an intrinsic state χ_K are therefore a direct measure of the $C^K_{j\ell}$ expansion coefficients for that state. When the nuclear structure factors are displayed as a function of energy, the resulting characteristic pattern is called a fingerprint (see, e.g. Elbek and Tjøm 1971, p.291). Comparing experimental fingerprints to theoretical or empirical fingerprints is one way in which Nilsson assignments are made. A disadvantage of this procedure is that level spins and parities must be experimentally determined before nuclear structure factors can be calculated. An alternative technique is to compare the relative cross sections of the band members directly with theoretical values. Both procedures, however, depend upon the DWBA calculations being reasonably realistic.

2.6 Distorted-wave Born approximation.

Several authors (e.g. Bassel et al. 1962, Satchler 1964) have given derivations of an expression for the single particle cross section in the distorted-wave Born approximation. The mathematics are tedious, so only the main points in the treatment will be presented in this section. In the present work, single particle cross sections were calculated with the computer program DWUCK4 (Kunz 1974). The relationship between $\phi_{j\ell}(\theta)$ in Eqs. 36 and 46 and the cross section calculated by DWUCK4, $\sigma_{DW}^{\ell sj}$, is

$$\phi_{j\ell}(\theta) = \frac{(N\times 10^4)}{2j+1}\,\sigma_{DW}^{\ell sj}(\theta) \quad , \tag{48}$$

where N is a normalization factor peculiar to the particular reaction, and the factor 10^4 is introduced to convert from the units given by DWUCK(fm^2/sr) to μb/sr. The DWUCK4 cross section for the reaction A(a,b)B is given by

$$\sigma_{DW}^{\ell sj}(\theta) = \frac{1}{4\pi}\,\frac{I}{E_a E_b}\,\frac{k_b}{k_a}\left(\frac{C^2}{AB}\right)^2\,\frac{2\ell+1}{2S+1}\sum_{m,m_a m_b}\left|\beta_{\ell sj}^{m\ m_a m_b}\right|^2 , \tag{49}$$

where

$$\beta_{\ell sj}^{m\ m_a m_b} = \sum_{L_b}\beta_{\ell sj,L_b}^{m\ m_a m_b}\ P_{L_b}^{m_a-m-m_b}(\theta) \tag{50}$$

and

$$\beta^{m\, m_a m_b}_{\ell sj;L_b} = \sum_{J_a L_a J_b} i^{L_a - L_b - \ell} \langle L_a S_a 0 m_a | J_a m_a \rangle$$

$$\times \langle L_b S_b m_a - m - m_b m_b | J_b m_a - m \rangle \langle J_b\ j\ m_a - m\ m | J_a\ m_a \rangle$$

$$\times (2L_b+1) \langle L_b \ell 00 | L_a 0 \rangle \sqrt{(2S_a+1)(2j+1)(2J_b+1)(2L_a+1)}$$

$$\times \begin{Bmatrix} L_b & S_b & J_b \\ \ell & s & j \\ L_a & S_a & J_a \end{Bmatrix} \sqrt{\frac{(\ell - |m|)!}{(\ell + |m|)!}}\ I^{\ell sj}_{J_a L_a J_b L_b} \qquad (51)$$

The quantity in curly brackets in Eq. (51) is a 9-j symbol. The last factor in that equation is a radial integral defined by

$$I^{\ell sj}_{J_a \ell_a J_b L_b} = \int dr\ \chi_{J_b L_b}(k_b, \frac{A}{B} r) f_{\ell sj}(r) \chi_{J_a L_a}(k_a, r) \ , \qquad (52)$$

where the χ's are the radial part of the distorted wavefunctions of the incoming and outgoing particles. They are solutions of the equation

$$\left[\frac{d^2}{dr^2} + k^2 - \frac{L(L+1)}{r^2} - \frac{2\mu}{\hbar^2} (U + U_c + U^J_L) \right] \chi_{JL}(k, r) = 0 \ , \qquad (53)$$

where $U(r)$ is the central optical potential, $U_c(r)$ is the Coulomb potential and $U^J_L(r)$ is the spin-orbit coupling. The form factor, $f_{\ell sj}(r)$, is the normalized radial wavefunction of the transferred particle, and is also found by solving an equation of the form (53).

Many assumptions and approximations have been made to arrive at these expressions. Here are the more important ones:

a) the incoming and outgoing particles move in the average field of the nucleus. Elastic scattering is the most important process, and effects due to inelastic processes can be treated as perturbations. The reaction is therefore regarded as a single-step process.

b) in a direct reaction, only a few nucleons are involved. The nuclear core is not affected by the reaction (except possibly to gain rotational angular momentum), and exchange effects between free and bound particles can be neglected.

c) integrations over products of wavefunctions are simplified by making the zero-range approximation, which effectively requires the incoming and outgoing particles to be present at the same point in space when the reaction occurs.

d) the potential is local, i.e. independent of particle velocity.

e) the nucleus is spherical. Since deformed target nuclei are randomly oriented in a sample, aspherical effects will tend to average out, making this assumption a reasonable one.

f) the incident particle and the target nucleus are unpolarized.

Assumptions (c) and (d) are usually found to be quite good for light projectiles, but approximate corrections for the errors produced can be included in the calculation (Kunz 1974). Only the non-local correction has been used in the present work. It is a factor which multiplies the wavefunctions of the incoming, outgoing and transferred

particles, and is given by

$$W_{NL}(r) = \exp\left(\frac{\beta_i^2 m_i}{4h^2} U_i(r)\right) , \qquad (54)$$

where β_i is the non-local correction parameter, m_i is the mass of particle i, and $U_i(r)$ is its optical potential

The normalization factor N in Eq. (48) can be calculated if wave-functions are assumed for the projectile and ejectile. The value calculated for the (d,p) reaction agrees quite well with experimental findings. Values calculated for other reactions do not always agree well with experiment (when they can be checked), so empirical values are often used. The theoretical relationship between $N_{(a,b)}$ for a pickup reaction and $N_{(b,a)}$ for the inverse stripping reaction is

$$N_{(b,a)} = \frac{2S_a+1}{2S_b+1} N_{(a,b)} , \qquad (55)$$

where b = a + x, x being the transferred nucleon, and S_a and S_b are the particle spins.

A variety of forms may be assumed for the optical model potentials in Eq. (53). In this work, the form

$$U(r)+U_L^J(r) = V_R f(X_R) + i V_I f(X_I) - \left[V_{SO} \frac{1}{r} \frac{d}{dr} f(X_{SO}) \right] \vec{L}.\vec{S} \qquad (56)$$

was used, where

$$f(X_i) = \left[1 + \exp \frac{r - r_{oi} A^{1/3}}{a_i} \right]^{-1} \qquad (57)$$

is a Woods-Saxon potential. The Coulomb potential is given (for particle a) by:

$$U_c(r) = \frac{Z_A Z_a e^2}{(2 r_{oc} A^{1/3})} \left| 3 - \frac{r^2}{(r_{oc} A^{1/3})^2} \right| \quad \text{for } r \leq r_{oc} A^{1/3} ,$$

$$= \frac{Z_A Z_a e^2}{r} \quad \text{for } r > r_{oc} A^{1/3} . \qquad (58)$$

The optical model parameters in Eqs. (56) and (57) are usually found by fitting theoretical angular distributions to elastic scattering data. In the case of the transferred particle, the real well depth is varied to reproduce the binding energy of the particle.

Once distorted waves and form factors have been calculated for a given reaction, it is trivial to calculate the cross sections of both the original reaction and the time reversed reaction. It is also a fairly straightforward matter to calculate the polarizations of the outgoing particles for both reactions. In the particular case of the (t,α) reaction, the outgoing alphas, being spinless, are of course unpolarized. For the time reversed reaction (α,t), however, the spin - 1/2 tritons leave with some vector polarization, $P_t(\theta) = \langle S_t \rangle / S_t$. The vertical projection of this polarization, $P_y(\theta)$, is equal to the analyzing power, $A_y(\theta)$, of the $(\vec{t},\alpha)$ reaction. This equality is a consequence of the time reversal invariance of the reaction, and is discussed by Darden (1971). The $(\vec{t},\alpha)$ cross section is given by

$$\frac{d\sigma}{d\Omega}(\theta) = \left(\frac{d\sigma}{d\Omega}(\theta)\right)_0 (1+P_y A_y(\theta)) \quad (59)$$

where the quantity with the subscript "0" is the unpolarized cross section and P_y is now the vertical component of the beam polarization (the reaction plane is horizontal). If the direction of the beam polarization is taken into account explicitly, this may be written

$$\left(\frac{d\sigma}{d\Omega}(\theta)\right)_{\pm} = \left(\frac{d\sigma}{d\Omega}(\theta)\right)_0 (1 \pm P_{\pm} A_y(\theta)) \quad (59a)$$

Here the subscript + (-) refers to beam polarized up (down), and P is the magnitude of the polarization. When a DWUCK4 calculation for the unpolarized (t,α) reaction is done, cross sections and polarizations for the time reversed $(\alpha,\vec{t})$ reaction are also calculated. Since $P_y(\theta,(\alpha,\vec{t})) = A_y(\theta,(\vec{t},\alpha))$, this calculation provides all the information required for analysis of the polarized (t,α) reaction.

CHAPTER III

EXPERIMENTAL DETAILS

In this chapter, the experimental procedures and apparatus used in the experiments performed in 1975 and 1976 will be described. The techniques used for the 1971 experiments will not be discussed here because of the very limited usefulness of the results.

3.1 Triton beam production.

Two different ion sources were used in the course of this study. Unpolarized tritons were produced by a standard duoplasmatron ion source. Los Alamos is the only nuclear structure laboratory with a tritium ion source of this type, simply because it is the only one with the experience and facilities for handling the amounts of highly radioactive tritium gas required.

Polarized tritons were produced in a Lamb-shift polarized ion source, specifically designed for use with tritium (Hardekopf et al. 1976 a,b). The principles of operation of this type of ion source have been described by Ohlsen (1970), and will not be discussed here. The beam polarization was measured using the quench-ratio method, as outlined by Ohlsen et al. (1971). Essentially, this method consists of altering conditions in the source to quench the polarized part of the beam, and then measuring the remaining unpolarized current. If Q is the ratio of unquenched to quenched beam current, the polarization is given by P=1-1/Q. This method has been calibrated using reactions of known analyzing powers ($A_y = \pm 1.0$),

and is accurate to better than ± 0.5% (Hardekopf et al. 1978a,b).

Once negative tritium ions (polarized or unpolarized) were produced, they were injected into a model FN tandem Van de Graaff accelerator. At the time these experiments were begun, a body of (t,α) data already existed for 15 MeV tritons. To facilitate comparison with these data, the unpolarized (t,α) experiments into rhenium were done with tritons of this energy. The experiments with polarized tritons were, however, done at 17 MeV incident energy because DWBA calculations and previous experience indicated that the magnitudes of the analyzing powers increased quite rapidly with increasing beam energy. This was the maximum polarized-triton energy that could easily and reliably be obtained with the LASL accelerator.

After leaving the accelerator, the ions were transported 40m to the spectrometer target chamber by a system of four quadrupole doublet magnets and three magnetic steerers. Flynn et al. (1975) have described the beam transport system in some detail. The end result was a beam spot 0.75 mm wide by about 3mm high on target. Typical beam currents achieved through the target were ∿ 1.0μA for unpolarized tritons and ∿ 50nA for polarized tritons. The accelerator tends to enhance the beam polarization, so the quench ratio measurements were taken with a Faraday cup after the analyzing magnet. The polarization was in the range 73 to 80% for all Os($\vec{t}$,α) experiments.

3.2 Target preparation.

Osmium metal in powder form was obtained from the Isotope Sales Division of the Oak Ridge National Laboratory. The isotopic enrichments

of the samples used to make targets for the (t,α) experiments were: 97.7% for ^{188}Os, 95.5% for ^{190}Os and 98.7% for ^{192}Os. For the ($\vec{t}$,α) experiments, the sample enrichments were: 94.5% for ^{188}Os, 95.5% for ^{190}Os and 99.1% for ^{192}Os. The targets were made by vacuum evaporating the osmium metal onto carbon backings 50μg/cm^2 thick. The thickness of the osmium for the (t,α) experiments was ∿ 50μg/cm^2. Because of the much lower beam current available with polarized tritons, the thickness of the osmium for the ($\vec{t}$,α) experiments was increased to ∿ 150μg/cm^2.

3.3 The Q3D spectrometer.

The Q3D spectrometer is a recent addition to the series of magnetic spectrometers designed by Harald Enge. It represents a considerable improvement over its forerunners in several respects: larger solid angle, the ability to accurately compensate for kinematic aberrations, higher resolving power and larger dispersion. In this section the design characteristics of the Q3D which yield these properties will be discussed.

Two main types of Q3D spectrometer have been constructed: Type I with a maximum-to-minimum energy ratio of 1.2, and Type II with E_{max}/E_{min}=1.5. The instrument installed at the LASL tandem accelerator laboratory is of the latter type, and a schematic diagram of it is given in Fig. 3. There is a quadrupole element followed by three dipoles; hence the name of the spectrometer.

The Q3D spectrometer was designed with a maximum solid angle of acceptance of ∿ 14 msr, significantly larger than that of any earlier spectrometer. This is a necessary feature whenever the intensity of the reaction products of interest is low, due to small reaction cross sections,

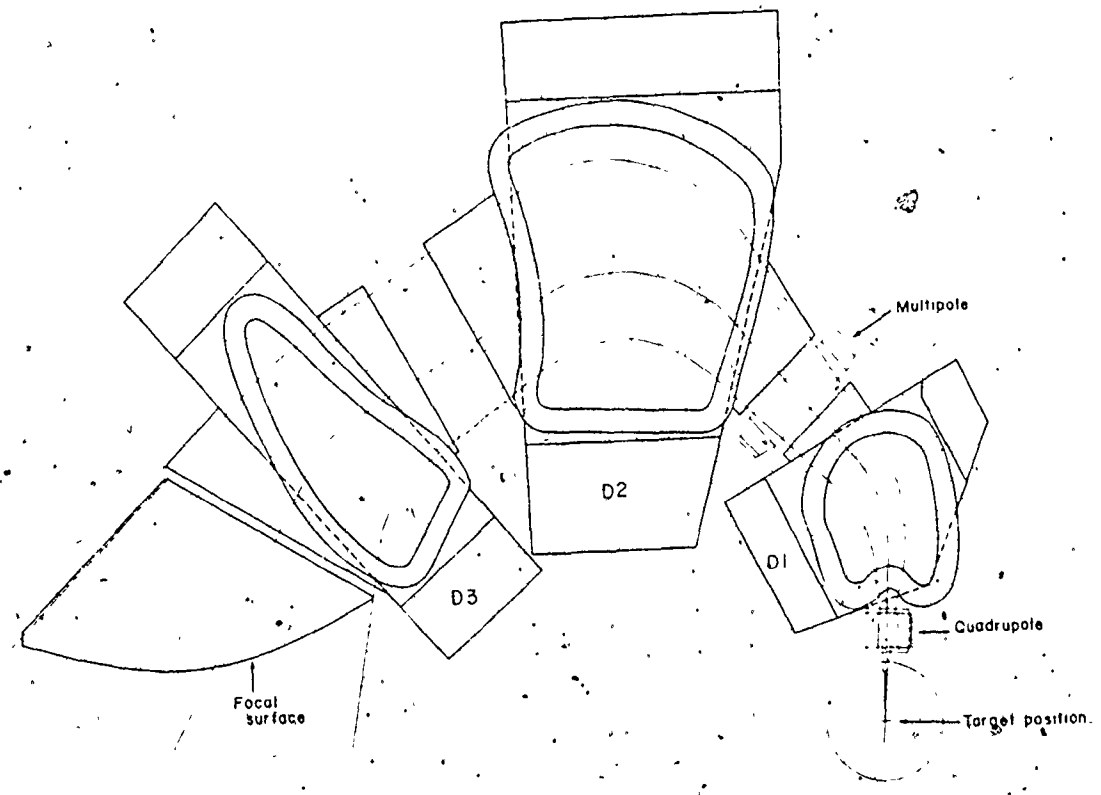

Figure 3. Schematic diagram of the Type II Q3D magnetic spectrometer (top view). The mean particle radius of curvature is 90 cm, the focal surface radius is 215 cm and its length is 240 cm.

low beam currents or thin targets. A large solid angle makes it possible to accumulate a useful amount of data in a reasonable amount of time. The energy of outgoing particles depends upon the reaction angle, however, so a large angle of acceptance in the reaction plane results in kinematic aberrations. If these are not corrected, different particles leaving the nucleus in the same state of excitation are not brought to the same point on the focal surface by the spectrometer; this is called kinematic line broadening and it results in poor energy resolution. The aberration may be expressed as a polynomial in the angles of acceptance, where the power of the angles is the order of the aberration. In the Q3D, the entrance quadrupole is focussing in the vertical direction, producing a cross-over between the first and second dipoles. Near this vertical waist, corrections may be made in the horizontal plane without coupling in undesirable effects in the vertical direction. These corrections can be made to fourth order by a multipole magnet with components up to decapole.

A spectrometer is initially designed assuming infinitesimal spot size and solid angle. Because both of these are actually of finite extent, another type of aberration comes into the system, again limiting resolving power. It is possible to correct for these aberrations by using suitably shaped magnet boundaries. The Q3D has six effective dipole boundaries, and the shape of each is described by a non-linear five parameter equation. Hence much flexibility was available for designing the system in such a way that the geometrical aberrations were reduced. Numerical calculations indicated that corrections could be made in the dispersive plane to fifth order in the solid angle and spot size. The optimum design values of the boundary shape parameters

were determined by using a numerical ray-tracing computer program to minimize the theoretical aberrations on the focal surface. The actual energy resolution possible with the LASL Q3D has been measured to be $E/\Delta E = 3200$ for a solid angle of 14 msr (Flynn et al. 1975).

In addition to its focussing action in the vertical plane, the entrance quadrupole defocusses in the horizontal (reaction) plane. This increases the dispersion of the spectrometer, and, together with the long particle path length through the dipoles, results in a dispersion of 10.2 cm/% momentum. This figure means that two particles of the same charge differing by 1% in momentum will be separated by 10.2 cm on the focal surface. The advantage of high dispersion is that lower spatial resolution is required of the focal plane detector. Hence it is possible to use existing electronic detection systems rather than higher-resolution nuclear emulsions. A disadvantage is that a typical spectrum having a 3 MeV energy range may be spread over nearly a meter of the focal surface, so that the detection system must be quite long if the entire spectrum is to be collected at one time.

3.4 The helix detector.

The particle detector used on the focal surface of the LASL Q3D spectrometer is a helical-cathode position-sensitive proportional counter (Flynn et al. 1973, Flynn et al. 1975, Orbesen et al. 1976). The helix is rectangular in cross section, and is made from 75μm diameter copper clad aluminum wire wound on an insulating frame with a pitch of 1 mm. One side of the helix forms the rear cathode of the proportional chamber; the front cathode is a sheet of 2.5μm aluminized polycarbonate and the anode

consists of nine active coplanar 25μm diameter gold plated tungsten wires running through the center of the chamber. These wires are parallel to the reaction plane and perpendicular to the helix windings. The total depth of the chamber is 6 mm from the front cathode to the rear cathode, and its active height is 3 cm. It is filled with a gas mixture consisting of 70% Ar and 30% CO_2 to a pressure of from 200 to 550 torr, depending on the experiment. When an ionizing particle passes through the gas, a pulse is induced in the helix, and is propagated towards both ends at a rate of 1.5 ns/mm. From the difference in the times at which the pulse reaches the two ends of the helix, the position of the particle along the focal plane is found.

Particle identification is achieved using two additional pieces of information. From the size of the pulse induced in the anode wires by each event, the energy loss in the chamber, dE/dx, can be found. In general, the differential energy loss of particles of the same magnetic rigidity will depend upon the particle type, so by gating on the anode signal particles can be identified. After passing through the helix, particles are stopped in a plastic scintillator, and the resulting light output is measured by two photomultiplier tubes. The output signals from the dynodes are summed and used as a measure of the total remaining energy of the particle, thereby providing an additional means for particle identification.

In Fig. 4 a block diagram of the electronics associated with the helix detector is shown. In addition to their particle identification functions, the signals from the anode wires and photomultipliers are used to establish coincidences, thereby greatly reducing background due

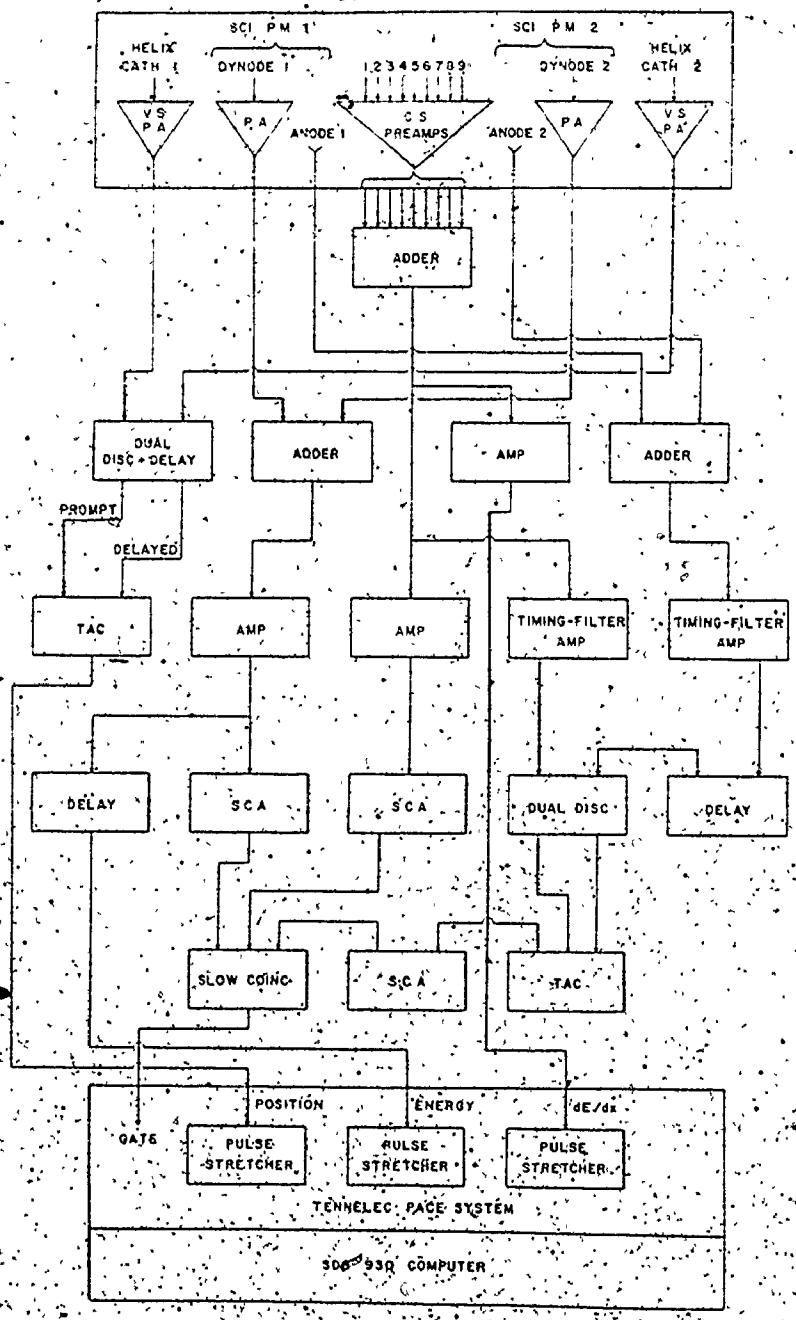

Figure 4. Block diagram of electronics associated with the helix detector (from Flynn et al. 1975). V.S.=voltage sensitive, C.S.=charge sensitive, P.A.=preamplifier, SCI.=scintillator, P.M.=photomultiplier, S.C.A.=single channel analyzer.

to gamma rays and neutrons. A fast coincidence is required between the photomultiplier anode signal and the signal from the anode wires. The anode wire signal and the summed photomultiplier dynode signals are put through single-channel analyzers to eliminate low-level noise due, for example, to neutrons passing through the counter or the scintillator. Then a slow coincidence is required among these two signals and the pulse resulting from the fast coincidence. When all coincidence requirements are satisfied, the position, dE/dx and E signals from the detectors are digitized by either a Tennelec PACE-TC 501 or a Victoreen analog-to-digital converter system and then read by an SDS 930 on-line computer.

The computer is capable of displaying three dimensional plots with dE/dx versus position or E versus position; examples obtained during a (t,α) experiment are shown in Figs. 5 and 6. Gates may be set on displayed particle groups in either type of spectrum by moving three cursors to appropriate locations on corresponding two-dimensional contour displays. A quadratic polynomial is fit to the three cursor points and the resulting curve defines a boundary between two regions. In Fig. 5, a gate has been set on the alpha particles. All particles entering the detector are represented on this plot, but of the three particle types indicated, only the alpha particles were of interest. Although the alphas appear well separated from the tritons in Fig. 5, the valley became less distinct as more events were stored. In Fig. 6, an E gate was set on the group containing alphas and deuterons. If only events occuring in this gate are recorded, the dE/dx spectrum becomes like that shown in Fig. 7; the tritons have been eliminated. It is clearly a simple matter to distinguish between the remaining deuteron and alpha particle groups.

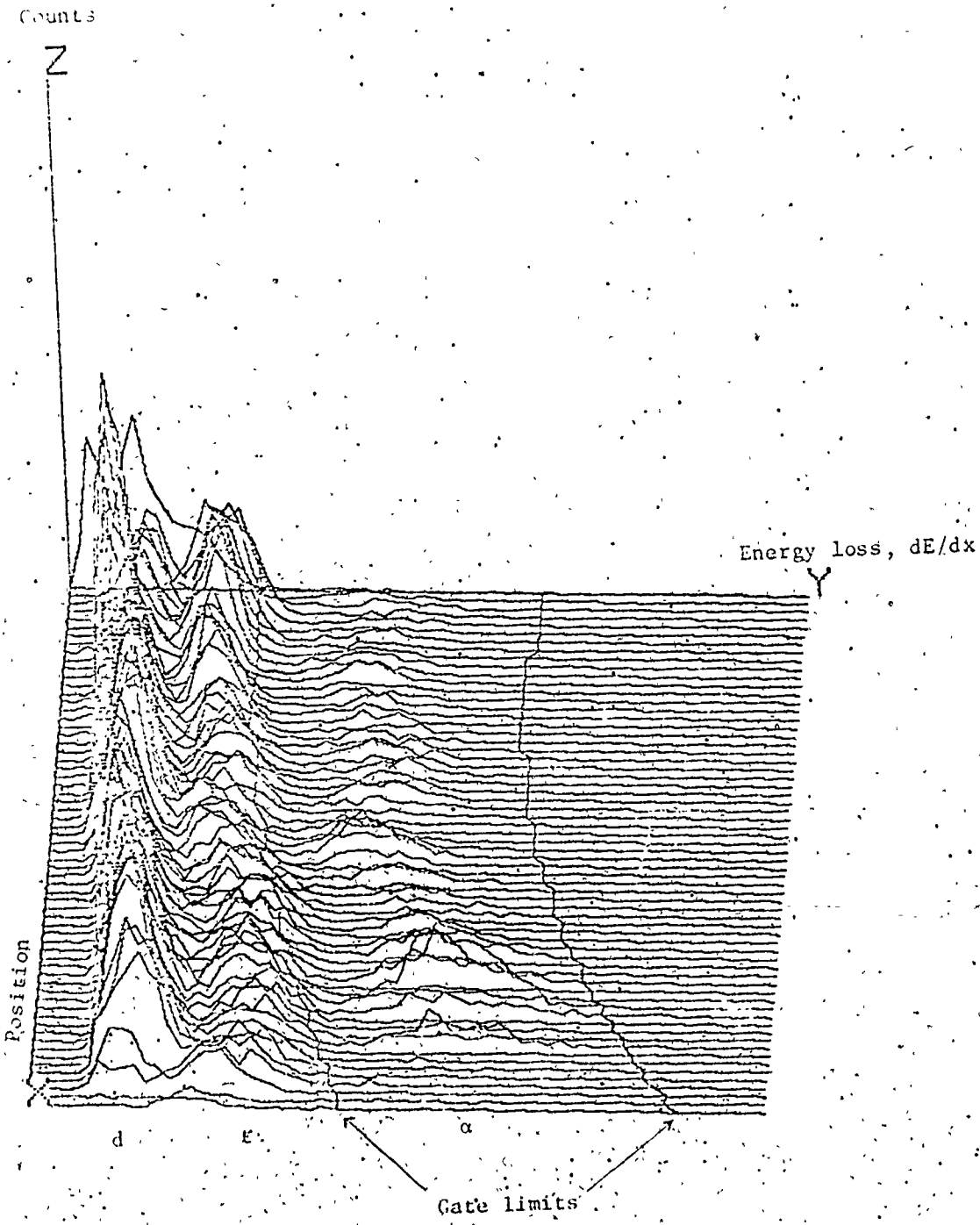

Figure 5. Plot of energy loss versus position obtained during (t,α) experiment with no total energy gate set.

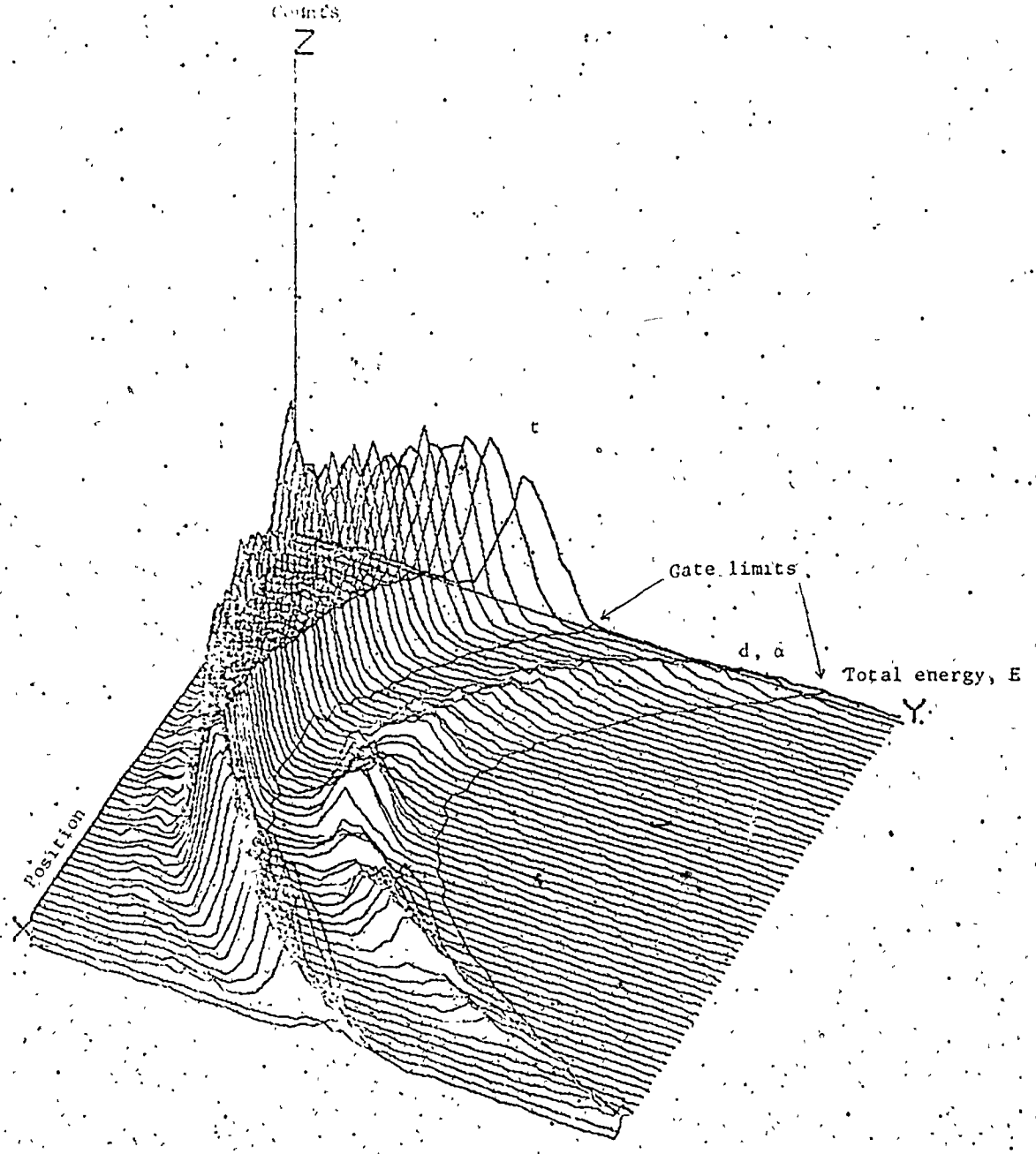

Figure 6. Plot of total energy deposited in scintillator versus position obtained during (t,α) experiment.

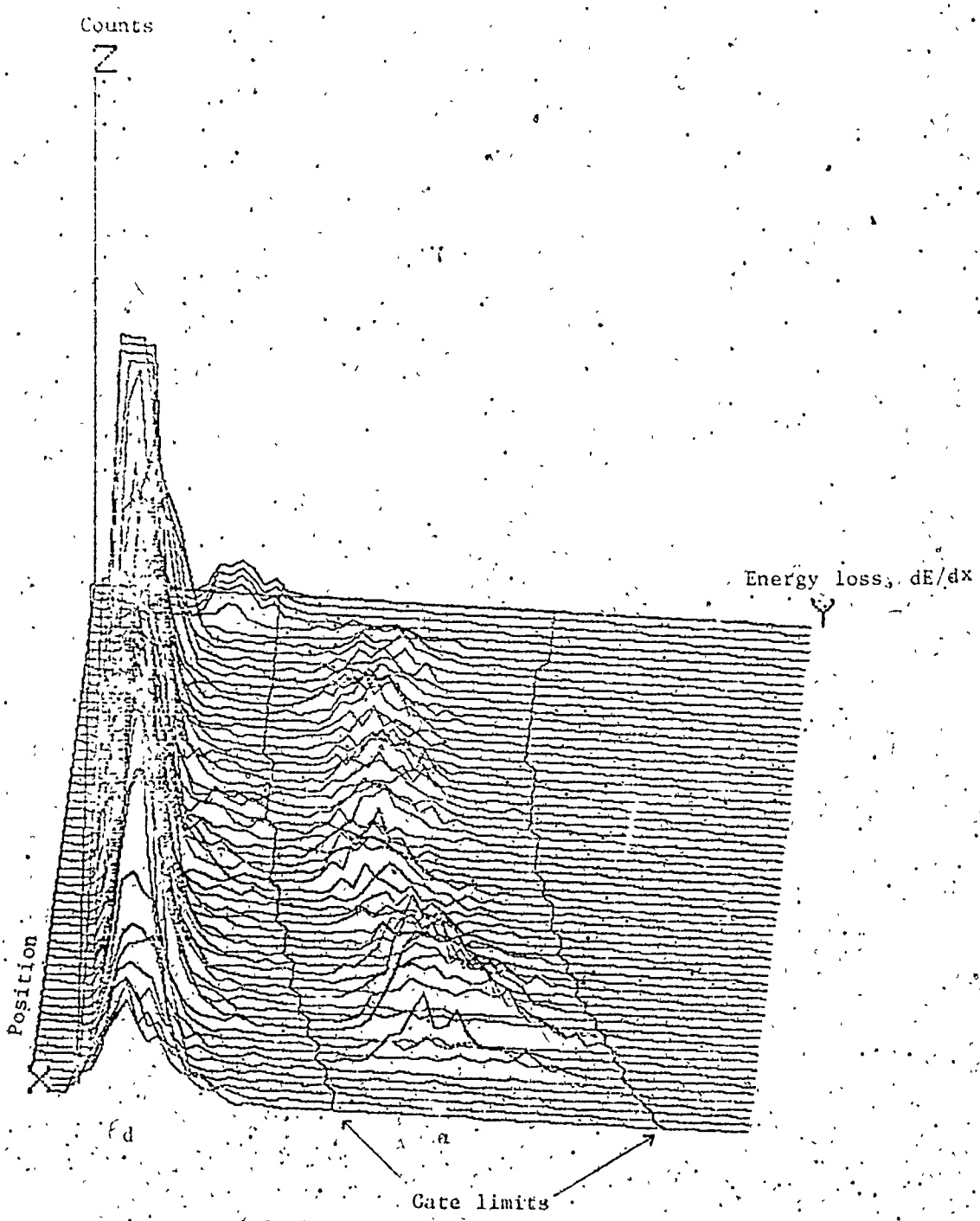

Figure 7: Plot of energy loss versus position obtained during (t,x) experiment with total energy gate set as shown in fig. 6.

For moderate count rates (the system can handle an event rate of 3kHz), the resulting alpha spectra have little or no background, as will be seen in the next chapter. At the end of each run, the position spectrum and related information (such as the monitor spectrum, see section 3.6, below) were printed out on a fast line printer and also written onto magnetic computer tape.

The experiments described in this thesis were done using two different models of helix detector. For the experiments with unpolarized tritons, a detector 50 cm in length with the scintillator behind the helix was used. In order to observe states ranging in energy from 0 to 3 MeV, it was necessary to obtain two overlapping alpha spectra. This was done by taking exposures for two different positions of the detector on the focal surface. By the time the $(\vec{t},\alpha)$ experiments were begun about one year later, a new one-meter long counter with the scintillator inside the helix was operational. It was possible to collect the full region of excitation of interest in one step with this detector. Tests with X-ray sources have shown the spatial resolution to be $\sim$ 0.5 mm for the 50 cm and $\sim$ 1.0 mm for the one meter helix. Observed spectral line widths are somewhat larger than these values, so the detector is not the resolution-limiting factor.

3.5 Energy calibration.

Due to small variations in amplifier gains and slight nonuniformities in the helix wire, it is not possible to accurately obtain absolute position information from the helix detector. The detector must therefore be calibrated. In the present case, this was done by first performing the ^{166}Er(t,α)^{165}Ho reaction, whose Q-value is similar

to that for the $^{188}Os(t,\alpha)^{187}Re$ reaction, and is accurately known. The excitation energies of states in ^{165}Ho have previously been measured (Wagner et al. 1975), so the energies of the resulting α-particles could be calculated using standard kinematic equations. Then, knowing the magnetic field through which the particles passed, their radii of curvature, ρ, were calculated. From these values of ρ and the mean position of the corresponding particle groups in the spectrum, a quadratic polynomial relating ρ to channel number was found by a least squares fit routine. This polynomial was then used for the reactions into the rhenium isotopes to calculate E_α values and hence excitation energies. Since the Q-value of the $^{166}Er(t,\alpha)$ reaction was about 100 keV too low for a complete energy overlap with the $^{188}Os(t,\alpha)$ reaction, known levels up to $\sim$ 400 keV in ^{187}Re were also used in determining the calibration polynomial. This procedure was followed for the unpolarized (t,α) experiments, and the energies were compared with known values for many levels above 400 keV in ^{187}Re, and with those found for ^{189}Re in the 1971 study. Good agreement was observed in all cases. Because the targets for the $(\vec{t},\alpha)$ experiments were about three times thicker than those for the unpolarized experiments, the resolution was significantly poorer. Consequently, no accurate energy calibration was attempted, and the energies obtained from the higher-resolution experiments with unpolarized beams were adopted.

3.6 Cross section normalization.

To determine absolute cross sections, the observed particle intensities must be normalized to a known quantity. In the LASL Q3D, a

cooled surface barrier detector is mounted in the target chamber to monitor the number of elastically scattered particles. The energy spectrum from this detector is accumulated during an experiment, and the number of counts in the peak corresponding to tritons elastically scattered in the target material (but not in the carbon backing) is obtained. Once the geometry of the detector, the solid angle of the spectrometer and the efficiency of the helix detector are known the absolute reaction cross section may be calculated for each peak in the position spectrum. If N_r is the number of counts in a peak, the reaction cross section is

$$\left(\frac{d\sigma}{d\Omega}\right)_r = Y_{NORM} N_r \qquad (60)$$

If the helix detector is assumed to be 100% efficient (approximately true for low count rates), the normalization factor, Y_{NORM}, is given by:

$$Y_{NORM} = \left(\frac{d\sigma}{d\Omega}(\theta_{mon})\right)_{el} \frac{d\Omega_{mon}}{d\Omega_{sp}} \frac{\eta_{sp}}{\xi N_{mon}} , \qquad (61)$$

where $\left(\frac{d\sigma}{d\Omega}(\theta_{mon})\right)_{el}$ is the elastic cross section at the angle of the monitor detector (usually given by an optical model calculation), $d\Omega_{mon}$ and $d\Omega_{sp}$ are the solid angles of the monitor and spectrometer, η_{sp} is the correction factor for computer deadtime, N_{mon} is the number of elastic events (corrected for monitor ADC deadtime) and ξ is the isotopic enrichment of the target. Theoretical cross sections are normally calculated in the center of mass coordinate system; Eqs. (60) and (61) give the experimental cross sections in the laboratory system. Thus an

additional factor must be applied to the experimental results before a comparison can be made. For experiments of the type reported here, this factor is close to unity.

There is also a Faraday cup in the target chamber which stops the unscattered beam. It provides an additional check on the monitor detector, since if there are no changes in the target thickness during an experiment, the ratio of the number of elastic events recorded by the monitor to integrated beam current should remain constant. This was observed to be the case to within $\sim$ 2% during the experiments described here. For the unpolarized (t,α) experiments, the monitor detector was mounted at $\theta_{mon} = 45^{\circ}$, while in the $(\vec{t},\alpha)$ experiments, it was at $\theta_{mon}=30^{\circ}$. In both cases its solid angle of acceptance was $d\Omega_{mon}=0.0866$ msr, and that of the spectrometer was $d\Omega_{sp}$ = 14 msr.

The relative efficiency of the helix detector as a function of position along its length was tested by stepping the detector along the focal plane, thus exposing successive parts of it to a strong particle group. In this way, it was learned that the efficiencies of both helix detectors were constant to within ± 6% over the entire length except for a few centimeters near each end. Only the region of constant efficiency was used for collecting data to be analyzed.

On the basis of observed repeatability of experimental cross sections, their relative errors are estimated to be ± 10%, and their absolute errors ± 15%.

CHAPTER IV

EXPERIMENTAL RESULTS AND DATA ANALYSIS

4.1 Unpolarized (t,α) results.

In the 1971 experiments, data were obtained at $\theta = 45^{\circ}$ and 60° for ^{187}Re and ^{189}Re. The results for ^{187}Re have not been used for the reasons given in Chapter I, but the energies measured for ^{189}Re have provided a check on the more recent data.

In 1975, spectra were acquired for all three rhenium isotopes at the laboratory angles $\theta = 30$, 40 and 50°. Ground state regions were obtained at all three angles, and excited state regions at one or more angles for each isotope. The energy resolution achieved was in the range 8-12 keV (FWHM). The best spectra for each isotope are shown in Figs. 8, 9 and 10. To facilitate analysis, the spectra were smoothed using a standard method (Bevington 1969). This consists of taking half the counts in a given channel, adding one quarter of the number of counts from each adjacent channel, and putting the total back into the initial channel. The process is repeated for each channel in the spectrum. This procedure does not change the positions of the centroids nor the peak areas. It may result in slightly poorer resolution, but not significantly so in the present case. After smoothing, the spectra were analyzed using program SPECTR on the McMaster University CDC 6400 computer (O'Neil 1970). This is a fitting program which uses a standard line shape (determined from a well-resolved peak in the spectrum) to find peak centroids and areas. Excitation energies and cross sections were calculated, and are

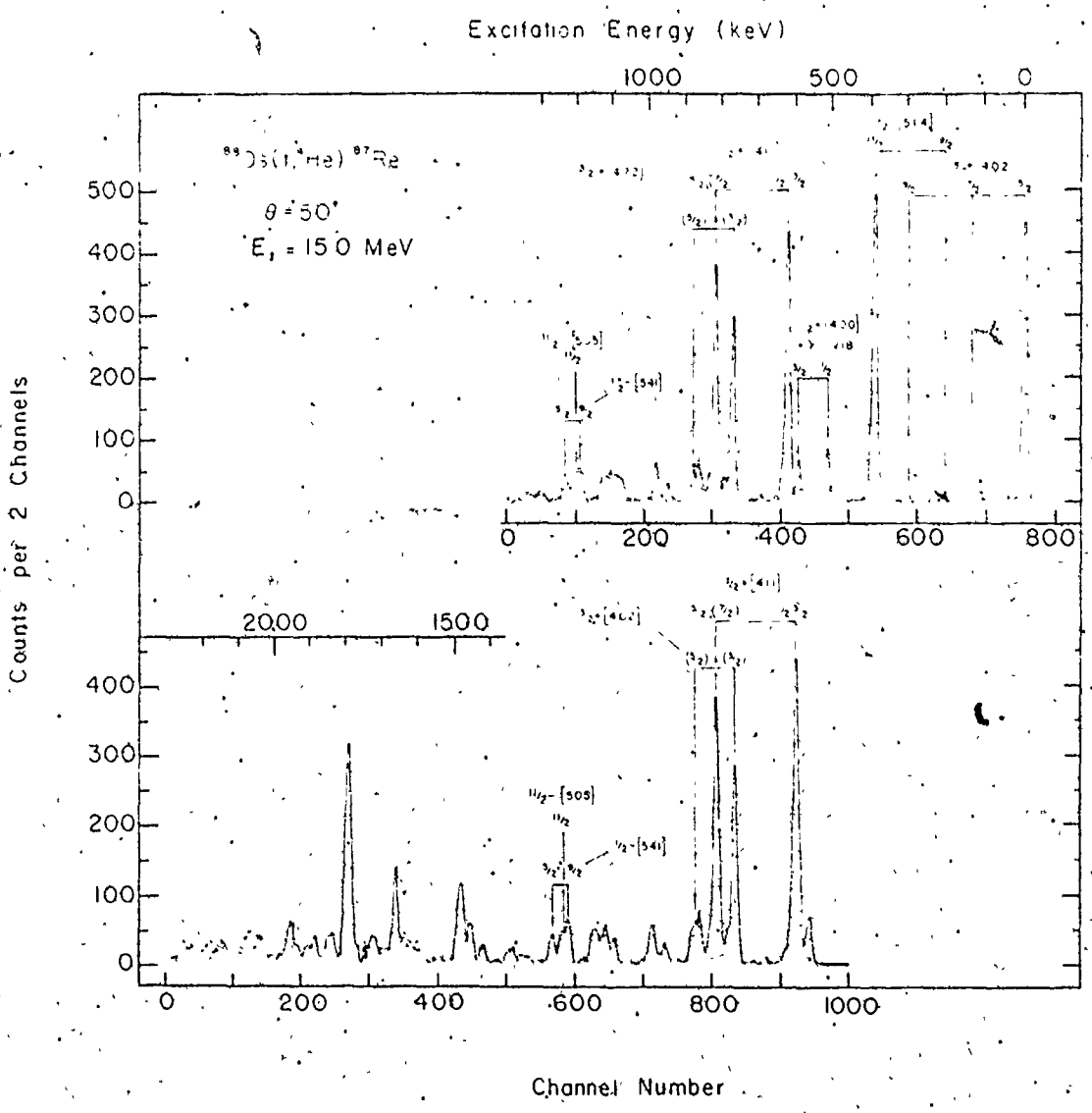

Figure 8. The (t,α) spectra for ^{187}Re at a reaction angle of 50°. The upper spectrum is the ground state bite; the lower one includes higher excitations. Note that, because the exposures were not of the same length, the vertical axes have different scales. Observed levels assigned by Lu and Alford (1971) have been indicated.

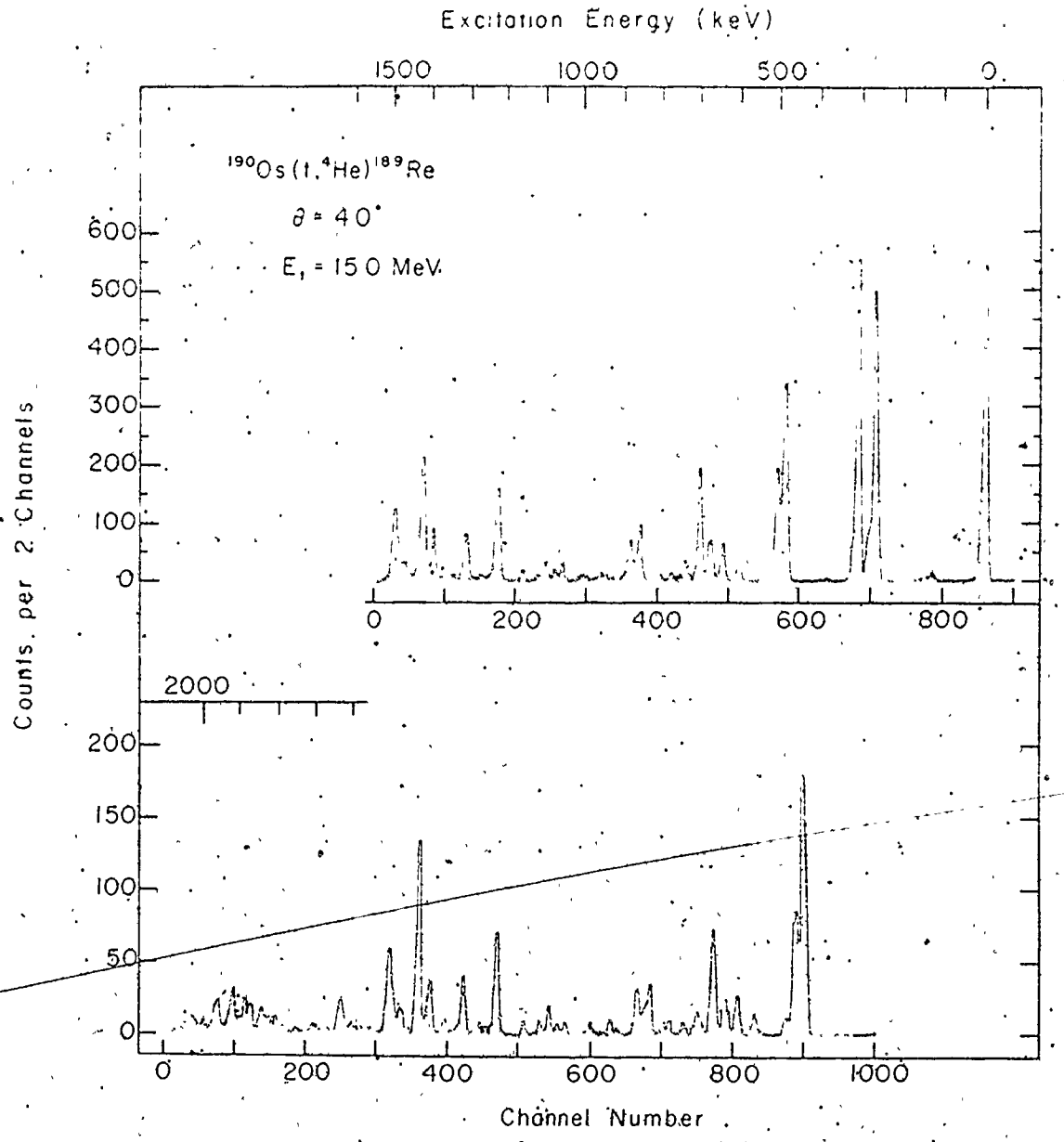

Figure 9. The (t,^{4}He) spectra for ^{189}Re at a reaction angle of 40°. See caption to fig. 8.

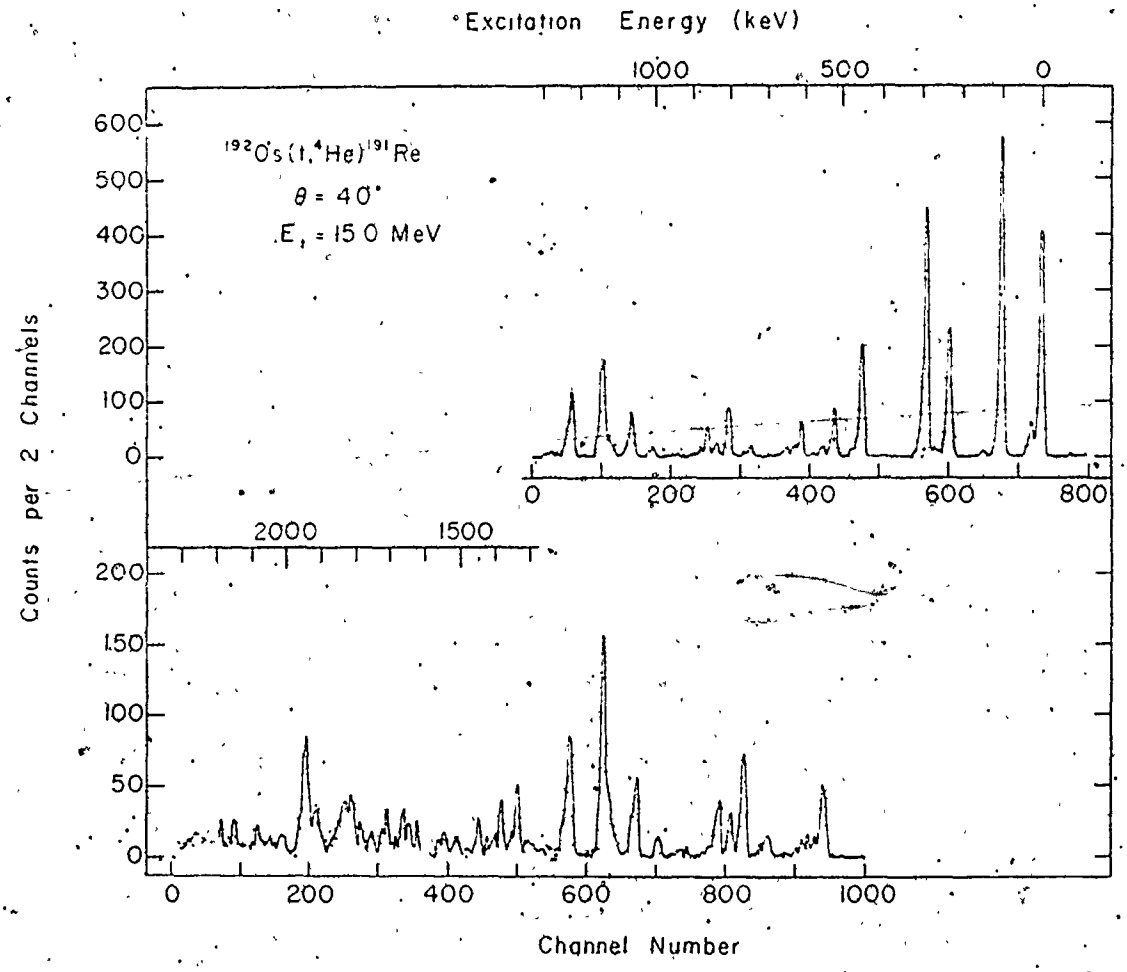

Figure 10. The (t,α) spectra for ^{191}Re at a reaction angle of 40°. See caption to fig. 8.

given in Tables 1, 2 and 3. In Table 1, energies of levels in ^{187}Re found by other researchers (Ellis 1974) are given for comparison with the present results. The assignments indicated are those made in other studies. In Table 2, energies for ^{189}Re are given from the 1971 study using the Elbek-type spectrograph, and energies and cross sections are given from the 1975 study using the Q3D spectrometer. The average energies obtained for ^{191}Re are given in Table 3. In each case the (t,α) cross sections given correspond to the spectra shown in Figs. 8, 9 and 10. In all cases, the energies at different angles have been checked for systematic shifts which would indicate that the associated peaks were due to impurities in the targets; none of significance were found. The estimated errors given in the tables are based upon observed variations about the mean values and, where possible, upon comparison with γ-decay data.

Ground-state Q-values have been calculated for each of the three reactions studied, and are given in Table 4. These results have essentially utilized the precisely known ^{166}Er(t,α)^{165}Ho Q-value as a standard as described in section 3.5. The errors in the Q-values in Table 4 are estimated from the variations in the values making up the average presented for each isotope. Previous values and their errors are from the 1971 Atomic Mass Evaluation (Gove and Wapstra 1972). The previous value for ^{188}Os(t,α) is accurately known, and the present value is in good agreement with it. For ^{190}Os(t,α) the error for the previous value is larger than that for the present, but again the agreement is good. Finally, the previous Q-value for ^{192}Os(t,α) was estimated from systematics, and therefore may be in error by several hundred keV.

Table 1

Energies and (t,α) Cross Sections for Levels in ^{187}Re (E_t=15 MeV)

Excitation Energy (keV) Previous Work	Present[a]	Assignment[b]	$\frac{d\sigma}{d\Omega}(50^\circ)$ (μb/sr)
0	0	5/2 5/2$^+$[402]	137
134	133	7/2 5/2$^+$[402]	1.9
206	207	9/2 9/2$^-$[514]	4.2
301	303	9/2 5/2$^+$[402]	1.7
390	389	11/2 9/2$^-$[514]	138
512	514	1/2{1/2$^+$[400] + 5/2$^+$[402],2$^+$}	25
589	591	3/2{1/2$^+$[400] + 5/2$^+$[402],2$^+$}	19
618	621	1/2,3/2 1/2$^+$[411])	130
773	771	(3/2 3/2$^+$[402]	83
817	817	5/2, 7/2 1/2$^+$[411]	99
865	864	3/2{3/2$^+$[411] + 1/2$^+$[411],2$^+$}	17
880	878	(5/2 3/2$^+$[402]	11.5
	948		8.8
	979		19
1187	1189		14.9
1200	1200	(9/2 1/2$^-$[541])	8.3
1208	1211	(11/2 11/2$^-$[505])	8.5
1233	1232	(5/2 1/2$^-$[541])	10.8
	1458		19
1488	1484		38
	1661		37
1789	1790		100

a) Energies up to 1400 keV are believed accurate to ± 3 keV and those above 1400 keV to ≈ ± 6 keV.

b) From Lú and Alford (1971).

Table 2-

Energies and (t,α) Cross Sections for Levels in ^{189}Re (E_t=15 MeV)

Excitation Energy (keV) 1971 data	1975 data[a]	$\frac{d\sigma}{d\Omega}$ (40°) (μb/sr)
0	0	153
	125	4.3
134	{	
	146	2.1
259	260	135
277	279	17
304	303	146
483	481	105
500	501	50
598	599	9.9
640	640	18
668	670	20
696	697	47
847	852	28
876	877	19
1096	1097	9.3
1224	1223	50
1308	1308	25
1393	1396	22
1422	1423	67
	1502	31
1624	1632	11.6
1917	1916	19
(1951)	1959	11.2

[a] Errors on energies up to 1500 keV are estimated to be ± 3 keV. Above 1500 keV, they may be ± 10 keV.

Table 3

Energies and (t,α) Cross Sections for Levels in ^{191}Pe (E_t=15 MeV)

Excitation Energy (keV)[a]	dσ/dΩ (40°) (μb/sr)
0	134
27	20
97	174
145	3.6
227	79
254	1.7
264	4.6
285	137
299	11.7
449	66
521	27
550	3.7
555	3.2
606	17
622	2.5
627	5.0
741	6.4
758	2.1
799	30
832	8.5
858	15.5
876	3.9
1004	4.9
1015	2.0
1064	27
1112	7.1
1128	12.5
1145	64
1229	37
1243	12.7
1367	21
1408	13.6
1468	9.8
1524	6.2
1560	8.2
1663	16
1715	12.8
1835	22
1904	18
1937	43

a) Errors on energies up to 1300 keV are estimated to be ± 3 keV. Above 1300 keV, ± 6 keV.

Table 4

Ground State Q-values

Reaction	Present value (MeV)	Mass table value (MeV)[a]
$^{188}Os(t,\alpha)^{187}Re$	12.604 ± 0.010	12.6055 ± 0.0012
$^{190}Os(t,\alpha)^{189}Re$	11.796 ± 0.010	11.794 ± 0.020
$^{192}Os(t,\alpha)^{191}Re$	10.993 ± 0.010	11.140[b]

a) Gove, N. B. and Wapstra, A. H., 1972. Nucl. Data Tables 11, 259-261

b) Value estimated from systematics, error may be several hundred keV.

The present value is 150 keV lower, and much more precise.

On the basis of relative (t,α) cross sections, systematic energy trends in the odd-A rhenium isotopes and the results of an early γ-decay study (Kuaranen and Ihochi 1965), it was possible to suggest some assignments in ^{189}Re (Hirning and Burke 1976). Three alternative level schemes were also suggested for low-lying levels in ^{191}Re. Because the later $(\vec{t},\alpha)$ data provided much more direct evidence for level assignments, the arguments leading to the earlier conclusions will not be presented here. Let it suffice to say that most of the conclusions of the 1975 study were substantiated by the results obtained in 1976.

4.2 Polarized (t,α) results.

Data were obtained with a polarized triton beam for reaction angles from 15° to 50° in 5° steps for all three rhenium isotopes, and also at 60° for ^{187}Re. The lower limit on the angular range results from the inability of the particle identification system to function well with the very high particle flux incident on the detector at forward angles. For $\theta < 15^{\circ}$, high background and poor resolution resulted in an alpha particle spectrum that was not usable. The problem could have been corrected by greatly reducing the beam current, but the time required for each run would then have been much longer, and it would not have been possible to obtain data at as many angles in the limited period available. The upper limit on the range of angles was chosen because there is little structure in the angular distributions at larger angles, and the cross sections decrease rapidly. At each angle a spectrum was acquired with the triton spin polarized down, then

with it polarized up. The beam polarization was measured before and after each run, and was found to be the same to within $\sim$ 1% in all cases. The spectra obtained at $\theta = 50^{\circ}$ are shown in Figs. 11, 12 and 13; the resolution is $\sim$ 20 keV (FWHM), and is typical of that achieved at all angles. These data were originally collected in a 2048 channel spectrum; they have been compressed to a 1024 channel spectrum by summing adjacent channels and also smoothed in the manner described in the last section. This procedure did not result in any apparent loss of information.

Analyzing powers and unpolarized cross sections were extracted from the data using two computer programs written for the purpose. The first program, called MANIP, read two of the original spectra from magnetic tape; these were specified to be a spin up and spin down spectrum at the same angle. These spectra were then bunched (reduced to 1024 channels), smoothed and summed together to produce a third spectrum. The resulting three spectra were printed and plotted. Using primarily the summed spectrum (which approximately corresponded to an unpolarized (t,α) spectrum) gate regions were set by inspection on those peaks which were well resolved or strongly populated. The gate limits and smoothed spectra, along with the information needed for cross section normalization, were then given as input to a second computer program, called POLAR. This program calculated the cross sections of the gated regions for each spin orientation using Eqs. (60) and (61). From this information, the analyzing powers and unpolarized cross sections were calculated, along with their statistical errors, using the equations given below.

The expression for the analyzing power may easily be found from

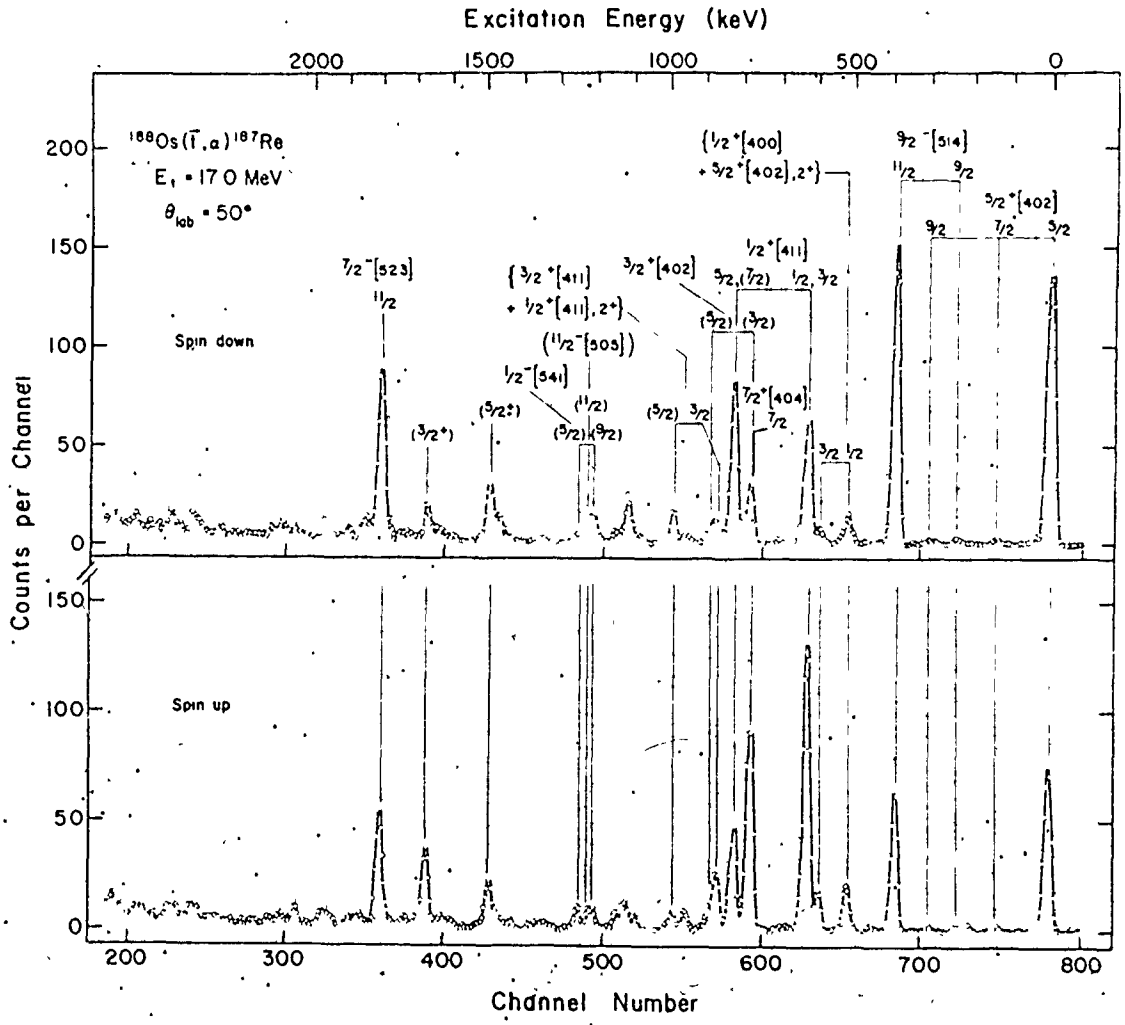

Figure 11. The $(\vec{t},\alpha)$ spectra for ^{187}Re at a reaction angle of 50°.

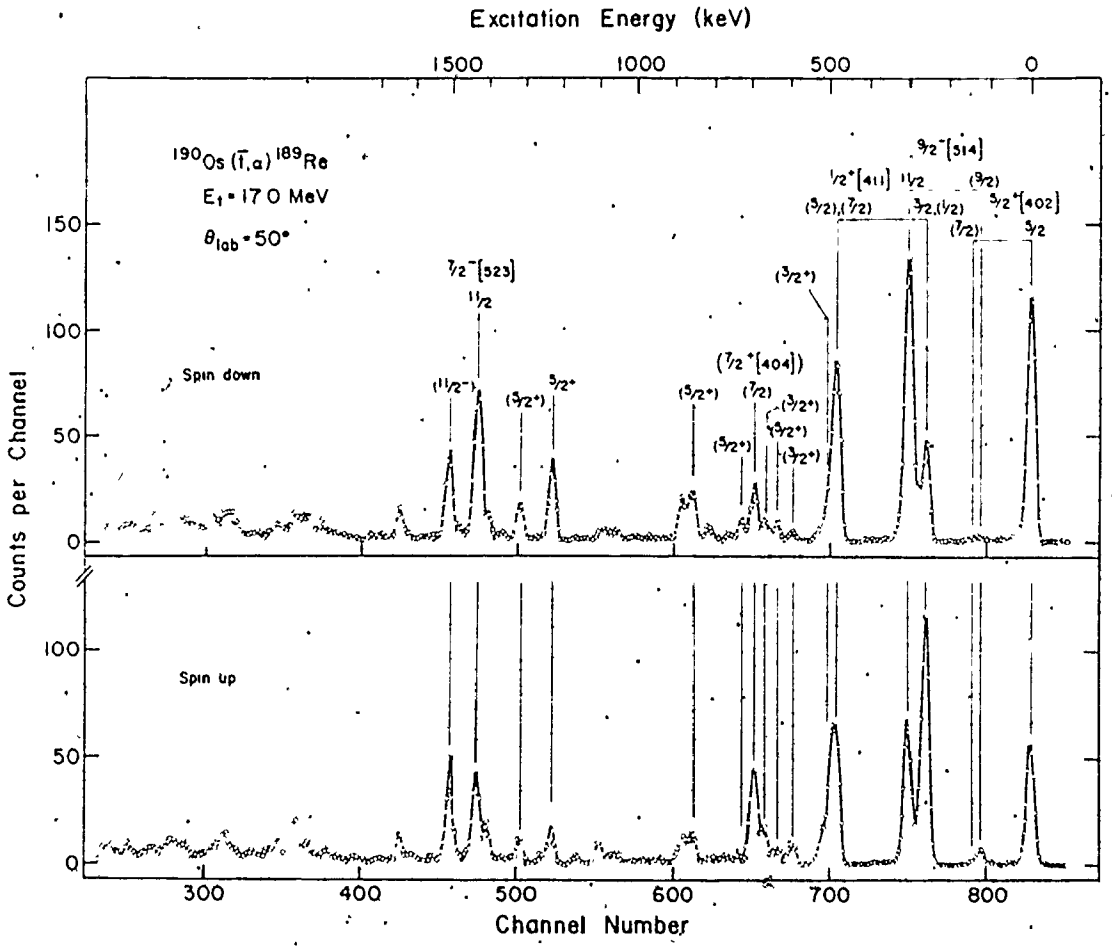

Figure 12. The ($\vec{t}$,α) spectra for ^{189}Re at a reaction angle of 50°.

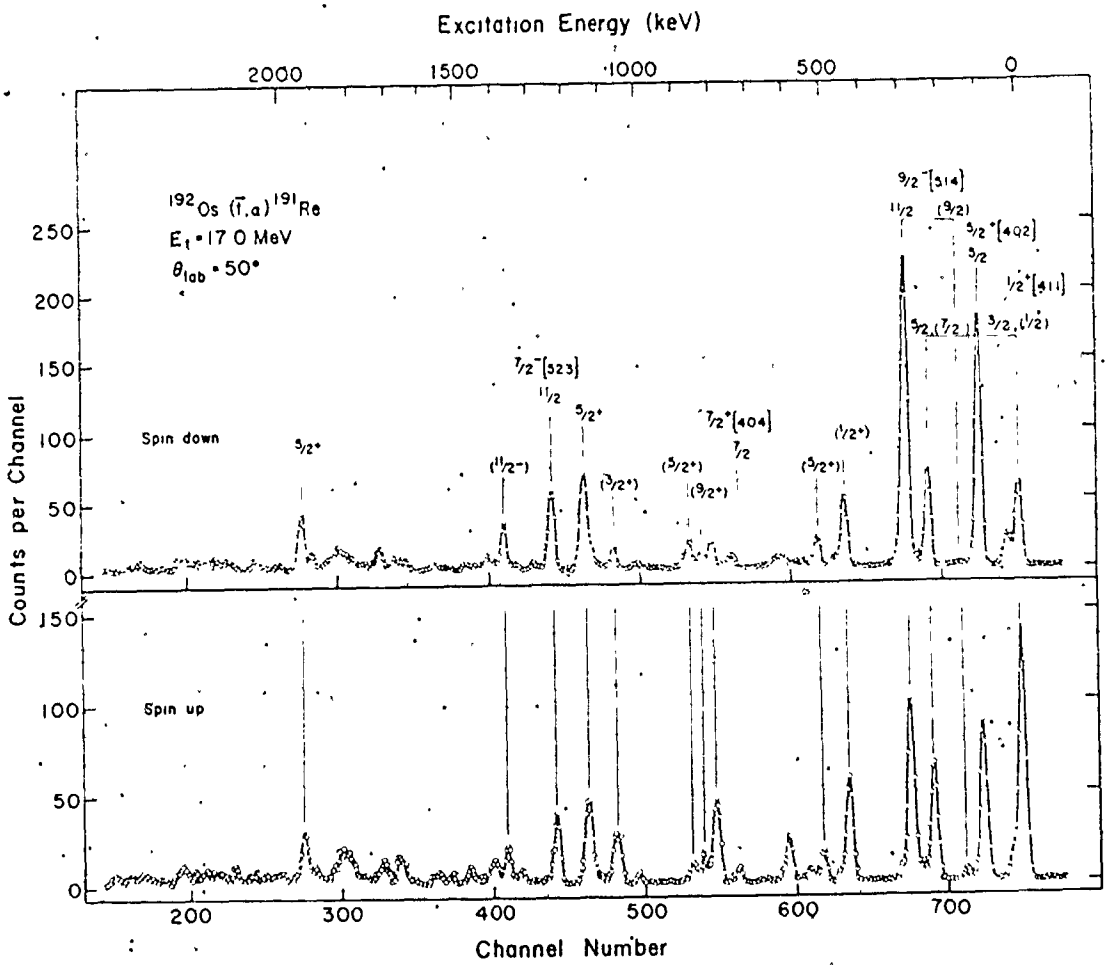

Figure 13. The (t,α) spectra for ^{191}Re at a reaction angle of 50°.

Eq. (59a) to be

$$A_y = \frac{\left(\frac{d\sigma}{d\Omega}\right)_+ - \left(\frac{d\sigma}{d\Omega}\right)_-}{P_-\left(\frac{d\sigma}{d\Omega}\right)_+ + P_+\left(\frac{d\sigma}{d\Omega}\right)_-} , \tag{62}$$

where the dependence on θ has been left out for simplicity. The convention is for particle detection to the left of the incident beam. Since in the LASL Q3D spectrometer particles are detected to the right of the incident beam, the sign of A_y as given by Eq. (62) is reversed. Assuming normalization factors and absolute polarization to be the same for both spin orientations, the error in the analyzing power is approximately

$$\Delta A_y = \frac{1}{\bar{P}}\left[\frac{1 - \varepsilon^2}{N_+ + N_-}\right]^{1/2} , \tag{63}$$

where

$$\bar{P} = \frac{1}{2}(P_+ + P_-)$$

is the average polarization, and

$$\varepsilon = \frac{N_+ - N_-}{N_+ + N_-}$$

is an asymmetry parameter. The N's are simply the original numbers of counts in the peaks. The unpolarized cross section is given by

$$\left(\frac{d\sigma}{d\Omega}\right)_0 = \frac{P_+\left(\frac{d\sigma}{d\Omega}\right)_- + P_-\left(\frac{d\sigma}{d\Omega}\right)_+}{P_+ + P_-} , \tag{64}$$

and the associated error is

$$\Delta\left(\frac{d\sigma}{d\Omega}\right)_0 = \frac{1}{2}\left[\left(\Delta\frac{d\sigma}{d\Omega}\right)_+^2 + \left(\Delta\frac{d\sigma}{d\Omega}\right)_-^2\right]^{1/2} \qquad (65)$$

The errors in the polarized cross sections are given by the usual $\sqrt{N}$ rule for Poisson statistics.

Angular distributions of analyzing powers and unpolarized cross sections are shown in Figs. 14, 15 and 16. The errors in cross sections indicated in these figures are either from Eq. (65) or 10%, whichever is larger. The unpolarized cross sections at $\theta = 50^\circ$ are also given in Tables 5, 6 and 7.

4.3. DWBA analysis of $(\vec{t},\alpha)$ results.

The angular distributions of analyzing powers obtained for levels of known spin and parity in ^{187}Re show a definite dependence of shape and magnitude on the transferred j- and ℓ- values. In particular, the results obtained for the known 5/2 $5/2^+[402]$, 11/2 $9/2^-[514]$, 3/2 $1/2^+[411]$ and $1/2\{1/2^+[400] + 5/2^+[402], 2^+\}$ levels provide characteristic (or "standard") shapes for the four values of I^π represented. The shapes of the distributions of unpolarized cross sections are less distinctive, but there are some significant differences; these will be discussed below. Since the analyzing powers and unpolarized cross sections are also dependent on the Q-value of the reaction, it is reasonable to compare the distributions of unassigned levels with those of known states

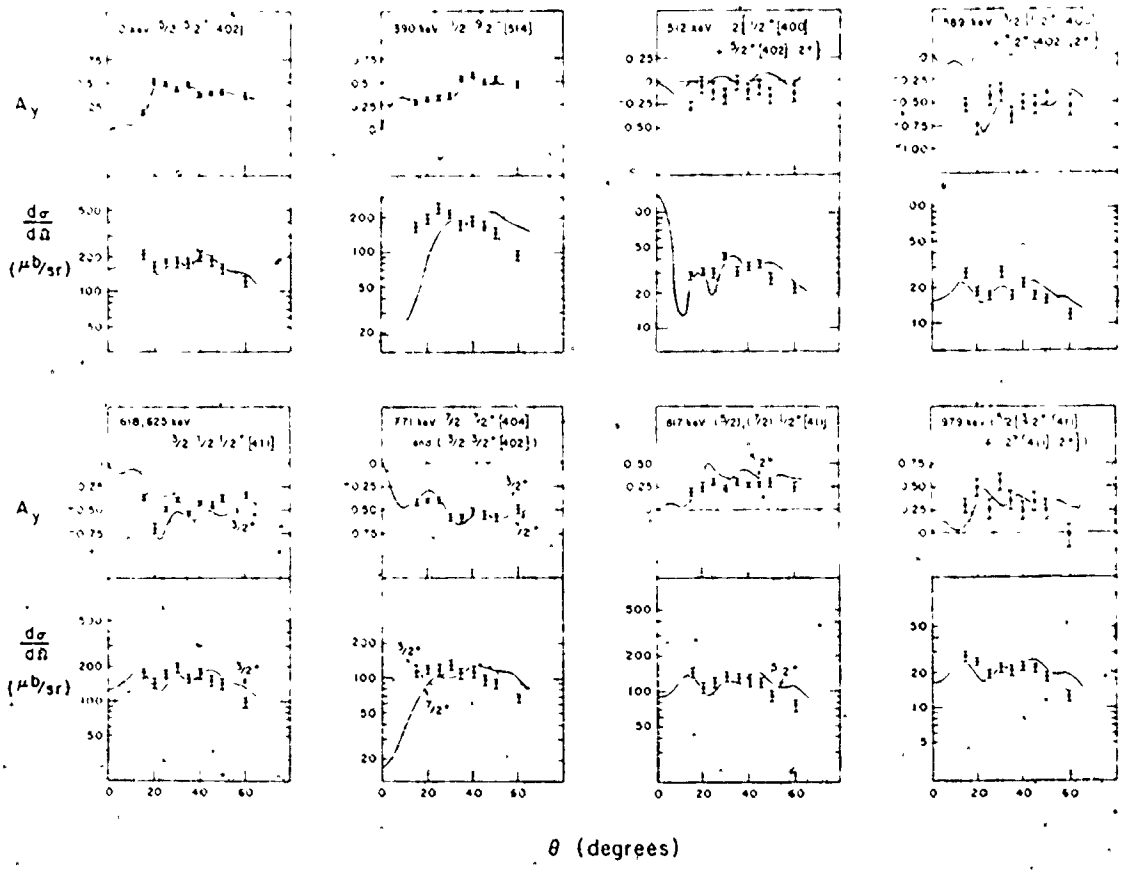

Figure 14(a). Angular distributions of analyzing powers and unpolarized cross sections for levels in ^{187}Re. The curves are from DWBA calculations.

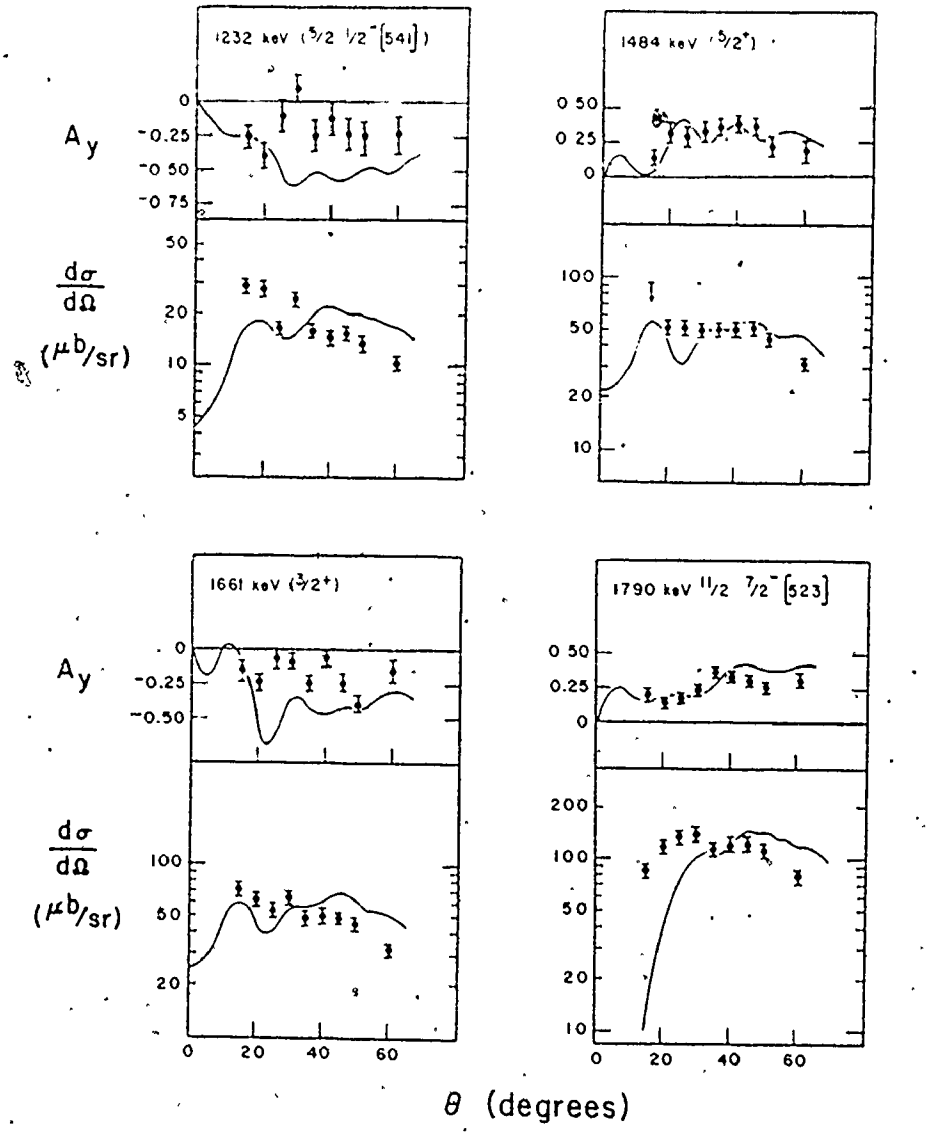

Figure 14(b). ^{187}Re cont'd. See caption to fig. 14(a).

Table 5

Levels in ^{187}Re Populated by the $(\vec{t},\alpha)$ Reaction (E_t=17 MeV)

Energy (keV)	I^π	Interpretation	$\frac{d\sigma}{d\Omega}_{unpol}(50^\circ)$ $\frac{\mu b}{sr}$ Expt.	Theory	Nuclear Structure Factor Expt.	Theory.
0	$5/2^+$	$5/2\ 5/2^+[402]$	158 ± 16	164	0.56	0.57
134	$7/2^+$	$7/2\ 5/2^+[402]$	4.0 ± 0.7	3.1	0.04	0.03
206	$9/2^-$	$9/2\ 9/2^-[514]$	2.7 ± 0.6	0.5	0.03	0.005
301	$9/2^+$	$9/2\ 5/2^+[402]$	2.9 ± 0.6	1.1	0.02	0.01
390	$11/2^-$	$11/2\ 9/2^-[514]$	148 ± 15	147	1.28	1.27
512	$1/2^+$	$1/2\{1/2^+[400]+5/2^+[402],2^+\}$	27 ± 3		0.06	
589	$3/2^+$	$3/2\{1/2^+[400]+5/2^+[402],2^+\}$	16 ± 2		0.06	
618	$3/2^+$	$3/2\ 1/2^+[411]$	144 ± 14	166		0.61
625	$1/2^+$	$1/2\ 1/2^+[411]$		55		0.12
771	$7/2^+$	$7/2\ 7/2^+[404]$	92 ± 9	89		1.00
	$(3/2^+)$	$(3/2\ 3/2^+[402])$		4.6		0.02
817	$5/2^+$	$5/2\ 1/2^+[411]$	93 ± 9	34		0.11
	$(7/2^+)$	$(7/2\ 1/2^+[411])$		8.6		0.10

continued...

Table 5 (continued)

Levels in ^{187}Re Populated by the $(\vec{t},\alpha)$ Reaction (E_t=17 MeV)

Energy (keV)	I^{π}	Interpretation	$\frac{d\sigma}{d\Omega}_{unpol}(50^{\circ})$ $\frac{\mu b}{sr}$ Expt.	Theory	Nuclear Structure Factor Expt.	Theory
865	$3/2^+$	$3/2\{3/2^+[411]+1/2^+[411],2^+\}$				
880	$(5/2^+)$	$(5/2\ 3/2^+[402])$	40 ± 4	12		0.04
948	$(1/2^+, j=\ell-1/2)$		11 ± 2			
979	$(5/2^+)$	$(5/2\{3/2^+[411]+1/2^+[411],2^+\})$	18 ± 2		0.06	
1189						
1200	$(9/2^-)$	$(9/2\ 1/2^-[541])$	36 ± 3	2.5		0.03
1211	$(11/2^-)$	$(11/2\ 11/2^-[505])$				
1232	$(5/2^-)$	$(5/2\ 1/2^-[541])$	13 ± 2	1.8	0.04	0.006
1458	$j=\ell-1/2$		16 ± 2			
1484	$(5/2^+)$		38 ± 4		0.12	
1661	$(1/2^-,3/2^+,5/2^-)$	$(3/2^+)$	39 ± 4		0.14	
1790	$11/2^-$	$11/2\ 7/2^-[523]$	100 ± 10	106	1.14	1.21

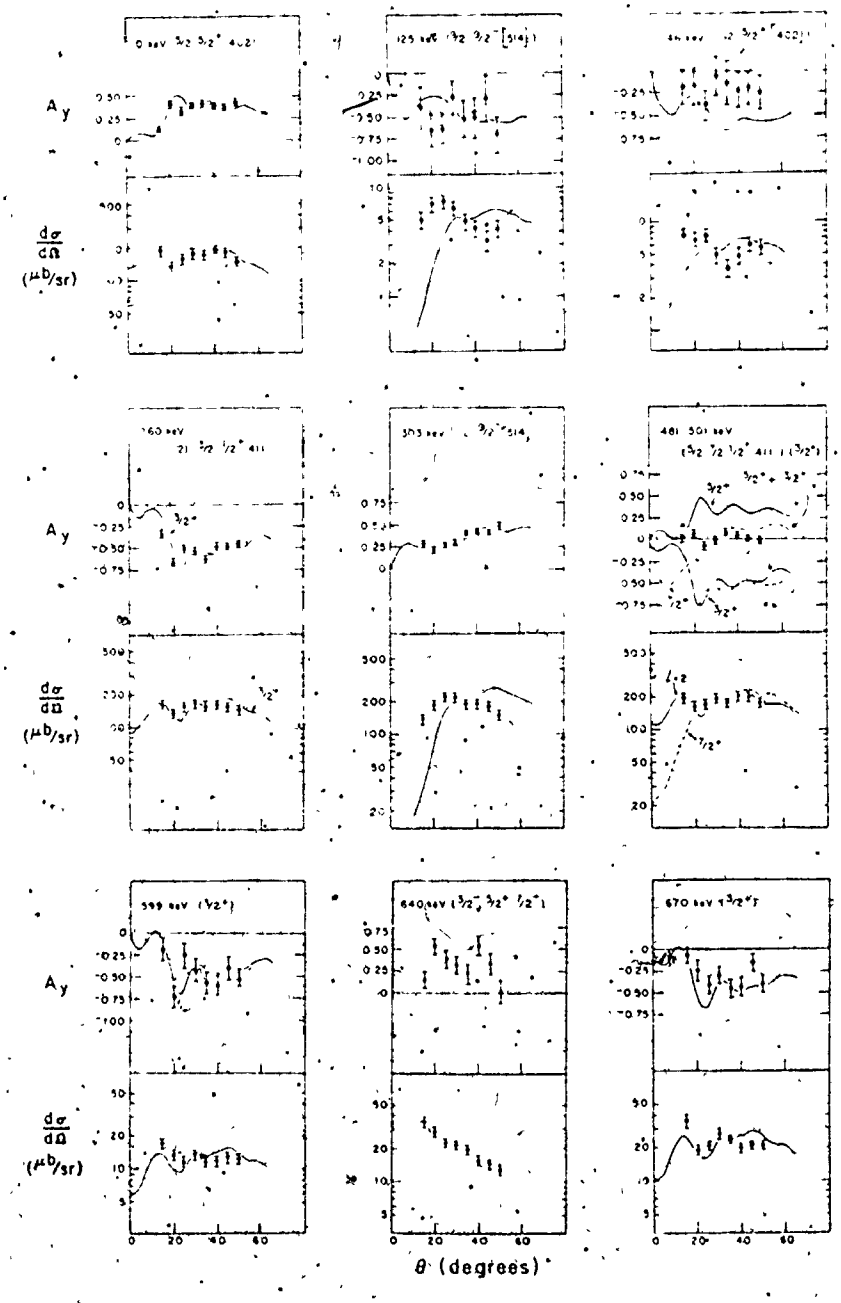

Figure 15(a). Angular distributions of analyzing powers and unpolarized cross sections for levels in ^{189}Re. The solid lines are from DWBA calculations. The line marked "$5/2^+ + 3/2^+$" for the 481-501 keV multiplet represents $A_y(5/2^+) + 0.5A_y(3/2^+)$.

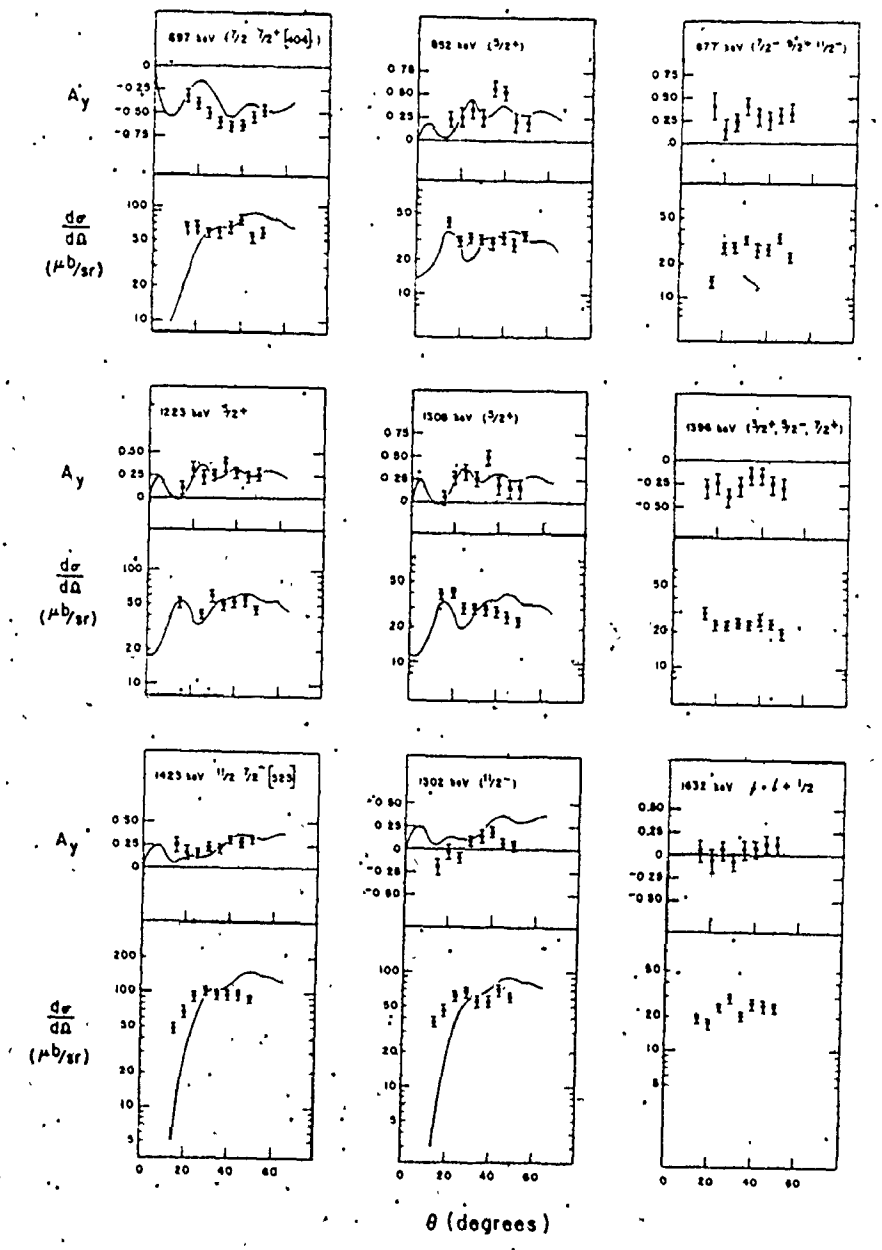

Figure 15(b). ^{189}Re cont'd. See caption to fig. 15(a).

Table 6

Levels in ^{189}Re Populated by the $(\vec{t},\alpha)$ Reaction (E_t=17 MeV)

Energy (keV)	I^{π}	Interpretation	$\frac{d\sigma}{d\Omega}_{unpol}(50^{\circ})\frac{\mu b}{sr}$ Expt.	Theory	Nuclear Structure Factor Expt.	Theory
0	$5/2^+$	5/2 5/2$^+$[402]	148 ± 15	170	0.49	0.56
125	$(7/2^+,9/2^-)$	(9/2 9/2$^-$[514])	4.7 ± 0.7	0.4	0.05	0.005
146	j=ℓ-1/2	(7/2 5/2$^+$[402])	5.9 ± 0.9	2.8	0.07	0.03
260	$3/2^+$	3/2 1/2$^+$[411]	145 ± 14	151		0.54
	$(1/2^+)$	(1/2 1/2$^+$[411])		56		0.12
279			151 ± 15			
303	$11/2^-$	11/2 9/2$^-$[514]		140	<1.48	1.38
481	$(5/2^+)$	(5/2 1/2$^+$[411])	174 ± 17	38		0.12
	$(7/2^+)$	(7/2 1/2$^+$[411])		7.2		0.08
501	j=ℓ-1/2	$(3/2^+)$				
599	$(3/2^+)$		13 ± 2		0.04	
640	$(3/2^-;5/2^+,7/2^-)$		13 ± 2			

continued...

Table 6 (continued)

Levels in ^{189}Re Populated by the $(\vec{t},\alpha)$ Reaction (E_t=17 MeV)

Energy (keV)	I^{π}	Interpretation	$\frac{d\sigma}{d\Omega}_{unpol}(50^{\circ})\frac{\mu b}{sr}$ Expt.	Theory	Nuclear Structure Factor Expt.	Theory.
670	$(3/2^+)$		21 ± 2		0.08	
697	$(7/2^+)$	$(7/2\ 7/2^+[404])$	59 ± 6	80	0.72	0.97
852	$(5/2^+)$		33 ± 3		0.11	
877	$(7/2^-,9/2^+,11/2^-)$		23 ± 2		0.26	
1223	$5/2^+$		45 ± 4		0.15	
1308	$(5/2^+)$		23 ± 2		0.08	
1396	$(1/2^-,3/2^+,5/2^-)$		19 ± 2			
1423	$11/2^-$	$11/2\ 7/2^-[523]$	86 ± 9	72	1.10	0.93
1502	$(7/2^-,9/2^+,11/2^-)$	$(11/2^-)$	62 ± 6		0.82	
1632			24 ± 2			

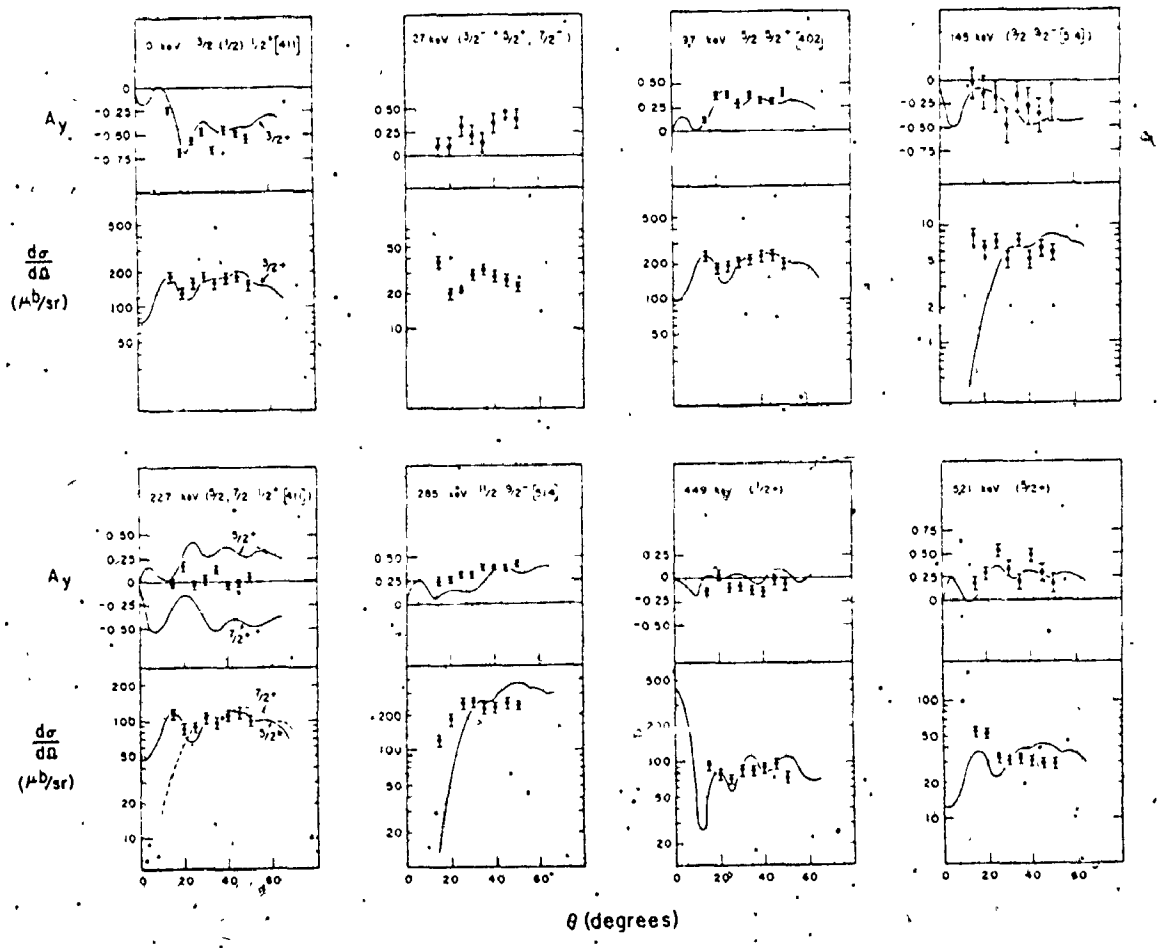

Figure 16(a). Angular distributions of analyzing powers and unpolarized cross sections for levels in ^{191}Re. The curves are from DWBA calculations.

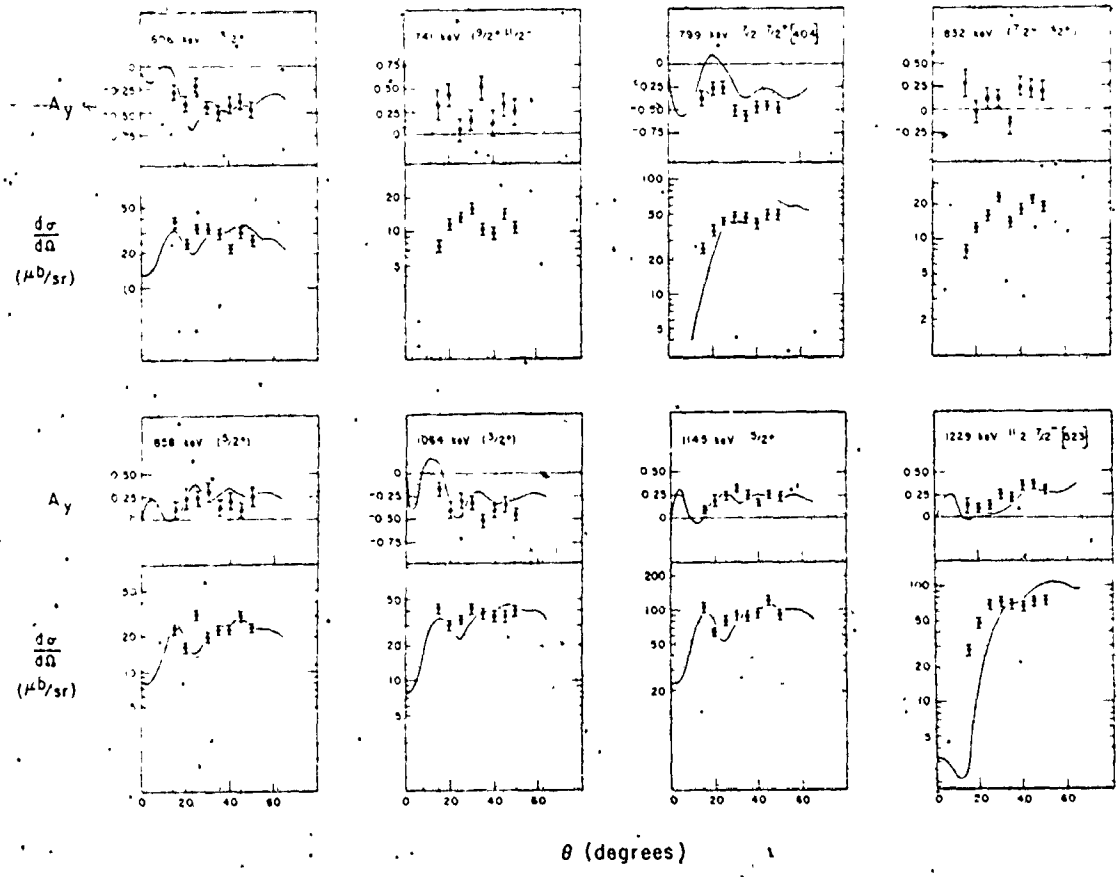

Figure 16(b). [191]Re cont'd. See caption to fig. 16(a).

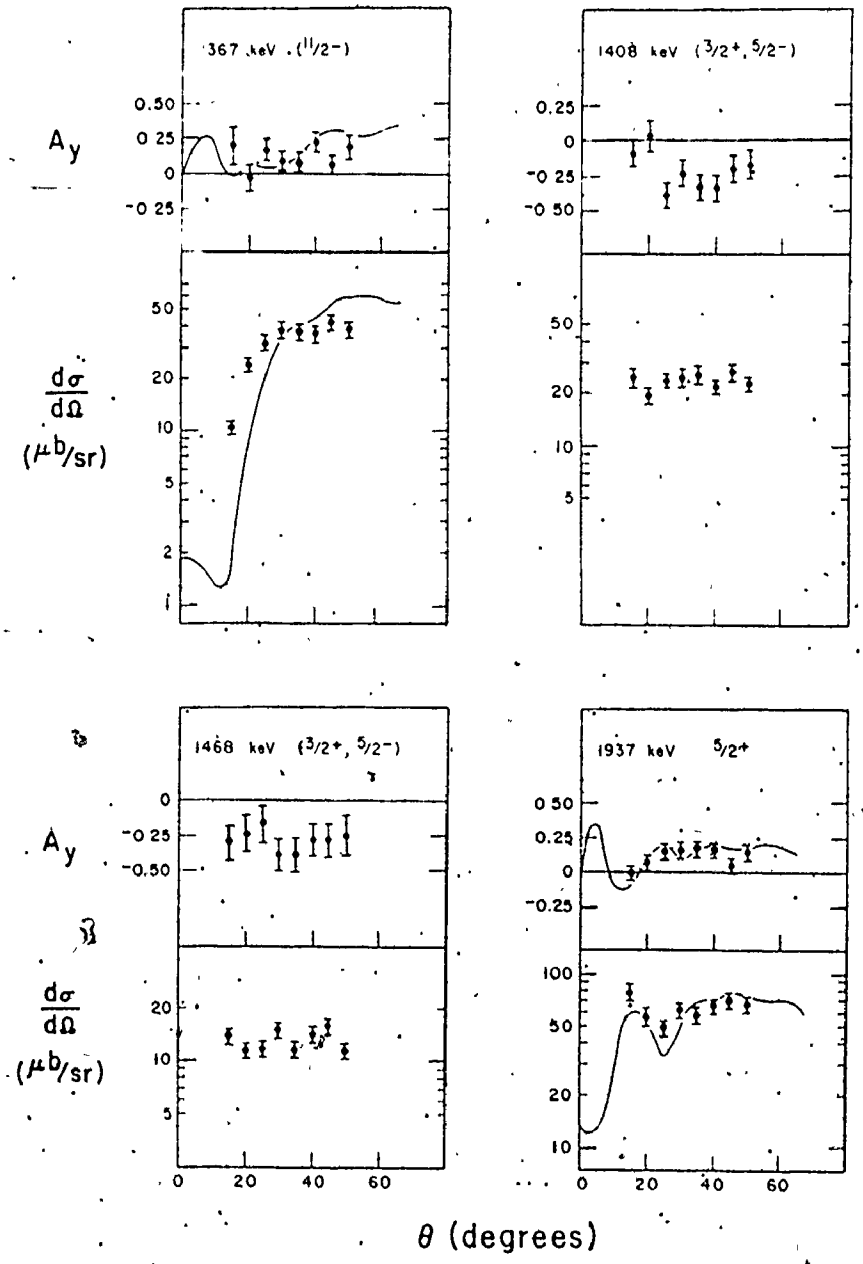

Figure 16(c). [191]Re cont'd. See caption to fig. 16(a).

Table 7

Levels in ^{191}Re Populated by the $(\vec{t},\alpha)$ Reaction (E_t=17 MeV)

Energy (keV)	I^π	Interpretation	$\frac{d\sigma}{d\Omega}_{unpol}(50^\circ)\frac{\mu b}{sr}$ Expt.	Theory	Nuclear Structure Factor Expt.	Theory
0	$3/2^+$	$3/2\ 1/2^+[411]$	156 ± 16	114		0.41
	$(1/2^+)$	$1/2\ 1/2^+[411]$		48		0.09
27	$(3/2^-,5/2^+,7/2^-)$		23 ± 2			
97	$5/2^+$	$5/2\ 5/2^+[402]$	200 ± 20	228	0.65	0.74
145	$(9/2^-)$	$(9/2\ 9/2^-[514])$	5.8 ± 0.9	0.3	0.09	0.005
227	$(7/2^+)$	$(7/2\ 1/2^+[411])$	100 ± 10	3.7		0.05
	$(5/2^+)$	$5/2\ 1/2^+[411]$		22		0.07
285	$11/2^-$	$11/2\ 9/2^-[514]$	234 ± 24	139	2.73	1.64
449	$(1/2^+)$		74 ± 7		0.13	
521	$(5/2^+)$		29 ± 3		0.10	
606	$(1/2^-,3/2^+,5/2^-)$	$(3/2^+)$	26 ± 3		0.09	
741	$(7/2^-,9/2^+,11/2^-)$		11 ± 2			

continued...

Table 7 (continued)

Levels in ^{191}Re Populated by the $(\vec{t},\alpha)$ Reaction (E_t=17 MeV)

Energy (keV)	I^π	Interpretation	$\frac{d\sigma}{d\Omega}_{unpol}(50^\circ)\frac{\mu b}{sr}$ Expt.	Theory	Nuclear Structure Factor Expt.	Theory
799	$7/2^+$	$7/2\ 7/2^+[404]$	49 ± 5	70	0.70	1.00
832	$(9/2^+)$		19 ± 2			
858	$(3/2^-,5/2^+)$	$(5/2^+)$	24 ± 2		0.08	
1064	$(3/2^+)$		40 ± 4		0.15	
1145	$5/2^+$		92 ± 9		0.32	
1229	$11/2^-$	$11/2\ 7/2^-[523]$	75 ± 7	63	1.17	0.97
1367	$(7/2^-,9/2^+,11/2^-)$	$(11/2^-)$	38 ± 4		0.61	
1408	$(3/2^+,5/2^-)$		23 ± 2			
1468	$(3/2^+,5/2^-)$		11 ± 2			
1937	$5/2^+$		57 ± 6		0.23	

only when their Q-values are similar. In order to assign I^{π} values to levels having Q-values considerably different from those of the standards, some method of taking into account the Q dependence of the distributions must therefore be used. In the present work, it has been assumed that the Q dependence could be adequately reproduced by DWBA calculations.

First, it was necessary to find a set of DWBA parameters which could reproduce the experimental results for known levels. Several sets of optical model parameters obtained from elastic scattering experiments were available in the literature. Parameters potentially suitable for the present reaction were given by Flynn et al. (1969) and Hardekopf et al. (1975) for tritons, and by McFadden and Satchler (1966) for alpha particles. Using the computer program DWUCK4 (Kunz 1974), DWBA calculations were done for all possible combinations of these parameters. The predictions of the calculations were compared to the experimental results for the four known levels listed above. The best overall agreement was achieved using the parameters given in Table 8; the triton parameters are from Flynn et al. (1969), except for the depth of the spin orbit potential, which was suggested by Hardekopf et al. (1975), and the alpha parameter set is one of the four given by McFadden and Satchler (1966). It was found that the results of the calculation were fairly insensitive to the choice of the alpha parameter set; this is in contrast to the findings of Flynn et al. (1976). The zero-range approximation was made, but a non-local correction (see Eq. (54)) was included, with non-local parameters 0.25 for the incident triton, 0.20 for the emergent alpha particle and 0.85 for the transferred proton (Kunz 1974).

Table 8

Optical Model Parameters used in DWBA Analysis

	t	α	p
V_R	-181.2	-249.5	a)
r_{or}	1.16	1.236	1.25
a_r	0.752	0.592	0.65
V_I	-11.4	-27.5	
r_{oi}	1.498	1.236	
a_i	0.817	0.592	
V_{so}	-24.0		
r_{so}	1.16		
a_{so}	0.752		
r_{oc}	1.25	1.30	1.25
PNLOC	0.25	0.20	0.85
VSOR[b)]			8.0

a) Varied to reproduce the proton binding energy.

b) Thomas spin-orbit factor

In an earlier proton transfer experiment (Lu and Alford 1971) it was found that better agreement was obtained between theoretical and experimental (^{3}He,d) angular distributions if a lower cutoff of 0.6 fm were used in the radial integral (Eq. (52)). In the present case, several values for the lower cutoff were tried, and the best agreement was obtained with no lower cutoff.

The results of the DWBA calculations are shown as solid lines in Fig. 14. Agreement between theoretical and experimental analyzing powers is very good for the $5/2^+$, $11/2^-$ and $3/2^+$ standards. The agreement is not as good for $1/2^+$, but the DWBA calculation does correctly predict small magnitudes for the analyzing power at all angles.

It was mentioned in Chapter I that the cross section angular distributions for the (t,α) reaction have not shown much variation from one ℓ-value to another. Figure 17 shows the distributions predicted by DWBA for ℓ=0 to 5 for the ^{188}Os(t,α) reaction at Q=12.0 MeV. The shapes are not very distinctive for reaction angles $\theta \geq 15^\circ$. It would evidently have been useful to obtain data at smaller angles, but this was not possible for the reason given in the last section. For $\theta \geq 15^\circ$, then, the ℓ=0, 1 and 2 distributions are seen to have very similar shapes, as do those for ℓ=4 and 5. There is, however, some difference between the two groups: the high-ℓ transfers exhibit a forward minimum while the low-ℓ transfers do not. The shape of the ℓ=3 distribution is intermediate between ℓ =2 and ℓ=4. The theoretical angular distributions for ℓ=0 and 2 agree quite well with experiment; that for ℓ=5 does not agree very well. The forward minimum for the high-ℓ transfer is experimentally found to be less deep than predicted. The difference in shape between

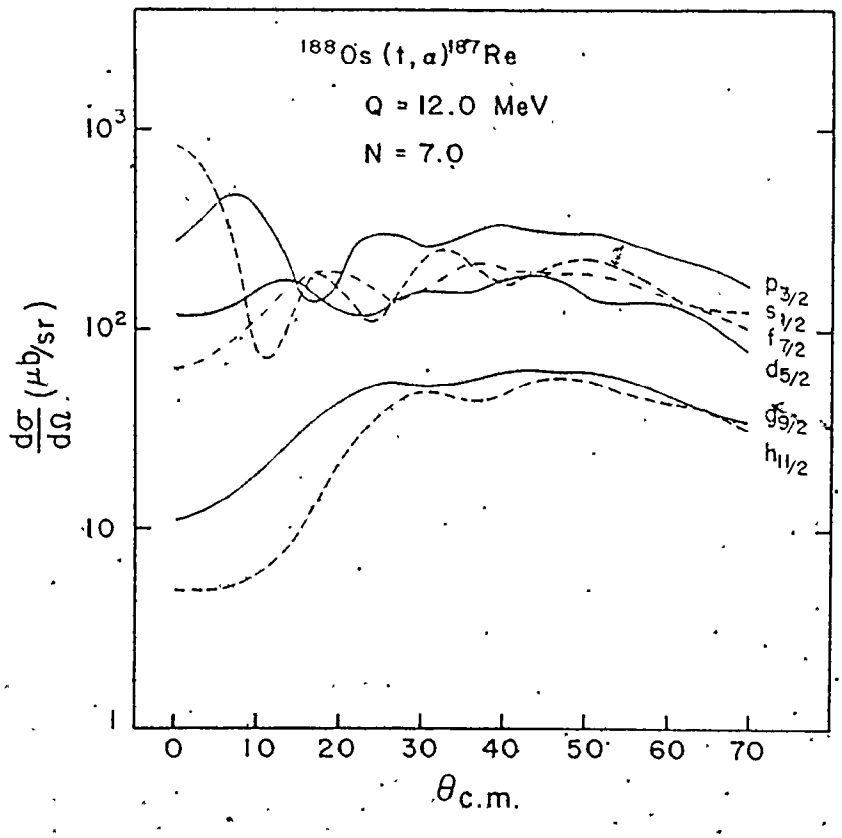

Figure 17. Unpolarized cross section angular distributions predicted by DWBA calculations for the ^{188}Os(t,α)^{187}Re reaction for 0-7.6.

high- and low-ℓ transfers is therefore somewhat smaller than one might expect from the DWBA calculations. Nonetheless, it is sufficient to be observed experimentally for well-resolved levels.

The procedure for assigning j- and ℓ- values to levels in the three rhenium isotopes was as follows. For those levels which were well resolved and strongly populated, it was usually found that the analyzing power distribution matched only one of those given by DWBA at the appropriate Q-values; hence a unique I^{π} assignment was immediately possible. In less clear cases, the analyzing powers determined whether $j=\ell+1/2$ (A_y predominantly positive), $j=\ell-1/2$ (A_y predominantly negative) or $\ell=0$ ($A_y \sim 0$). As well, the shape of the cross section angular distribution often restricted the possible ℓ-values to either $\ell \leq 3$ (no significant forward minimum) or $\ell \geq 3$ (distinct forward minimum). Using this reasoning, the possible assignments for a given level could usually be limited to two or three alternatives. In some cases, where one of the possibilities looked much more probable than the others, a single tentative I^{π} value was assigned. Assignments made on the basis of angular distributions of analyzing powers and cross sections are given in column 2 of Tables 5-7; note that they are independent of any nuclear structure model.

CHAPTER V

INTERPRETATION OF RESULTS

For rhenium, with atomic number 75, neither the spherical shell model nor the Nilsson model predicts any low-lying proton hole states having ℓ=1 or 3 which would be strongly populated in a single particle transfer reaction. On the basis of this very general observation, it is sometimes possible to choose among several tentative assignments for a given level. For example, the spin and parity of a low-lying strongly populated level may be limited to $1/2^-$, $3/2^+$ or $5/2^-$ by its angular distributions. (Here, and henceforth, "angular distributions" refers to both analyzing powers and cross sections unless otherwise specified.) Since one does not expect to find any significant ℓ=1 or 3 strength at low energy, the $3/2^+$ assignment is the most probable of the three. Where this reasoning has been applied, the model-dependent choice is indicated as a tentative assignment in the third column of Tables 5,6 and 7.

5.1 Nilsson model calculations.

Previous studies of the light odd-A rhenium isotopes (e.g. Lu and Alford 1971) have indicated that most of the observed single particle states can be described quite well by the Nilsson model. In the present work, an effort has therefore been made to interpret levels in ^{189}Re and ^{191}Re also in terms of this model. Calculations have been performed using a slightly modified version of the computer program CREAT

(O'Neil 1971). First, using a routine due to Chi (1966), the Nilsson wavefunctions were calculated. Then, following the theory outlined in Chapter II, the effects of the pairing interaction and Coriolis band mixing were simulated. The resulting perturbed energies, nuclear structure factors and cross sections could then be compared with the experimental results.

The $C^K_{j\lambda}$ expansion coefficients of the Nilsson wavefunctions (Eq. (19)) were calculated assuming a simple quadrupole deformation. Values chosen for the deformation parameter were $\delta = 0.20$ for ^{187}Re, 0.18 for ^{189}Re and 0.16 for ^{191}Re; the choice is not very critical because the wavefunctions do not depend strongly on δ for deformations of this magnitude. The potential parameters $\kappa = 0.062$ and $\mu = 0.614$ were adopted from Nilsson et al. (1969).

For the pairing calculations, the diffuseness parameters, Δ, used for ^{188}Os and ^{190}Os were 0.85 and 0.95 MeV respectively, taken from Fig. 5 of Neergård and Vogel (1970). A value of 1.0 MeV was used for ^{192}Os. The Fermi energy, λ, was set at 100 keV above the orbital forming the final ground state in all three cases. This is a reasonable estimate based on systematics, and again results are not very sensitive to the value of this parameter (except for cross sections to the ground state band).

The spirit of the Coriolis coupling calculations was not to vary all the parameters possible in order to get the best fit. No fitting procedure was used. Only the unperturbed bandhead energies and rotational parameters were systematically varied in an attempt to reproduce the observed spectrum. All other parameters were fixed at "reasonable" values,

usually taken from the literature. All Coriolis matrix elements were attenuated by 0.75, a factor which has been found necessary in other studies (e.g. Cheung et al. 1974). Those states which were not assigned, but which were expected to be significant in the calculation, were given energies consistent with systematics in the rhenium isotopes, and with the Nilsson model.

It was discovered that in order to approximately reproduce the experimental cross sections for known levels in ^{187}Re, a normalization factor of N=7 was required (Eq. (48)). The theoretical value for this factor (Kunz 1974) is N=23. Other researchers have obtained better agreement between DWBA results and their data if larger normalization factors were used for the (t,α) reaction. A value of N=54 has been used for the ^{208}Pb(t,α)^{207}Tl reaction (Barnes et al. 1970) and N=34 was found to be suitable for the ^{210}Po(t,α)^{209}Bi reaction (Barnes et al. 1972). According to Eq. (55), the theoretical normalization factor for the (α,t) reaction is N=46. Again, researchers have found that much higher values are indicated experimentally; Price et al. (1971) used N=118 for the ^{190,192}Os(α,t)^{191,193}Ir reactions. Analysis of data for the ^{166}Er($\vec{t}$,α)^{165}Ho reaction (Løvhøiden et al. 1976), which were acquired at the same time as the Os($\vec{t}$,α)Re data, have similarly indicated a low value of N (N=10.6) is suitable if the same optical model parameters are used for the DWBA calculations. The differences between theory and experiment are not regarded as a serious problem since the value of N required for these reactions is strongly dependent upon the choice of optical model parameters, and the relative cross sections are the quantities which are most important.

Once the normalization factor was determined, the experimental nuclear structure factor could be calculated (see Eqs. (46) and (48)) for each case where a unique spin and parity were assigned. These are given in column 6 of Tables 5-7.

5.2 Levels in ^{187}Re.

Most of the level assignments for ^{187}Re indicated in Table 5 have been adopted from previous studies. The ^{188}Os$(\vec{t},\alpha)^{187}$Re reaction was regarded primarily as a test case for the reaction process. Nonetheless, several new assignments have been made, and it is of interest to see how well the experimental results compare with model predictions. The unpolarized cross sections and nuclear structure factors predicted by the model are compared with the experimental values in Table 5, and the level energies from the model calculations are compared with experimental energies in Table 9. The latter table also gives the rotational parameters and decoupling parameters used for each band. It may be seen that the energies correspond quite well, with the exception of the $1/2^-[541]$ band. The decoupling parameter predicted by the model for this band is not large enough to produce the inverted order of the $5/2^-$ and $9/2^-$ band members, which were tentatively assigned by Lu and Alford (1971). Because this band mixes very little with others included in the calculation, the possible discrepancy does not affect the results for other levels.

The first three members of the $5/2^+[402]$ ground state band are observed in ^{187}Re. No strong mixing is predicted for this band, and the theoretical and experimental nuclear structure factors are in good

Table 9

Comparison of experimental and model energies for ^{187}Re

Orbital	I^{π}	Experimental energy (keV)	Model		
			Energy (keV)	$\hbar^2/2I$ (keV)	a
$5/2^+[402]$	$5/2^+$	0	0	20	
	$7/2^+$	134	138		
	$9/2^+$	301	314		
$9/2^-[514]$	$9/2^-$	206	206	20.5	
	$11/2^-$	390	386		
$1/2^+[411]$	$1/2^+$	625	624	22	-1.03
	$3/2^+$	618	616		
	$5/2^+$	817	811		
	$(7/2^+)$		814		
$3/2^+[402]$	$(3/2^+)$	773	773	19	
	$(5/2^+)$	880	885		
$7/2^+[404]$	$7/2^+$	771	773	20	
$11/2^-[505]$	$(11/2^-)$	1211	1209	20	
$1/2^-[541]$	$(5/2^-)$	1232	1232	20	4.18
	$(9/2^-)$	1200	1385		
$7/2^-[523]$	$11/2^-$	1790	1792	20	
$1/2^+[400]$	$1/2^+$	*	901	20	0.42
$3/2^+[411]$	$3/2^+$	*	2500	20	
$5/2^-[523]$	$5/2^-$	*	2659	20	
$5/2^+[413]$	$5/2^+$	*	3001	20	
$3/2^-[541]$	$3/2^-$	*	3131	20	
$1/2^-[550]$	$1/2^-$	*	3250	20	-5.83

* Not experimentally assigned, but included in the calculation.

agreement. Several small peaks which do not correspond to any known levels in ^{187}Re are observed in the unpolarized (t,α) spectra in the region of the ground state band. The target had a 6.7% impurity of ^{189}Os, and the ground state Q value for ^{189}Os(t,α)^{188}Re (Gove and Wapstra 1972), is about 50 keV lower than that for ^{188}Os(t,α)^{187}Re. The first of the unidentified peaks occurs at an apparent excitation energy of 46 keV in ^{187}Re, so these are believed to be due to ^{188}Re.

Lu and Alford (1971) identified the $9/2^-[514]$ orbital as a low-lying hole state, and the present results are consistent with this description. The band is expected to mix strongly with other orbitals originating from the $h_{11/2}$ shell model state. With this mixing taken into account, the predicted strength of the $11/2^-$ member agrees very well with the experimental result. The $9/2^-$ member is too weakly populated to permit a valid comparison with the model prediction.

The $1/2^+[411]$ band is strongly decoupled, with the order of the $1/2^+$ and $3/2^+$ members inverted. Previous work indicates an energy separation of 7 keV between these members, which is less than the peak widths in the present experiments. They are therefore expected to form an unresolved doublet with the $3/2^+$ member dominant. A peak is observed at an energy between the adopted energies for these levels and its analyzing power is consistent with the DWBA prediction for $I^\pi = 3/2^+$. Its cross section, however, is only 65% of the sum of the predicted cross sections. The $5/2^+$ and $7/2^+$ members of the band are also expected to be inverted and unresolved, although the latter has not been previously assigned. Again, a peak is observed which could correspond to a doublet with a dominant $I^\pi = 5/2^+$ member, but its cross section is 2.2 times the

sum of the calculated cross sections. All but the $1/2^+$ member are predicted to mix strongly with members of the $3/2^+[402]$ band originating from the same $d_{3/2}$ shell model state. Although the total strength in the band is similar to that predicted, the distribution is different. It has not yet been possible to provide an explanation for this discrepancy.

It has been shown (Lu and Alford 1971) that the $3/2^+[402]$ orbital is a particle state lying well above the Fermi surface, so it is not expected to be strongly populated in a pickup reaction. Levels are observed within 2 keV of the two known members of this band, but the strength for the level at 771 keV is much too large to be due solely to the 3/2 $3/2^+[402]$ state. The Nilsson model predicts the $7/2^+[404]$ orbital to occur as a low-lying hole state in the Re isotopes, and the bandhead should be strongly populated by a proton pickup reaction. The 771 keV group has values of A_y which are in better agreement with a spin of $7/2^+$ than with $3/2^+$ so it has been interpreted as a doublet with the major contribution coming from the 7/2 $7/2^+[404]$ state. With this assignment, the total predicted cross section agrees well with that observed. The cross section angular distribution of the doublet does not decrease as rapidly at forward angles as would be expected for $I^\pi = 7/2^+$; this may be partly due to the $3/2^+$ component, but $7/2^+$ states assigned in ^{189}Re show similar distributions.

The $11/2^-[505]$ and $1/2^-[541]$ negative-parity particle orbitals were tentatively assigned by Lu and Alford (1971). These are only weakly populated in the present experiments, so a comparison with model predictions is not meaningful.

A second strongly populated $11/2^-$ state has been identified at 1790 keV, and is assigned to the $7/2^-[523]$ rotational band as this is the next Nilsson hole state originating from the $h_{11/2}$ shell. Since the theoretical angular distributions of cross sections for $\ell=5$ do not agree well with experiment, the very good agreement between theoretical and experimental strengths for both the 11/2 $9/2^-[514]$ and $11/2\cdot 7/2^-[523]$ states is somewhat fortuitious. Nonetheless, the good agreement of relative cross sections shows that Coriolis coupling can account for the distribution of strength.

Since the model used in the present work does not take into account the possibility of vibrational excitations, it is not possible to compare predicted strengths with those observed for quasiparticle-vibration mixed states populated by the (t,α) reaction. It is, however, of some interest to indicate which states of this type have been populated. The $1/2^+$ and $3/2^+$ members of the previously identified band based on the $\{1/2^+[400] + 5/2^+[402], 2^+\}$ state are observed at 512 and 589 keV. The $3/2^+$ bandhead of the K_0-2 gamma vibrational band based on the $1/2^+[411]$ state is seen at 865 keV. This vibrational band is expected to contain a significant admixture of the $3/2^+[411]$ single proton state (Malov et al. 1969), which is characterized by a large spectroscopic strength to the $I = 5/2$ rotational member. A level at 979 keV has been tentatively assigned $I^\pi = 5/2^+$, and a $5/2\{3/2^+[411] + 1/2^+[411], 2^+\}$ interpretation is suggested. Finally, there are two levels of significant strength at 1484 and 1681 keV which have been tentatively assigned $I^\pi = 5/2^+$ and $3/2^+$ respectively. No levels of these spins and intensities are predicted by the Nilsson model at this energy, but it is apparent that

vibrational states are important in ^{187}Re, and these levels may also be due to particle-vibration coupling.

5.3 Levels in ^{189}Re.

Prior to the present study, no level assignments had been made in ^{189}Re. The rather limited information which was available has been outlined in Chapter 1. Using the results of the (t,α) and ($\vec{t}$,α) experiments, it has been possible to make a number of I^{π} assignments and several Nilsson model assignments. Experimental and theoretical unpolarized cross sections and nuclear structure factors are compared in Table 6. The level energies, rotational parameters and decoupling parameters used in the calculations are given in Table 10; the energies correspond quite closely to the experimental values.

On the basis of its angular distributions, the ground state of ^{189}Re is assigned $I^{\pi} = 5/2^{+}$, which is consistent with the observed log ft value for decay to ^{189}Os (Lewis 1974). It is interpreted as the $5/2^{+}$[402] bandhead, which is found to be the ground state in the lighter isotopes. The calculated strength of this state is slightly less than observed, but in view of the sensitivity of the ground state cross section to the position of the Fermi surface, the agreement is quite good. There are weakly populated levels at 125 and 146 keV, either of which could be $7/2^{+}$ on the basis of their distributions. A more reasonable level spacing is found if the 7/2 $5/2^{+}$[402] state is assigned to the 146 keV level.

A strongly populated $11/2^{-}$ state at 303 keV is assigned to the $9/2^{-}$[514] band. In the ($\vec{t}$,α) spectra, it was not resolved from a much weaker level at 279 keV, but the total cross section for the doublet is

Table 10

Comparison of experimental and model energies for ^{189}Re

Orbital	I^π	Experimental energy (keV)	Model		
			Energy (keV)	$\hbar^2/2\mathfrak{I}$ (keV)	a
$5/2^+[402]$	$5/2^+$	0	-2	21	
	$(7/2^+)$	146	142		
$9/2^-[514]$	$(9/2^-)$	125	124	22	
	$11/2^-$	303	300		
$1/2^+[411]$	$(1/2^+)$	260	268	23	-1.07
	$3/2^+$		259		
	$5/2^+$	481	488		
	$(7/2^+)$		471		
$7/2^+[404]$	$(7/2^+)$	697	696	21	
$7/2^-[523]$	$11/2^-$	1423	1425	21	
$3/2^+[402]$	$3/2^+$	*	702	21	
$1/2^+[400]$	$1/2^+$	*	900	21	0.41
$11/2^-[505]$	$11/2^-$	*	1113	21	
$1/2^-[541]$	$1/2^-$	*	1400	21	4.37
$3/2^+[411]$	$3/2^+$	*	2500	21	
$5/2^-[532]$	$5/2^-$	*	2501	21	
$3/2^-[541]$	$3/2^-$	*	2982	21	
$5/2^+[413]$	$5/2^+$	*	3001	21	
$1/2^-[550]$	$1/2^-$	*	3100	21	-5.86

* Not experimentally assigned, but included in the calculation.

slightly greater than the theoretical cross section for the 11/2 $9/2^-$[514] state. If the 125 keV level is assigned to be the $9/2^-$[514] bandhead, a very credible level spacing results. The predicted cross section for the 9/2 $9/2^-$[514] state is much less than what is observed; this is often found to be the case for weakly populated levels and is believed to be due to the simplicity of the structure and reaction models used.

The angular distributions for the level at 260 keV are in accord with a spin assignment of $I^\pi = 3/2^+$, and the level is interpreted as the 3/2 $1/2^+$[411] state. The $1/2^+$ member of the $1/2^+$[411] band is predicted to lie 9 keV above the $3/2^+$ member, so it seems likely that the 260 keV peak is in fact a doublet. Since the $1/2^+$ member is expected to have less strength than the $3/2^+$ member, it is reasonable that the distributions are compatible with $I^\pi = 3/2^+$. The possibility that the unassigned level at 279 keV is the 1/2 $1/2^+$[411] state has been considered, but such a large spacing between the two band members would be inconsistent with the situation found in ^{187}Re. The level at 481 keV is believed to be a doublet containing the $5/2^+$ and $7/2^+$ members of the $1/2^+$[411] band, with the former state dominant. This is supported by the γ-decay results of Kuaranen and Ihochi (1965). The relative intensities and energy spacing of the (1/2,3/2) and the proposed (5/2,7/2) doublets are in very good agreement with those found in ^{187}Re. Unfortunately, the 481 keV level was not resolved from that at 501 keV in the $(\vec{t},\alpha)$ experiments, so it was not possible to obtain analyzing powers for each level. Changes in the peak shape from one spin orientation to the other seem to indicate that the 481 keV level has a positive analyzing power, supporting the assignment given above, while that at 501 keV has a

negative analyzing power.

The analyzing power for the complete (481,501) keV multiplet shown in Fig. 15(a) is seen to be very close to zero at all angles. This could be explained most easily if the 501 keV level had $I^{\pi} = 3/2^{+}$. Other $j=\ell-1/2$ assignments cannot be definitely ruled out, but the almost complete cancellations of analyzing powers for the multiplet suggests the main components have the same ℓ-value. The angular distribution of the cross section for the multiplet is consistent with $\ell=2$.

The level at 697 keV has been tentatively interpreted as the $7/2^{+}[404]$ bandhead. It has a high ℓ-value, a j-value of $\ell-1/2$, and its large strength makes it the most likely candidate for this Nilsson assignment.

Another strongly populated level at 1223 keV has been assigned $I^{\pi} = 5/2^{+}$. It has a strength comparable to the 1484 keV level in ^{187}Re, but the Nilsson configuration is not known.

A second strongly populated $11/2^{-}$ state is observed at 1423 keV and is attributed to the $7/2^{-}[523]$ band. Another strongly populated level at 1502 keV may also have $I^{\pi} = 11/2^{-}$ although this is less certain. It can be seen from Table 6 that the strengths of the $11/2\ 9/2^{-}[514]$ and $11/2\ 7/2^{-}[523]$ levels are reproduced quite well by the calculations. The basic Nilsson model with only a quadrupole deformation does not predict additional $11/2^{-}$ states with significant (t,α) strength at low excitation energies and would therefore not explain another $I^{\pi} = 11/2^{-}$ level at 1502 keV. However, it will be seen in Chapter VI that for reasonable hexadecapole deformations the low-K orbitals from the $h_{11/2}$ shell would become very closely spaced. As they would also be strongly

mixed by the Coriolis interaction, the distribution of strength would be expected to depend strongly upon the single particle energies for these states.

Finally, several other I^{π} assignments are listed in Table 6 but there is not sufficient information available to justify speculation on their nature.

5.4 Levels in ^{191}Re.

No information was previously available on the nuclear structure of ^{191}Re. As in ^{189}Re, the present study has made possible the assignment of many I^{π} values and several Nilsson orbitals. Table 7 shows the experimental and theoretical cross sections and nuclear structure factors, while Table 11 gives the energies used for the model calculations. As for the other two isotopes, the theoretical energies are quite close to the experimental values. An exception, however, is the predicted 25 keV separation between the $5/2^+$ and $7/2^+$ members of the $1/2^+[411]$ band; a separation this large would have resulted in the peaks being resolved in the (t,α) experiments, which they are not.

The first interesting feature of the structure of ^{191}Re is that the ground state is not the same as that found in all the lighter rhenium isotopes. Angular distributions indicate $I^{\pi} = 3/2^+$ for the first observed peak, suggesting that the $1/2^+[411]$ orbital forms the ground state band in this nuclide. It is not clear whether the bandhead of this orbital or the $3/2^+$ rotational member forms the ground state, as these are expected to be closely spaced. In this study, the $3/2^+$ state is assumed to be at 0 keV. The possibility that the level at 27 keV is

Table 11

Comparison of experimental and model energies for ^{191}Re

Orbital	I^{π}	Experimental energy (keV)	Model		
			Energy (keV)	$\hbar^2/2\mathcal{I}$ (keV)	a
$1/2^+[411]$	$(1/2^+)$	0	12	23	-1.11
	$3/2^+$		0		
	$5/2^+$	227	234		
	$(7/2^+)$		209		
$5/2^+[402]$	$5/2^+$	97	97	24	
$9/2^-[514]$	$(9/2^-)$	145	141	22	
	$11/2^-$	285	295		
$7/2^+[404]$	$7/2^+$	799	799	23	
$7/2^-[523]$	$11/2^-$	1229	1223	23	
$3/2^+[402]$	$3/2^+$	*	702	23	
$1/2^+[400]$	$1/2^+$	*	901	23	0.40
$1/2^-[541]$	$1/2^-$	*	1600	23	4.54
$5/2^-[532]$	$5/2^-$	*	1885	23	
$3/2^-[541]$	$3/2^-$	*	2386	23	
$3/2^+[411]$	$3/2^+$	*	2400	23	
$1/2^-[550]$	$1/2^-$	*	2500	23	-5.89
$5/2^+[413]$	$5/2^+$	*	2901	23	

* Not experimentally assigned, but included in the calculation.

the 1/2 $1/2^+[411]$ state has been considered, but it is made unlikely by the $(\vec{t},\alpha)$ data. The analyzing powers for the 27 keV level, determined according to the procedure described in section 4.2, were close to zero, as would be expected for $I^\pi = 1/2^+$, but a significant tail from the $3/2^+$ peak at 0 keV was present in the 27 keV gate, especially for the spin up case. The spectra have been examined more closely by using the peak shape of the 97 keV level to determine the contribution of the tail under the 27 keV peak. Although the uncertainties are quite large, the resulting analyzing powers, shown in Fig. 16(a), are definitely positive. Further, a distinct forward minimum is not observed in the cross section angular distribution, suggesting $\ell \leq 3$. The possible assignments for the 27 keV level are therefore $3/2^-$; $5/2^+$ or $7/2^-$, but no convincing interpretation has yet been found for it. It is assumed that the 1/2 $1/2^+[411]$ state is unresolved from the more strongly populated $3/2^+$ member of the band, as in ^{187}Re. The $5/2^+$ and $7/2^+$ members of the $1/2^+[411]$ band are found as an unresolved doublet at 227 keV. The intensities of the two doublets attributed to the $1/2^+[411]$ band in ^{191}Re agree well with the corresponding intensities in ^{187}Re and ^{189}Re, providing further support for the assignments. In all three isotopes, however, the $(5/2^+,7/2^+)$ doublet is stronger, relative to the $(1/2^+,3/2^+)$ one, than predicted.

The $5/2^+[402]$ bandhead, which forms the ground state in all other odd-mass rhenium isotopes, is found at 97 keV in ^{191}Re. Its spectroscopic strength is in good agreement with the predicted result. It was not possible to identify the weakly populated 7/2 $5/2^+[402]$ state. A $7/2^+$ state at 799 keV is interpreted as the $7/2^+[404]$ bandhead. As

was found for the corresponding state in ^{189}Re, the nuclear structure factor is ∿ 70% of the predicted value.

There is a level at 449 keV which appears to have $I^{\pi} = 1/2^{+}$. This may be analagous to the 512 keV vibrational state in ^{187}Re, although the experimental strength is about twice as large in ^{191}Re. As in the other two isotopes, a strongly populated $5/2^{+}$ state is observed above 1 MeV in excitation, in this case at 1145 keV. Another $5/2^{+}$ state is observed at 1937 keV. No interpretations are presented for these levels, but it is quite possible that they result from particle-vibrational coupling.

If the states originating from the $h_{11/2}$ shell model state displayed some unusual properties in ^{189}Re, it appears to be an even greater challenge to explain their behaviour in ^{191}Re. The $11/2\ 9/2^{-}[514]$ state at 285 keV is populated very strongly with the (t,α) reaction. The observed nuclear structure factor is 2.7, which is significantly larger than the calculated value of 1.64. A second $11/2^{-}$ state, found at 1229 keV, also has a large strength and has been assigned $11/2\ 7/2^{-}[523]$ in analogy with ^{187}Re and ^{189}Re. (It is to be realized, of course, that these states would be strongly mixed and the Nilsson quantum numbers are at best an indication of the main admixture.) There is another level at 1367 keV which has also been tentatively assigned $I^{\pi} = 11/2^{-}$. None of the Coriolis coupling calculations which were performed using only a quadrupole deformation in the Nilsson potential have been able to reproduce the observed strengths for these $11/2^{-}$ states. Attempts to explain the experimental results with the inclusion of a hexadecapole term in the deformation are described in the next chapter.

CHAPTER VI

LEVEL SYSTEMATICS AND THE EFFECTS OF HEXADECAPOLE DEFORMATIONS

In Chapter II, several theoretical calculations of equilibrium quadrupole and hexadecapole deformations were briefly described. The results of those calculations for the W, Re and Os isotopes with A $\sim$ 190 are given in Table 12. In general, the trend is for both ε_2 and ε_4 to decrease with increasing mass. The hexadecapole deformation is $0.04 \leq \varepsilon_4 \leq 0.09$ for all the nuclei shown. It should also be noted that the calculations of Nielsen and Bunker (1975) indicate an appreciable variation in deformation for different Nilsson orbitals in the same nucleus. Götz et al. (1972) found that if ε_4 were neglected, ^{188}Os was predicted to be oblate. Taking the hexadecapole deformation into account, the transition from prolate to oblate did not occur until ^{194}Os. The deformation energy of ^{192}Os was predicted to be nearly independent of γ; this gives level energies for the first two 2^+ states and the first 4^+ vibrational state which are consistent with experimental results (Lederer et al. 1967). No equilibrium triaxial shapes were predicted for any of the nuclei listed in Table 12.

Experimental measurements of deformation parameters are not as numerous as theoretical results. In general, two different techniques have been used: Coulomb excitation and inelastic scattering, usually of alpha particles. Analysis of the results of the former type of experiment gives the shape of the Coulomb field, while the second gives the

Table 12

Equilibrium nuclear deformations in the A∿190 region

	Reference	Nucleus	State	ε_2	ε_4
Theory:	I.-L. Lamm (1969)	^{185}Re	g.s.	0.207	0.058
	S.G. Nilsson et al(1969)	^{186}W	g.s.	0.195	0.060
		^{188}W	g.s.	0.170	0.060
		^{188}Os	g.s.	0.175	0.055
		^{190}Os	g.s.	0.160	0.050
		^{192}Os	g.s.	0.140	0.050
	Götz et al.(1972)	^{186}W	g.s.	0.20	0.09
		^{188}W	g.s.	0.18	0.08
		^{188}Os	g.s.	0.18	0.08
		^{190}Os	g.s.	0.16	0.06
		^{192}Os	g.s.	0.14	0.04
	Neilson & Bunker(1975)	^{185}Re	$5/2^+[402]$	0.213	0.067
			$9/2^-[514]$	0.212	0.064
			$1/2^+[411]$	0.205	0.060
			$11/2^-[505]$	0.202	0.057
			$1/2^-[541]$	0.227	0.064
		^{187}Re	$5/2^+[402]$	0.200	0.067
			$9/2^-[514]$	0.197	0.064
			$1/2^+[411]$	0.190	0.060
			$11/2^-[505]$	0.187	0.057
			$1/2^-[541]$	0.207	0.064
Experiment:	Lee et al.(1974)*	^{186}W	g.s.b.	0.16	0.07
	Baker et al.(1976)*	^{188}Os	g.s.b.	0.14	0.025
		^{190}Os	g.s.b.	0.14	-
		^{192}Os	g.s.b.	0.12	0.02
	Bernthal et al.(1974)	^{187}Os		∿ 0.19	∿ 0.06

* Parameters scaled according to Hendrie (1973) procedure.

shape of the nuclear field. When both methods have been used on the same nucleus, the Coulomb deformation parameters have consistently been larger than the nuclear parameters. The difference may be eliminated or significantly reduced by applying a scaling procedure to the results obtained by inelastic scattering. Hendrie (1973) describes this procedure and provides a simple justification for it. Results from (α,α') experiments on ^{186}W(Lee et al. 1974) and on ^{188,190,192}Os (Baker et al. 1976) are given in Table 12; these parameters have been scaled using Hendrie's prescription. The experimental quadrupole deformation parameters are all slightly less than predicted, as are the values of ε_4 for ^{188}Os and ^{192}Os. There is, however, considerable uncertainty in the hexadecapole parameters, and Baker et al. (1976) claim only to have shown that $\varepsilon_4 > 0$ for the osmium isotopes.

Bernthal et al. (1974) used the perturbed band structure in ^{187}Os of neutron states originating from the $i_{13/2}$ shell model state to estimate the hexadecapole deformation. They found that ε_4 must be less than ~ 0.08 for the predicted band structure to agree with experiment. In a study of odd-A tungsten isotopes using neutron pickup reactions (Kleinheinz et al. 1973), it was found that a deformation of $\varepsilon_4 \approx 0.06$ was needed to interpret the resulting spectra.

For the present study, single particle energies have been calculated using the computer program NILS, due originally to Bjorn Nilsson. The results of the calculations for $\varepsilon_4 = 0$ and $\varepsilon_4 = 0.06$, with $0.10 \leq \varepsilon_2 \leq 0.20$, are shown in Fig. 18. Again the values used for the potential well parameters were $\kappa = 0.062$ and $\mu = 0.614$, adopted from

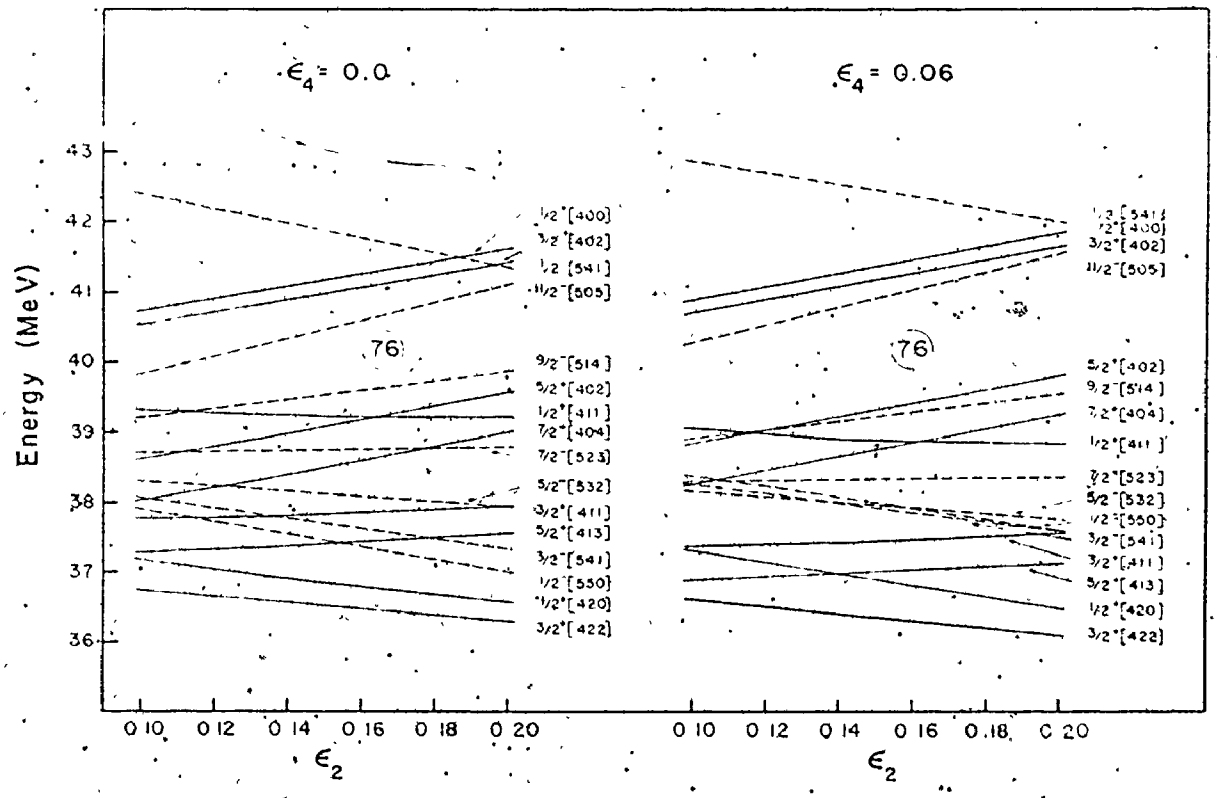

Figure 18. Energy level diagrams for proton states, $50 \leq Z \leq 82$, and $0.10 \leq \varepsilon_2 \leq 0.20$. The scheme on the left is for no hexadecapole deformation; that on the right is for $\varepsilon_4 = 0.06$. The circled numbers refer to the number of protons required to fill the energy levels to that point.

Nilsson et al. (1969). The value of 0.06 chosen for ε_4 is an approximate average of the theoretical values given in Table 12, and is consistent with the experimental values listed there. The calculations for $\varepsilon_4 = 0$ essentially reproduce part of Fig. 1. When a hexadecapole deformation is introduced, it can readily be seen that significant changes are produced in the level ordering. The composition of the wavefunctions is not, however, greatly affected by the introduction of an ε_4 deformation of this magnitude. Hence no new Coriolis coupling calculations were done using $C_{j\ell}$-values from the hexadecapole calculation.

Energy systematics for the five odd-A rhenium isotopes from ^{183}Re to ^{191}Re are shown in Fig. 19. Data for ^{183}Re and ^{185}Re are taken from Lu and Alford (1971), while data for levels in ^{187}Re are taken from Ellis (1974) where possible. Of particular interest is the rapid decrease in energy of the $1/2^+[411]$ orbital with increasing mass, until in ^{191}Re it forms the ground state. The Nilsson model without ε_4 deformation predicts a crossing between the $5/2^+[402]$ and the $1/2^+[411]$ orbitals at a deformation of $\varepsilon_2 \sim 0.16$, but it also indicates that the $9/2^-[514]$ orbital should form the ground state for deformations down to $\varepsilon_2 \sim 0.11$. On the other hand, the level scheme in Fig. 18 for $\varepsilon_4 = 0.06$ correctly predicts the ground state to be the $5/2^+[402]$ orbital down to $\varepsilon_2 \sim 0.12$, where the $1/2^+[411]$ orbital becomes the ground state. Both level schemes in Fig. 18 show the $7/2^+[404]$ orbital to have approximately the same energy relative to the $5/2^+[402]$ orbital for all values of ε_2, in agreement with the systematics. If the $1/2^+[411]$ orbital were shifted slightly upwards in the $\varepsilon_4 = 0.06$ diagram so that it intersected the $5/2^+[402]$ orbital at somewhat higher deformation, and was above the

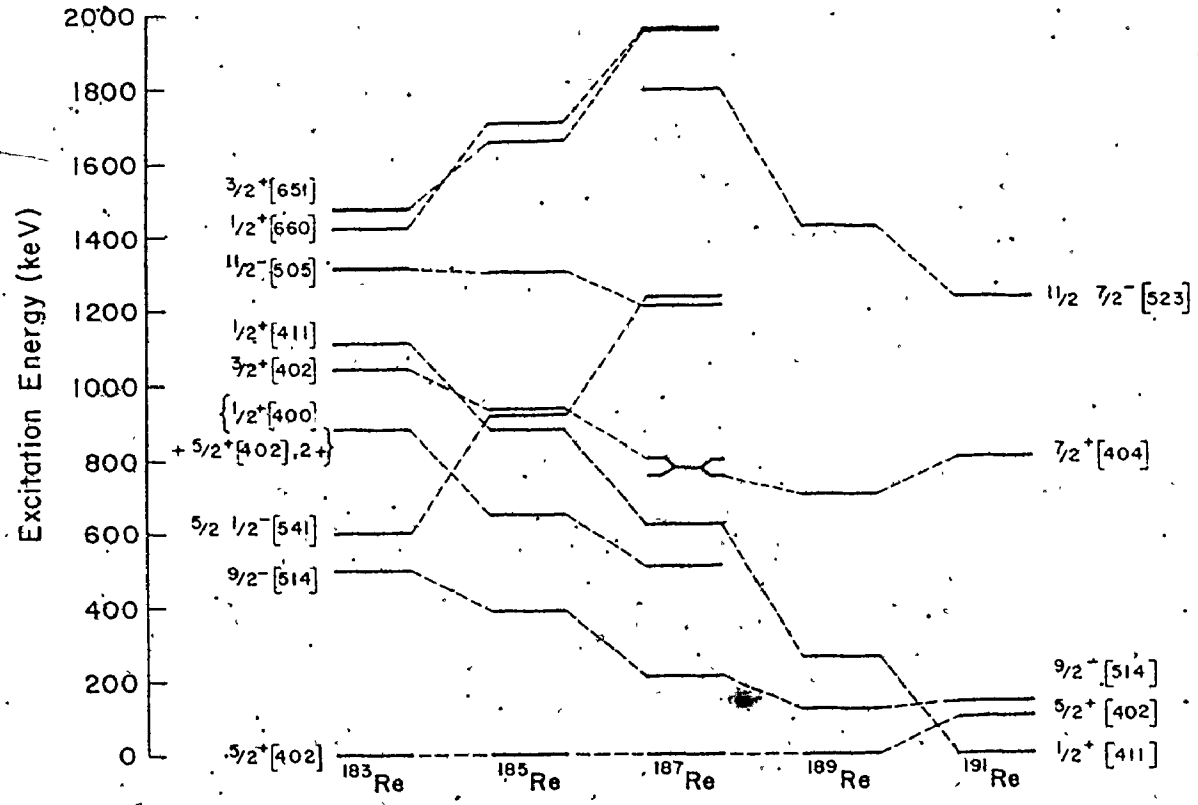

Figure 19. Energy systematics for the odd-A rhenium isotopes. The results for ^{183}Re and ^{185}Re are from Lu and Alford (1971), and most of the ^{187}Re energies are from Ellis (1974).

$7/2^+[404]$ state for most of the range shown, agreement between this level scheme and the systematics shown in Fig. 19 would be very good for the positive parity states.

Another interesting result of including a significant hexadecapole deformation is that the three lowest Nilsson orbitals originating from the $h_{11/2}$ shell model state are predicted to be nearly degenerate for $0.10 \leq \varepsilon_2 \leq 0.20$. This is quite a general result for orbitals originating from high-j shell model states, and a simple physical explanation has been provided by Kleinheinz et al. (1973). A particle in a low-Ω orbital tends to travel about a prolate nucleus in a polar orbit, whereas one in a high-Ω orbital travels in an equatorial orbit. For a pure quadrupole deformation, the major axis of the orbit decreases fairly smoothly with increasing Ω, corresponding to an increasing harmonic, oscillator constant ω. Hence the orbitals originating from a single shell model state are spread out in energy as shown in Fig. 1. When a hexadecapole component of $\varepsilon_4 \sim 0.08$ is introduced, the shape of the nuclear potential changes as shown in Fig. 2; the major axes of the orbits of the lowest two or three orbitals become nearly the same, and thus the orbitals are approximately degenerate. Whereas the $I^\pi = 11/2^-$ strength and its distribution for ^{187}Re could be described quite well by the Coriolis mixing calculations, it is recalled that anomalous behaviour for $I^\pi = 11/2^-$ states was observed in ^{189}Re and ^{191}Re. There are five Nilsson orbitals from the $h_{11/2}$ shell which would be expected to lie below the Fermi surface and thus the nuclear structure factors for the $11/2^-$ states at all excitation energies should sum to ~ 5 in the present proton pick-up reaction. Using the basic Nilsson model with $\varepsilon_4 = 0$

it is seen from Fig. 18 that two of these five orbitals might be expected as hole states in the first 1-2 MeV of excitation. The sum of the nuclear structure factors for $11/2^-$ states in ^{187}Re is $\lesssim$ 2.7, which appears to be a reasonable value considering that some of the strength from the deeper hole states will be brought to lower excitation energies by the Coriolis mixing. However, the corresponding sums of $11/2^-$ strengths in ^{189}Re and ^{191}Re are $\sim$ 3.4 and 4.5, respectively, indicating at least in the latter case, that most of the expected hole state $11/2^-$ strength is found at < 1.4 MeV in excitation energy. One can attempt to explain this behaviour qualitatively by invoking ε_4 deformations for these isotopes which, as shown in Fig. 18, would tend to group the $7/2^-[523]$, $5/2^-[532]$, $3/2^-[541]$ and $1/2^-[550]$ orbitals together and also bring them closer to the ground state. This tendency should be more pronounced for the smaller quadrupole deformations (e.g. $\varepsilon_2 \sim 0.12$) expected for heavier isotopes. The large Coriolis matrix elements coupling these states could then result in very complicated distortions of the rotational bands, depending on the energy spacings of the unperturbed states. Therefore the overall trend of the $11/2^-$ strength does not appear to be unreasonable as the total strength of $\sim$ 4.5 in ^{191}Re is consistent with this explanation. However, some of the details cannot easily be reproduced. In particular, Coriolis mixing calculations were unable to duplicate the experimental value of 2.7 for the nuclear structure factor of the lowest $11/2^-$ state observed in ^{191}Re. All combinations of single particle energies yielding reasonable perturbed energies gave nuclear structure factors less than $\sim$ 2.0.

An alternative approach to explaining the behaviour of these levels

would be to invoke different deformations for various excited states than for the ground state. In the region of rapidly changing deformation near A $\sim$ 150 there are several known cases where states with quite different quadrupole deformations co-exist at low excitations. Although the deformation is not changing as rapidly in the A $\sim$ 190 region, the possibility of similar effects exists. For example, the 285 keV level in ^{191}Re, which has been interpreted as 11/2 $9/2^-$[514], could be a spherical state having a large fraction of the $h_{11/2}$ strength. On the basis of the data presently available, there is no good way to distinguish between these possible interpretations. This is because the Coriolis mixing usually produces a distribution of strengths which is very similar to that expected on the basis of a spherical shell model with some residual interactions.

In order to determine whether the experimental results could be interpreted more easily if other values of ε_4 were considered, calculations were also done for ε_4 = 0.03, 0.05, 0.07 and 0.09. The resulting level schemes for ε_4 = 0.05 and 0.07 were sufficiently similar to those for ε_4 = 0.06 that all three could be considered acceptable. However, the predicted level orderings for ε_4 = 0.03 and 0.09 were in significantly poorer agreement with the experimental results. As might be expected, the level scheme for ε_4 = 0.03 was midway between those shown for ε_4 = 0.00 and ε_4 = 0.06 in Fig. 18. The rhenium ground state was incorrectly predicted to be the $9/2^-$[514] orbital for nearly the full range of quadrupole deformations (again $0.10 \leq \varepsilon_2 \leq 0.20$). The level spacings of the lowest three negative parity orbitals originating from the $h_{11/2}$ state were compressed relative to the pure quadrupole case, but their energies were

not sufficiently perturbed to provide as good an explanation for the observed behaviour of the $11/2^-$ states in ^{191}Re. The results of the calculations for $\varepsilon_4 = 0.09$ showed the $1/2^+[411]$ orbital still lower in energy than predicted for $\varepsilon_4 = 0.06$. Since this orbital was already somewhat too low in the latter calculation, increasing the hexadecapole deformation has made agreement with experiment poorer. Also, the spacing between the $5/2^+[402]$ and the $9/2^-[514]$ orbitals was predicted to be considerably larger than observed. And finally, the lowest three negative parity orbitals were brought very close to the $7/2^-[523]$ orbital for the full range of quadrupole deformation. This would lead to another $11/2^-$ state being observed at low excitation in ^{187}Re, and a different distribution of strengths from what is observed would result. Thus, neither the calculation for $\varepsilon_4 = 0.03$ nor that for $\varepsilon_4 = 0.09$ provides as good an explanation of the data as that for $\varepsilon_4 = 0.06$.

CHAPTER VII

SUMMARY AND CONCLUSIONS

The nuclear structures of the transitional nuclei ^{187}Re, ^{189}Re and ^{191}Re have been studied using the (t,α) proton pick-up reaction. Excitation energies were determined using unpolarized tritons on thin osmium targets. Angular distributions of analyzing powers and cross sections were obtained using polarized tritons on thicker targets. It was possible to reproduce the experimental analyzing powers for known levels in ^{187}Re very well with a distorted-wave calculation. The angular distributions observed for unpolarized cross sections were also well reproduced for ℓ=0 and 2, and qualitative agreement was found for ℓ=4 and 5. By comparing DWBA predictions with results for other levels in all three rhenium isotopes, it has been possible to make many spin and parity assignments. The assignments have been interpreted in terms of the Nilsson model, which, with pairing corrections and Coriolis coupling included, provides quite a good description of many of the levels observed.

The 7/2 7/2$^+$[404] and 11/2 7/2$^-$[523] states have been assigned for the first time in all three isotopes. No previous assignments had been made for ^{189}Re and ^{191}Re; the present study has assigned the 5/2$^+$[402], 9/2$^-$[514] and 1/2$^+$[411] orbitals in these isotopes. Many additional I^π assignments have been made to levels which have not been amenable to interpretation in terms of the simple theoretical model of the nucleus which was used. A number of these are believed to result

from particle-vibration coupling.

The distribution of strength to members of the $1/2^+[411]$ rotational band was similar in all three isotopes, and is not consistent with Nilsson model predictions. Similar anomalies in this band have also been observed in ^{161}Ho and ^{163}Ho (Panar et al. 1977) and in ^{165}Tm (Cheung et al. 1974), but no good explanation has yet been proposed.

Several aspects of the observed rhenium systematics are better accounted for by adding a hexadecapole component to the nuclear potential. The ground state in all odd-A rhenium isotopes up to A=189 is $5/2^+[402]$; in ^{191}Re it was found to be $1/2^+[411]$. A single particle energy level scheme calculated assuming only a quadrupole deformation predicts a $9/2^-[514]$ ground state down to small deformations, whereas a calculation with $\varepsilon_4 = 0.06$ correctly predicts a $5/2^+[402]$ ground state, yielding to the $1/2^+[411]$ orbital at $\varepsilon_2 = 0.12$. More and more $11/2^-$ strength is observed below $\sim$ 2 MeV excitation as one goes from ^{187}Re to ^{191}Re. This also is not expected if the nuclear potential has only a quadrupole deformation. A hexadecapole deformation, however, brings low-Ω negative parity states down in excitation, resulting in increased mixing and hence more $11/2^-$ strength at low excitations. It has not been possible to reproduce the distribution of strength among observed $11/2^-$ states in ^{191}Re with Coriolis mixing calculations. Further work is required before this discrepancy can be understood. Calculations using other values of ε_4 indicate that the data are best described by assuming a value of $\varepsilon_4 = 0.06 \pm 0.01$. No clear evidence was found for an equilibrium asymmetric nuclear shape.

More about the structure of these nuclei might be learned when

a facility becomes available which is suitable for doing ($d,^3He$) experiments on osmium targets. Angular distributions and cross section ratios with the (t,α) cross sections presented here could make new assignments possible. The early γ-decay study of ^{189}Re by Kuaranen and Ihochi (1965) used the (n,α) reaction with 14 MeV neutrons on a target of ^{192}Os to produce ^{189}W. This was chemically separated and its decay studied with sodium iodide detectors. This experiment could now be repeated, using higher-resolution detectors and better coincidence electronics to improve the data, and to further elucidate the level structure of ^{189}Re. Gamma-ray studies of ^{191}Re are difficult because of its position far to the right of the line of stability in the chart of the nuclides.

These experiments represent the first time the $(\vec{t},\alpha)$ reaction has been used to study deformed nuclei. The large and distinctive analyzing powers which were obtained clearly show that the technique is a very useful one for nuclear spectroscopy in the deformed rare earth region. It is apparent that the low values of A_y found in the $W(\vec{d},p)$ experiments of Castén et al. (1973b) are not a general property of single particle transfer reactions on rare-earth deformed nuclei. There are still many heavy deformed nuclei which can be studied using the (t,α) reaction and for which no nuclear structure information exists at present. The results of this work show that in such cases (e.g. ^{191}Re) the (t,α) reaction is far more useful when the triton beam is polarized. The only limitation, and it is a rather severe one at present, is the very restricted availability of a beam of polarized tritons.

References

Baker, F.T., Kruse, T.H., Hartwig, W., Lee, I.Y., and Saladin, J.X. 1976. Nucl. Phys. A,258, 43.

Bardeen, J., Cooper, L.N., and Schrieffer, J.R. 1957. Phys. Rev. 108, 1175.

Barnes, P.D., Flynn, E.R., Igo, G.J., and Armstrong, D.D. 1970. Phys. Rev. C, 1, 228.

Barnes, P.D., Romberg, E., Ellegaard, C., Casten, R.F., Hansen, O., Mulligan, T.J., Broglia, R.A., and Liotta, R. 1972 Nucl. Phys. A, 195, 146.

Bassel, R.H., Drisko, R.M., and Satchler, G.R. 1962. Oak Ridge National Laboratory Report ORNL-3240.

Bernthal, F.M., Jeltema, B.D., Boyno, J.S., Khoo, T.L., and Warner, R.A. 1974. Phys. Rev. Lett. 33, 915.

Bevington, P.R. 1969. Data Reduction and Error Analysis for the Physical Sciences, p. 255. McGraw-Hill, New York.

Bohr, A. 1952. Mat. Fys. Medd. Dan. Vid. Selsk, 26, No. 14.

Bohr, A., Mottelson, B.R., and Pines, D. 1958. Phys. Rev. 110, 936.

Bromley, D.A., Gove, H.E., and Litherland, A.E. 1957. Can. J. Phys. 35, 1057.

Bunker, M.E., and Reich, C.W. 1971. Rev. Mod. Phys. 43, 348.

Burke, D.G., Waddington, J.C., and Johns, M.W. 1971. Private communication.

Casten, R.F., Cosman, E., Flynn, E.R., Hansen, O., Keaton, P.W., Jr., Stein, N., and Stock, R. 1973a. Nucl. Phys. A, 202, 161.

Casten, R.F., Keaton, P.W., Jr., and Lawrence, G.P. 1973b. Phys. Rev. C, 7, 1016.

Cheung, H.C., Burke, D.G., and Løvhøiden, G. 1974. Can. J. Phys. 52, 2108.

Chi, B.E. 1966. Nucl. Phys. 83, 97.

Darden, S.E. 1971. Proc. of the Third Int. Sym on Polarization Phenomena in Nuclear Reactions, Madison, 1970, p. 48. Ed. H.H. Barschall and W. Haeberli, U. of Wisconsin Press, Madison.

Elbek, B., and Tjøm, P.O. 1969. Advances in Nuclear Physics, 3, 759. Ed. M. Baranger and E. Vogt, Plenum Press, New York.

Ellis, Y.A. 1974. Nucl. Data Sheets 14, 347.

Flynn, E.R., Armstrong, D.D., Beery, J.G., and Blair, A.G. 1969. Phys. Rev. 182, 1113.

Flynn, E.R., Orbesen, S., Stein, N., Thiessen, H.A., Lee, D.M., and Sobottka, S.E. 1973. Nucl. Instr. and Meth. 111, 67.

Flynn, E.R., Orbesen, S., Sherman, J.D., Sunier, J.W., and Woods, R. 1975. Nucl. Instr. and Meth. 128, 35.

Flynn, E.R., Hardekopf, R.A., Sherman, J.D., Sunier, J.W., and Coffin, J.P. 1976. Phys. Rev. Lett. 36, 79.

Flynn, E.R., Hardekopf, R.A., Sherman, J.D., and Sunier, J.W. 1976a. Private communication.

Götz, E., Pauli, H.C., Alder, K., and Junker, K. 1972. Nucl. Phys. A. 192, 1.

Gove, N.B., and Wapstra, A.H. 1972. Nucl. Data Tables 11, 259.

Hardekopf, R.A., Veeser, L.R., and Keaton, P.W., Jr. 1975. Phys. Rev. Lett. 35, 1623.

Hardekopf, R.A., Ohlsen, G.G., Poore, R.V., and Jarmie, N. 1976a. Proc. of the Fourth Int. Sym. on Polarization Phenomena in Nuclear Reactions, Zurich, 1975, p. 903. Ed. W. Gruebler and V. König, Birkhauser, Basel and Stuttgart.

Hardekopf, R.A., Ohlsen, G.G., Poore, R.V., and Jarmie, N. 1976b. Phys. Rev. C, 13, 2127.

Hendrie, D.L. 1973. Phys. Rev. Lett. 31, 478.

Hirning, C.R., and Burke, D.G. 1976. Can. J. Phys. 54, 1360.

Ikeda, A. 1974. Tokyo Institute of Technology, unpublished.

Kleinheinz, P., Casten, R.F., and Nilsson, B. 1973. Nucl. Phys. A, 203, 539.

Kuaranen, P., and Ihochi, H. 1965. J. Inorg. Nucl. Chem. 27, 1451.

Kunz, P.D. 1974. University of Colarado, unpublished computer program DWUCK4 and associated write-up.

Lamm, I.-L. 1969. Nucl. Phys. A, 125, 504.

Lederer, C.M., Hollander, J.M., and Perlman, I. 1967. Table of Isotopes. Wiley, New York.

Lee, I.Y., Saladin, J.X., Baktosh, C., Holden, J.E., and O'Brien, J. 1974. Phys. Rev. Lett. 33, 383.

Lewis, M.B. 1974. Nucl. Data Sheets 12, 409.

Løvhøiden, G., Burke, D.G., and Hirning, C.R. 1976. Unpublished data.

Lu, M.T., and Alford, W.P. 1971. Phys. Rev. C, 3, 1243.

Malov, L.A., Solov'ev, V.G., and Fainer, U.M. 1969. Izv. Akad. Nauk. S.S.S.R., Ser. Fiz. 33, 1244.

McFadden, L., and Satchler, G.R. 1966. Nucl. Phys. 84, 177.

Meyer-ter-Veyn, J. 1975. Nucl. Phys. A, 249, 111,141.

Neergård, K., and Vogel, P. 1970. Nucl. Phys. A, 145, 33.

Nielsen, B.S., and Bunker, M.E. 1975. Nucl. Phys. A, 245, 376.

Nilsson, B. 1969. Nucl. Phys. A, 129, 445.

Nilsson, S.G. 1955. Mat. Fys. Medd. Dan Vid. Selsk. 29, No. 16.

Nilsson, S.G., Tsang, C.F., Sobiczewski, A., Szymanski, Z., Wycech, S., Gustafson, C., Lamm, I.-L., Möller, P., and Nilsson, B. 1969. Nucl. Phys. A, 131, 1.

Ohlsen, G.G. 1970. LASL Report LA-4451.

Ohlsen, G.G., McKibben, J.L., Lawrence, G.P., Keaton, P.W., Jr., and Armstrong, D.D. 1971. Phys. Rev. Lett. 27, 599.

O'Neil, R.A. 1970. Unpublished computer program SPECTR.

O'Neil, R.A. 1971. Unpublished computer program GREAT.

Orbesen, S.D., Sherman, J.D., and Flynn, E.R. 1976. LASL Report LA-6271-MS.

Panar, J.D., Straume, O., and Burke, D.G. 1977. Private communication.

Preston, M.A., and Bhaduri, R.K. 1975. Structure of the Nucleus. Addison-Wesley, Reading, Mass.

Price, R.H., Burke, D.G., and Johns, M.W. 1971. Nucl. Phys. A, 176, 338.

Rowe, D.J. 1970. Nuclear Collective Motion. Methuen, London.

Satchler, G.R. 1958. Annals of Physics 3, 275.

Satchler, G.R. 1964. Nucl. Phys. 55, 1.

Strutinsky, V.M. 1967. Nucl. Phys. A, 95, 420.

Wagner, L.K., Burke, D.G., Cheung, H.C., Kleinheinz, P., and Sheline, R.K. 1975. Nucl. Phys. A, 264, 43.

Yamazaki, Y., Sheline, R.K., and Burke, D.G. 1976. Private communication.

Yoshida, S. 1961. Phys. Rev. 123, 2122.